Probabilistic Post-Liquefaction Residual Shear Strength Analyses of Cohesionless Soil Deposits: Application to the Kocaeli (1999) and Duzce (1999) Earthquakes

Partahi Mamora Halomoan Lumbantoruan

Thesis submitted to the faculty of the Virginia Polytechnic Institute and State University
in partial fulfillment of the requirements for the degree of

Master of Science
In
Civil and Environmental Engineering Department

Dr. Marte S. Gutierrez, Committee Chair
Dr Jimmy Martin
Dr. Matthew Mauldon

October 7, 2005
Blacksburg, Virginia

Keywords: Flow Liquefaction, Undrained Liquefied Shear Strength,
First Order Reliability Method, Monte Carlo Simulation

Probabilistic Post-Liquefaction Residual Shear Strength Analyses of Cohesionless Soil Deposits: Application to the Kocaeli (1999) and Duzce (1999) Earthquakes

Partahi Mamora Halomoan Lumbantoruan

ABSTRACT

Liquefaction of granular soil deposits can have extremely detrimental effects on the stability of embankment dams, natural soil slopes, and mine tailings. The residual or liquefied shear strength of the liquefiable soils is a very important parameter when evaluating stability and deformation of level and sloping ground. Current procedures for estimating the liquefied shear strength are based on extensive laboratory testing programs or from the back-analysis of failures where liquefaction was involved and in-situ testing data was available. All available procedures utilize deterministic methods for estimation and selection of the liquefied shear strength. Over the past decade, there has been an increasing trend towards analyzing geotechnical problems using probability and reliability. This study presents procedures for assessing the liquefied shear strength of cohesionless soil deposits within a risk-based framework. Probabilistic slope stability procedures using reliability methods and Monte Carlo Simulations are developed to incorporate uncertainties associated with geometrical and material parameters. The probabilistic methods are applied to flow liquefaction case histories from the 1999 Kocaeli/Duzce, Turkey Earthquake, where extensive liquefaction was observed. The methods presented in this paper should aid in making better decisions about the design and rehabilitation of structures constructed of or atop liquefiable soil deposits.

ACKNOWLEDGEMENTS

The author wishes to express his ultimate gratitude to the Almighty God for giving an opportunity to work and complete this research.

The author presents a bouquet of thanks and appreciation to his advisor, Dr. Marte S. Gutierrez, for his guidance, encouragement, and support throughout the research.

The author also appreciates the input and suggestions from Dr. Jimmy Martin and Dr. Matthew Mauldon.

The author is also grateful to his associate, Morgan Eddy for his help, support, and friendship.

A special thanks to United States Geological Survey for funding this research project.

The author wants to express his sincere thanks to Virginia Tech for providing all the facilities, infrastructures, and friendly research environment.

Finally, the author also wants to express his special thanks to his father, mother, and brothers, for their love, support, and encouragement.

TABLE OF CONTENTS

ABSTRACT..……...……...ii
ACKNOWLEDGEMENTS……..……...…….……..…iii
TABLE OF CONTENTS……..…….....…...iv
LIST OF FIGURES……..……..vi
LIST OF TABLES…….....xi
CHAPTER 1 INTRODUCTION…….1
1.1 INTRODUCTION TO THE PROBLEMS…….……1
1.2 LIQUEFACTION……..…….8
1.2.1 Terminology……..……10
1.2.1.1 Flow Liquefaction……..10
1.2.1.2 Cyclic Mobility……..11
1.3 OBJECTIVES AND METHODOLOGY OF THE STUDY.……...12
1.4 ORGANIZATION AND SCOPE…….....13
CHAPTER 2 PROBABILITY/RELIABILITY METHODS FOR SLOPE STABILITY ANALYSIS…….……...14
2.1 INTRODUCTION TO SLOPE STABILITY ANALYSIS……..14
2.2 LIMIT EQUILIBRIUM METHOD……..14
2.3 THE ISHIHARA ET AL. (1990) SIMPLIFIED METHOD…….15
2.4 INTRODUCTION TO RELIABILITY METHODS FOR SLOPE STABILITY ANALYSIS…….17
2.5 VARIABILITY OF SOIL PARAMETERS…….18
2.6 METHOD OF PROBABILISTIC ANALYSIS……20
2.6.1 First Order Reliability Method..…….20
2.6.2 Monte Carlo Simulation…….21
CHAPTER 3 THE 1999 KOCAELI/DUZCE, TURKEY EARTHQUAKE…….23
3.1 INTRODUCTION……23
3.2 GEOLOGY OF TURKEY……26
3.3 GEOTECHNICAL EFFECT……28

CHAPTER 4 CASE HISTORIES BACK ANALYSIS…….30
4.1 INTRODUCTION……30
4.2 HOTEL SAPANCA LIQUEFACTION FAILURE……..32
4.2.1 Slope Stability Computation……..33
4.2.2 Parameter Uncertainty……...34
4.2.3 Probabilistic Stability Computation……...37
4.2.4 Reliability Computations……...38
4.3 OTHER CASE HISTORIES…….……...44
4.4 COMPARISON OF DATA FROM THIS STUDY AND PREVIOUS DATA FROM SEED AND HARDER (1990)…….…60
CHAPTER 5 CONCLUSIONS…….62
5.1 CONCLUSIONS……..62
5.2 FUTURE STUDY…….63
REFERENCES……..65
APPENDIX A……73
APPENDIX B……..111
VITA……118

LIST OF FIGURES

Figure 1.1 Types of failure induced by liquefaction of cohesionless soils……..2

Figure 1.2 Photograph of the Kawagashi-Cho Apartments following the 1964 Niigata earthquake in Japan……..3

Figure 1.3 Photograph of the Lower San Fernando Dam flow failure after the 1971 San Fernando earthquake near Los Angeles, California…….3

Figure 1.4 Relationship between corrected clean sand blowcount $(N_1)_{60\text{-}cs}$ and undrained residual strength (S_r)……5

Figure 1.5 Relationship between SPT blowcount and normalized residual shear strength from case histories……...7

Figure 1.6 SPT blowcount versus residual shear strength from flow liquefaction case histories……7

Figure 1.7 Building collapsed following soil liquefaction after 1964 Alaska earthquake……...9

Figure 1.8 Crane collapsed in Kobe Harbor following soil liquefaction after 1995 Kobe earthquake…….....10

Figure 1.9 Initiation of flow liquefaction by cyclic and monotonic loading. Although the stress conditions at the initiation of liquefaction are different for the two types of loading (points B and D), both lie on the flow liquefaction surface (FLS)…….….11

Figure 1.10 Three cases of cyclic mobility shown in stress path space: (a) no stress reversal and combined static and cyclic shear stress less than the steady state strength; (b) no stress reversal and momentary periods where combined static and cyclic shear stresses exceed the steady state strength; and (c) stress reversal and combined static and cyclic shear stresses less than the steady state strength……..….12

Figure 2.1 Simplified slope stability analysis……16

Figure 2.2 Uncertainty in soil properties……...……....18

Figure 3.1 Map of active faults in Turkey…….24

Figure 3.2 Location of earthquakes casualties and injuries of the 1999 Kocaeli/Duzce, Turkey earthquake…….25
Figure 3.3 Damaged refineries after the 1999 Kocaeli, Turkey earthquake……..26
Figure 3.4 Extension movement of Anatolia slab toward Hellenic-Greek slab and African plate……27
Figure 4.1 Liquefied shear strength relationship……..…….31
Figure 4.2 Hotel Sapanca after the 1999 Kocaeli Earthquake……..…….32
Figure 4.3 Cross section 1……..33
Figure 4.4 Cross section 2……..33
Figure 4.5 Normal PDF of corrected SPT blowcount from Hotel Sapanca…...……35
Figure 4.6 Normal PDF of fines content from Hotel Sapanca…….……..35
Figure 4.7 Normal PDF of equivalent clean sand SPT blowcount from Hotel Sapanca...36
Figure 4.8 Correlation matrix used for probabilistic infinite slope analysis……..37
Figure 4.9 Lognormal PDF of Liquefied Shear Strength from Hotel Sapanca…….38
Figure 4.10 Correlation matrix used for reliability analyses…….....39
Figure 4.11 Reliability computations of Hotel Sapanca case using mean value of $(N_1)_{60\text{-}cs}$……...……41
Figure 4.12 Lognormal PDF of factor of safety for the Hotel Sapanca failure…….42
Figure 4.13 Reliability computations of Hotel Sapanca case using minimum value of $(N_1)_{60\text{-}cs}$……...43
Figure 4.14 Lognormal PDF of Liquefied Shear Strength from Cark Canal…….45
Figure 4.15 Lognormal PDF of Liquefied Shear Strength from Cumruhiyet Avenue…..45
Figure 4.16 Lognormal PDF of Liquefied Shear Strength from Degirmendere Nose..….46
Figure 4.17 Lognormal PDF of Liquefied Shear Strength from Esme Nose…….46
Figure 4.18 Lognormal PDF of Liquefied Shear Strength from Police Station……....47
Figure 4.19 Normal PDF of Liquefied Shear Strength from Seyman Tea Garden……...47
Figure 4.20 Lognormal PDF of Liquefied Shear Strength from Soccer Field……...…....48
Figure 4.21 Lognormal PDF of Liquefied Shear Strength from Yakin Street……...48
Figure 4.22 Normal PDF of Liquefied Shear Strength from Yalova Harbor……....49
Figure 4.23 Normal CDF of reliability index using mean values of $(N_1)_{60\text{-}cs}$.....51

Figure 4.24 Relationship between reliability index, β, and probability of failure, *Pf*.....52
Figure 4.25 Lognormal PDF of factor of safety for the Cark Canal failure……..53
Figure 4.26 Lognormal PDF of factor of safety for the Cumruhiyet Avenue failure..…..53
Figure 4.27 Lognormal PDF of factor of safety for the Degirmendere Nose failure……54
Figure 4.28 Lognormal PDF of factor of safety for the Esme Nose failure……..…54
Figure 4.29 Lognormal PDF of factor of safety for the Police Station failure……..55
Figure 4.30 Lognormal PDF of factor of safety for the Seymen Tea Garden failure……55
Figure 4.31 Lognormal PDF of factor of safety for the Soccer Field failure…..……..56
Figure 4.32 Lognormal PDF of factor of safety for the Yakin Street failure……56
Figure 4.33 Lognormal PDF of factor of safety for the Yalova Harbor failure…….57
Figure 4.34 Probability of failure from FORM analyses versus probability of failure from Monte Carlo Simulation…….58
Figure 4.35 Normal CDF of reliability index using minimum values of $(N_1)_{60\text{-}cs}$…….60
Figure 4.36 Comparison of data from this study and previous data from Seed and Harder (1990)…….61
Figure A.1 Photograph of Cark Canal site……...……..75
Figure A.2 Cross section of Cark Canal site……..75
Figure A.3 Cross section of Cumruhiyet Avenue site……...78
Figure A.4 Photograph of Degirmendere Nose before the 1999 Kocaeli earthquake…...81
Figure A.5 Photograph of Degirmendere Nose after the 1999 Kocaeli earthquake……..81
Figure A.6 Bathymetry map of Degirmendere Nose site……..82
Figure A.7 Coastal failure and local geology at Degirmendere Nose site…….82
Figure A.8 Cross section I-I of Degirmendere Nose site……...83
Figure A.9 Pre and post earthquake geometry of Degirmendere Nose site……...83
Figure A. 10 Coastal failure and local geology at Esme Nose site……86
Figure A.11 Locations of SPT and CPT at Esme Nose site……...86
Figure A.12 Post earthquake shoreline at Esme Nose site…….87
Figure A.13 Aerial photograph of Hotel Sapanca…….90
Figure A.14 Ground cracking at Hotel Sapanca site after the 1999 Kocaeli earthquake..91
Figure A.15 Hotel Sapanca site map……..91
Figure A.16 Ground deformation map of the Hotel Sapanca site……..92

Figure A.17a-d Cross sections of Hotel Sapanca site……92
Figure A.18a Police Station site map……95
Figure A.18b-c Cross sections of Police Station site……95
Figure A. 19 Aerial photograph taken after the 1999 Kocaeli earthquake……98
Figure A.20 Liquefaction location at Seymen Tea Garden site……99
Figure A.21 Soccer Field site map……...101
Figure A.22a-b Cross sections of Soccer Field site……101
Figure A.23 Yakin Street site map……...104
Figure A.24 Yalova Harbor site map……...107
Figure A.25 Cross Section of Yalova Harbor site……...…108
Figure A.26 Ground Cracking at Yalova Harbor site……..108
Figure B.1 Reliability computations of Cark Canal case using mean value of $(N_1)_{60\text{-}cs}$…….....…113
Figure B.2 Reliability computations of Cumruhiyet Avenue case using mean value of $(N_1)_{60\text{-}cs}$…….……....114
Figure B.3 Reliability computations of Degirmendere Nose case using mean value of $(N_1)_{60\text{-}cs}$…….115
Figure B.4 Reliability computations of Esme Nose case using mean value of $(N_1)_{60\text{-}cs}$……..……...116
Figure B.5 Reliability computations of Police Station case using mean value of $(N_1)_{60\text{-}cs}$……...…..117
Figure B.6 Reliability computations of Seymen Tea Garden case using mean value of $(N_1)_{60\text{-}cs}$…….……118
Figure B.7 Reliability computations of Soccer Field case using mean value of $(N_1)_{60\text{-}cs}$…….119
Figure B.8 Reliability computations of Yakin Street case using mean value of $(N_1)_{60\text{-}cs}$…….120
Figure B.9 Reliability computations of Yalova Harbor case using mean value of $(N_1)_{60\text{-}cs}$…….121
Figure B.10 Reliability computations of Cark Canal case using minimum value of $(N_1)_{60\text{-}cs}$……...……..122

Figure B.11 Reliability computations of Cumruhiyet Avenue case using minimum value of $(N_1)_{60\text{-}cs}$…….123
Figure B.12 Reliability computations of Degirmendere Nose case using minimum value of $(N_1)_{60\text{-}cs}$…….124
Figure B.13 Reliability computations of Esme Nose case using minimum value of $(N_1)_{60\text{-}cs}$…….125
Figure B.14 Reliability computations of Police Station case using minimum value of $(N_1)_{60\text{-}cs}$…….126
Figure B.15 Reliability computations of Seymen Tea Garden case using minimum value of $(N_1)_{60\text{-}cs}$…….127
Figure B.16 Reliability computations of Soccer Field case using minimum value of $(N_1)_{60\text{-}cs}$…….128
Figure B.17 Reliability computations of Yakin Street case using minimum value of $(N_1)_{60\text{-}cs}$…….129
Figure B.18 Reliability computations of Yalova Harbor case using minimum value of $(N_1)_{60\text{-}cs}$…….130

LIST OF TABLES

Table 1.1 Case histories database……6
Table 2.1 Coefficient of variation of soil parameters……19
Table 2.2 COV for dry and moist unit weights of soils…….20
Table 2.3 COV for buoyant unit weight……20
Table 4.1 Location of case histories……..30
Table 4.2 Normal PDF parameters for Hotel Sapanca……..34
Table 4.3 Parameters used in the analyses…….44
Table 4.4 Summary of the probabilistic slope stability analyses.……..49
Table 4.5 Summary of the reliability computations using mean values of $(N_1)_{60\text{-}cs}$……...50
Table 4.6 Comparison of probability of failure from FORM and Monte Carlo Simulation……..58
Table 4.7 Summary of the reliability computations using minimum values of $(N_1)_{60\text{-}cs}$……...59

CHAPTER 1

INTRODUCTION

1.1 INTRODUCTION TO THE PROBLEMS

When earthquakes occur, the resulting death and destruction can be widespread and unforgiving. Liquefaction, a phenomenon where loose soil deposits lose considerable shear strength during earthquakes, is considered to be one of the primary causes of earthquake-related damage. Common examples of liquefaction-induced damage include, tilting or overturning of buildings, flow failure of steeply sloping ground such as dams and lateral spreading of softly to moderately sloping ground. While liquefaction is typically observed during earthquakes the condition can also occur under static loading such as placement of an additional lift during construction. Figure 1.1 illustrates types of failure induced by liquefaction of cohesionless soils. Limited deformation (non-flow) failure is associated with lateral spreading case, while unlimited deformation (flow) failure is associated with flow liquefaction case.

When structures are constructed atop or of liquefiable materials the consequences can be disastrous. During the 1964 Niigata earthquake numerous buildings experienced failure as a result of liquefied foundation soils. Figure 1.2 shows a photograph of the Kawagashi-Cho Apartments taken after the 1964 Niigata earthquake. During the 1971 San Fernando earthquake, failure of the Lower San Fernando Dam nearly released a large body of water from a reservoir into San Fernando, near Los Angeles, California. Figure 1.3 is a photograph of the dam following the earthquake; the reservoir level immediately following the quake came within 4-feet of the dam crest. If the dam had been overtopped, numerous lives would have been lost and thousands of homes and buildings destroyed. This potential catastrophic disaster from liquefaction brought attention from many

researchers (Seed et al., 1973; Castro et al., 1985; Seed, 1987; Davis et al., 1988; Castro et al., 1989; Seed et al., 1989; Vasquez-Herrera and Dobry, 1989; Seed and Harder, 1990; Castro et al., 1992; Stark and Mesri, 1992; Gu et al. 1993; Konrad and Watts, 1995; Baziar and Dobry, 1995; Wride et al., 1999; Olson and Stark, 2002, 2003; Ming and Li, 2003).

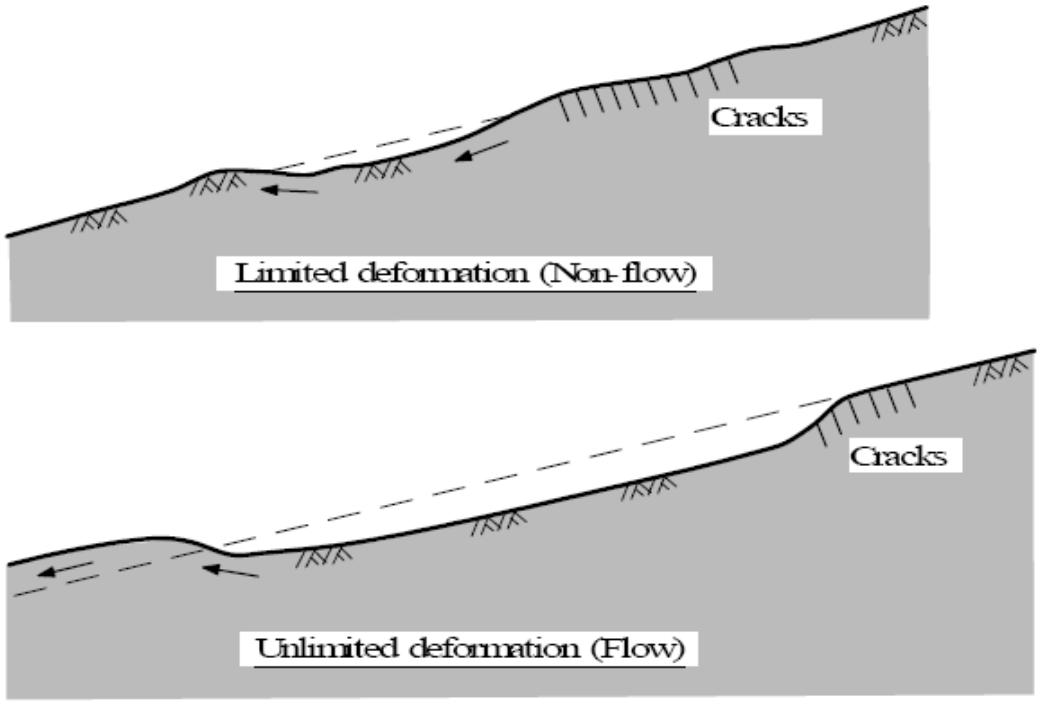

Figure 1.1 Types of failure induced by liquefaction of cohesionless soils (Ishihara, 2002)

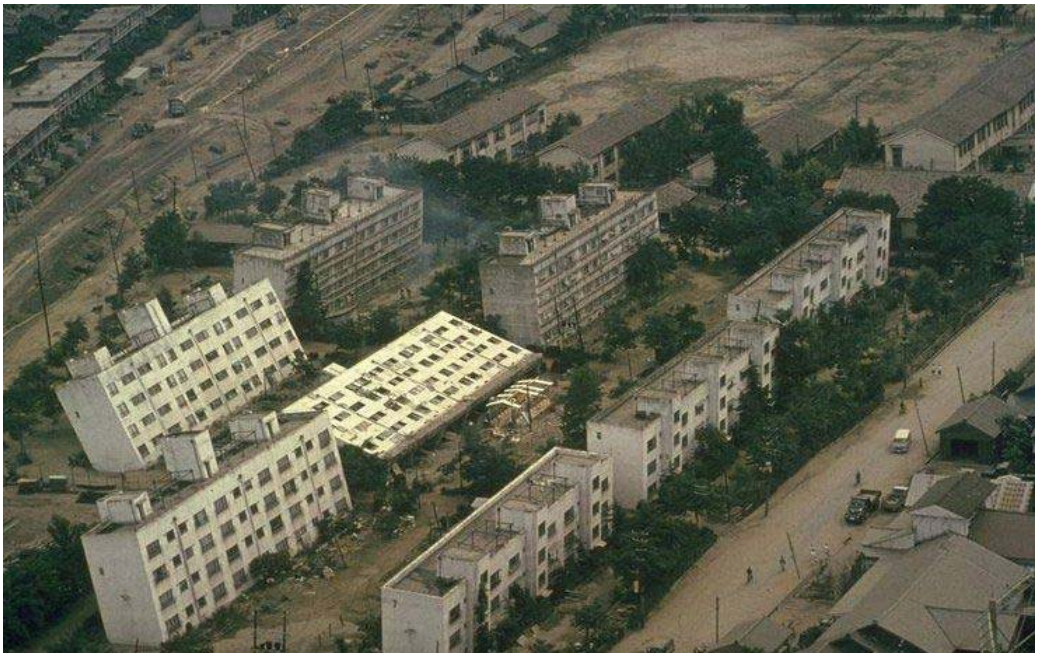

Figure 1.2 Photograph of the Kawagashi-Cho Apartments following the 1964 Niigata earthquake in Japan (www.ngdc.noaa.gov).

Figure 1.3 Photograph of the Lower San Fernando Dam flow failure after the 1971 San Fernando earthquake near Los Angeles, California (www.cee.engr.ucdavis.edu).

The residual shear strength is the main factor determining whether a soil mass will experience flow failure of large deformations due to earthquake loading. The cost and extent of remedial measures required to mitigate the liquefaction of soils deposits are, therefore, greatly influenced by the magnitude of the residual shear strength. As pointed out by Seed (1987), it may be adequate and economically advantageous simply to ensure the stability of an earth deposit or structure against post-liquefaction failure after the strength loss has been triggered than to prevent the triggering itself. The use of residual shear strength provides a very simple and attractive method to assess liquefaction potential. Since the residual shear strength should correspond to the minimum shear strength, its use predicts the worst-case scenario. Another advantage of using the residual shear strength in analysis and design is that the residual shear strength can be used to determine the post-liquefaction stability of both level and sloping grounds.

There are currently two methods for estimating the residual strength of soil deposits. One method is the case histories approach where the residual shear strength is back calculated from case histories of soil zones where Standard Penetration Tests (SPT) results were available. The other approach for determining the residual shear strength is the laboratory procedure.

Figure 1.4 developed by Seed and Harder (1990) is the commonly used chart to estimate residual shear strength based on Standard Penetration Tests (SPT). Several other researchers have developed similar charts including analysis of additional failures from recent earthquakes for estimating the residual shear strength or liquefied shear strength. The shear strengths are then used to assess structural stability and deformations with various techniques such as limit equilibrium, finite difference, and finite element analyses.

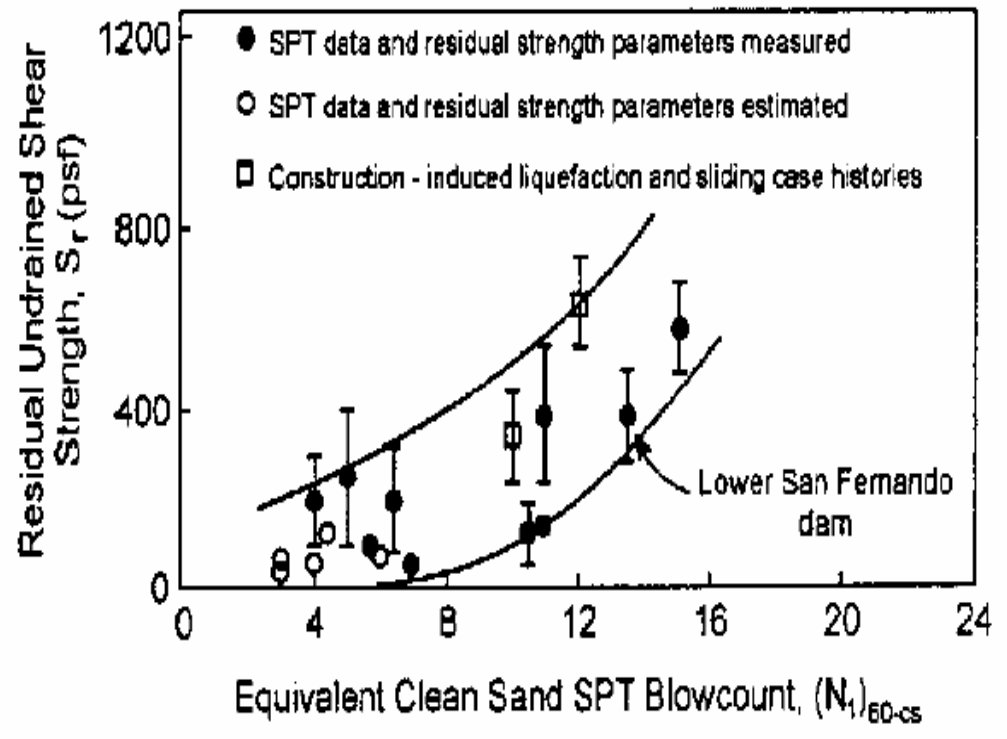

Figure 1.4 Relationship between corrected clean sand blowcount $(N_1)_{60\text{-}cs}$ and undrained residual strength (S_r) (Seed and Harder, 1990)

The Seed and Harder (1990) relationship is based on work previously performed by Dr. H. B. Seed (1987). The earlier relationship by Dr. H. B. Seed (1987) contains 12 case histories. Seed and Harder (1990) adds five new case histories to the relationship. The relationship is based on 10 field cases where SPT and residual strength measurements were available and five cases where the data were estimated. In addition to data from earthquake-induced liquefaction, data estimated from two cases of construction-induced liquefaction were included in the data set. Table 1.1 contains case histories presented by Seed and Harder (1990).

Table 1.1 Case histories database (modified from Seed and Harder, 1990)

Structure or Earth Structure	Apparent Cause of Sliding
Calaveras Dam	1918 Construction
Sheffield Dam	1925 Santa Barbara Earthquake (M=6.3)
Fort Peck Dam	1938 Construction
Solfatara Canal Dike	1940 El Centro Earthquake (M=7.2)
Lake Merced Bank	1957 San Fransisco Earthquake (M=5.7)
Kawagishi-Cho Building	1964 Niigata Earthquake (M=7.5)
Uetsu Railway Embankment	1964 Niigata Earthquake (M=7.5)
Snow River Bridge Fill	1964 Alaskan Earthquake (M=8.5)
Koda Numa Railway Embankment	1968 Tokachi-Oki Earthquake (M=7.9)
San Fernando Juvenile Hall	1971 San Fernando Earthquake (M=6.6)
Lower San Fernando Dam	1971 San Fernando Earthquake (M=6.6)
Upper San Fernando Dam	1971 San Fernando Earthquake (M=6.6)
Mochi-Koshi Tailings	1978 Izu-Oshima Earthquake (M=7.0)
Whiskey Springs Fan	1983 Borah Peak Earthquake (M=7.3)
La Marquesa Dam - U/S Slope	1985 Chilean Earthquake (M=7.8)
La Marquesa Dam - D/S Slope	1985 Chilean Earthquake (M=7.8)
La Palma Dam	1985 Chilean Earthquake (M=7.8)

Stark and Mesri (1992) presented a normalized approach where the residual shear strength of liquefied soils is normalized with respect to the initial effective vertical stress σ'_{vo} (Figure 1.5). The residual shear strengths were determined in a similar fashion as was done by Seed and Harder (1990), while the initial effective vertical stresses were estimated from the average value over the thickness of the liquefied layer. The advantage of a normalized approach is that the stress dependency of the residual shear strength can be incorporated in a post-liquefaction stability analyses. The normalized approach allows for the stability of the upstream and downstream slopes of existing slopes by allowing the shear strength to vary with effective stress level along the potential failure surface. Stark and Mesri (1990) proposed average, upper, and lower bound values of the normalized residual shear strength based on 20 case histories. Recently, Olson and Stark (2002) have

expanded the post-liquefaction database to include 33 case histories. Data from Olson and Stark (2002) are shown in Figure 1.6.

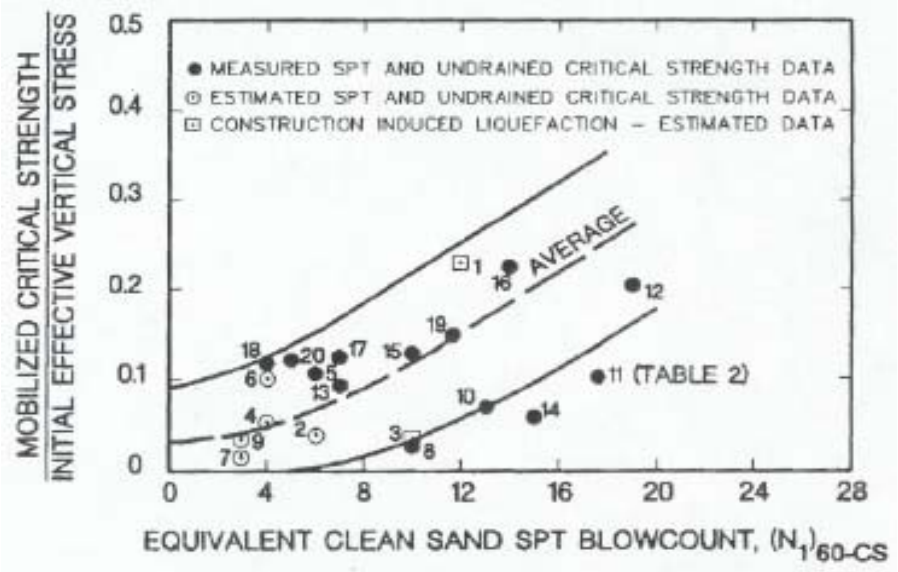

Figure 1.5 Relationship between SPT blowcount and normalized residual shear strength from case histories (Stark and Mesri, 1992)

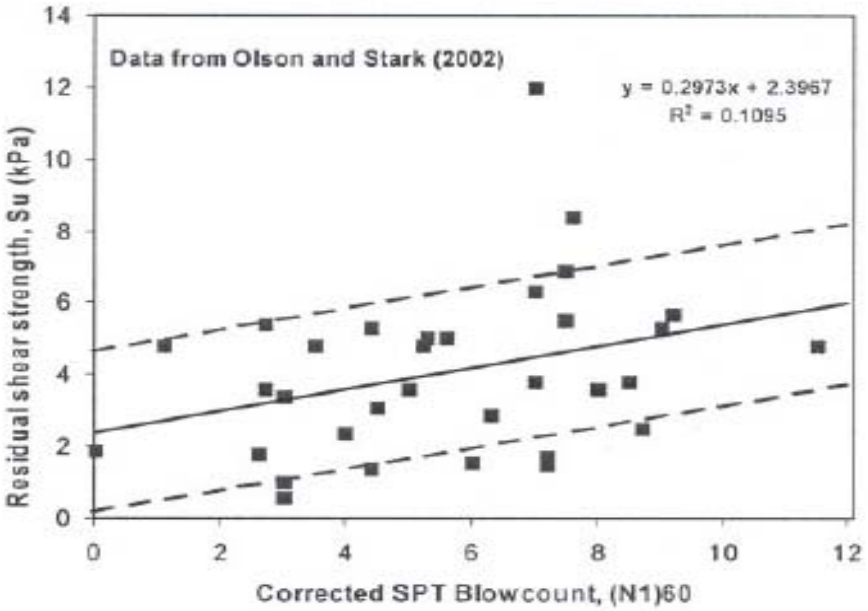

Figure 1.6 SPT blowcount versus residual shear strength from flow liquefaction case histories (data from Olson and Stark, 2002)

The liquefied shear strengths in Figure 1.4, Figure 1.5 and Figure 1.6 are based on the back-analysis of failures, where liquefaction was the apparent cause of failure, and SPT data or other in-situ data was available. The various studies have made great strides towards understanding liquefaction behavior based on the analysis of past failures, however, all procedures up to this point have been based on deterministic methods. Figure 1.4 illustrates how much uncertainty is involved in using such relationships; for example, the liquefied shear strength for a soil with a SPT blowcount of 8 ranges from 50 to 400 psf. The results of limit equilibrium and finite element analyses are highly dependent upon the selected value of liquefied shear strength. By using the lower bound shear strength the cost of structures may unnecessarily be increased through over-conservative designs; on the other hand the upper bound strength may result in unconservative designs leading to unwanted failures. It can also be seen from Figure 1.4 that very few data are available to estimate the residual undrained shear strength from in situ test.

1.2 LIQUEFACTION

For many years, soil liquefaction has been a major concern for geotechnical engineers, especially for designing structures with or on cohesionless soils. The phenomenon has been recognized for many years. Casagrande (1936) gave a brief explanation of early work in soil liquefaction analysis. The Niigata and Alaska earthquakes in 1964 are certainly the events that focused world attention on the phenomenon of soil liquefaction. Since 1964, much work has been carried out to explain and understand soil liquefaction. The progress of work on soil liquefaction has been described in detail in a series of state-of-the-art papers (e.g., Seed, 1979; Finn, 1981, 1991; Ishihara, 1993; and Robertson and Fear, 1995).

Figure 1.7 Building collapsed following soil liquefaction
after 1964 Alaska Earthquake (www.apsn.awcable.com)

Soil liquefaction is commonly associated with large earthquakes. The major earthquakes of Niigata in 1964, Alaska in 1964, Kobe in 1995, and Kocaeli/Duzce in 1999 have illustrated the significance and extent of damage caused by soil liquefaction. Numerous buildings and bridges collapsed are triggered by liquefaction events. Liquefaction was the cause of much of the damage to the port facilities in Kobe in 1995 (Figure 1.8). Soil liquefaction is also a major design program for large sand structures such as mine tailings impoundments and earth dams.

Figure 1.8 Crane collapsed in Kobe Harbor following soil liquefaction after 1995 Kobe earthquake (www.geoinfo.usc.edu)

1.2.1 Terminology

For many years, there are disagreements between experts about the terminology used to describe the liquefaction phenomenon. Casagrande (1975) pointed out that the reasons of these disagreements were: (1) they looked at different aspects of the same problem; (2) they generalized too much on the basis of different aspects of the same problem; and (3) they used the same terminology for different phenomenon. The terminologies used in this study are based on that suggested by Casagrande (1975), Robertson (1994), and Kramer (1996).

1.2.1.1 Flow Liquefaction

Flow liquefaction is the strain softening response of loose saturated cohesionless soils during undrained shear. This phenomenon can be triggered by monotonic or cyclic

loading, as shown in Figure 1.9 (Kramer, 1996). Flow liquefaction requires that the in-situ shear stress is greater than the undrained residual shear strength or undrained liquefied shear strength. Flow liquefaction can cause a failure of a dam, embankment or slope. An example of a flow failure induced by seismic loading is the Lower San Fernando Dam (Seed et al., 1973; Castro et al., 1989; Seed et al., 1989, Vasquez-Herrera and Dobry, 1989).

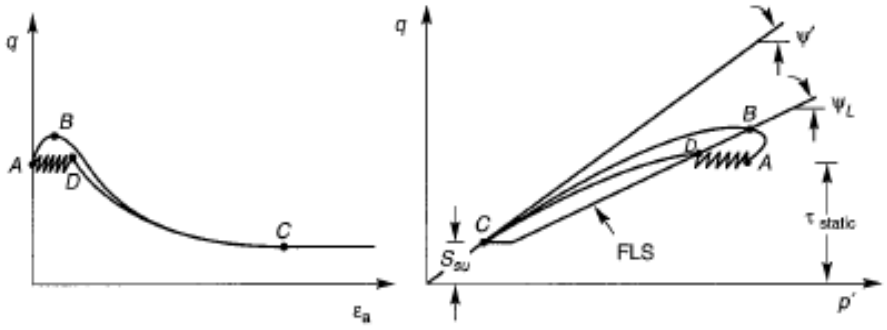

Figure 1.9 Initiation of flow liquefaction by cyclic and monotonic loading. Although the stress conditions at the initiation of liquefaction are different for the two types of loading (points B and D), both lie on the flow liquefaction surface (FLS) (Kramer, 1996)

1.2.1.2 Cyclic Mobility

Cyclic mobility is a liquefaction phenomenon, triggered by cyclic loading, occurring in soil deposits with static shear stresses lower than the soil strength. Deformations due to cyclic mobility develop incrementally because of static and dynamic stresses that exist during seismic or cyclic loading, as shown in Figure 1.10 (Kramer, 1996). In contrast to flow liquefaction, the static shear stress in cases of cyclic mobility is less than the undrained liquefied shear strength of the soil. Robertson (1994) pointed out that cyclic mobility can occur in almost any sand provided size and duration of cyclic loading is sufficiently large and no stress reversal occurs, and also can occur in dense

sand with shear stress reversal provided cyclic loading is not sufficient to cause zero effective stress to develop.

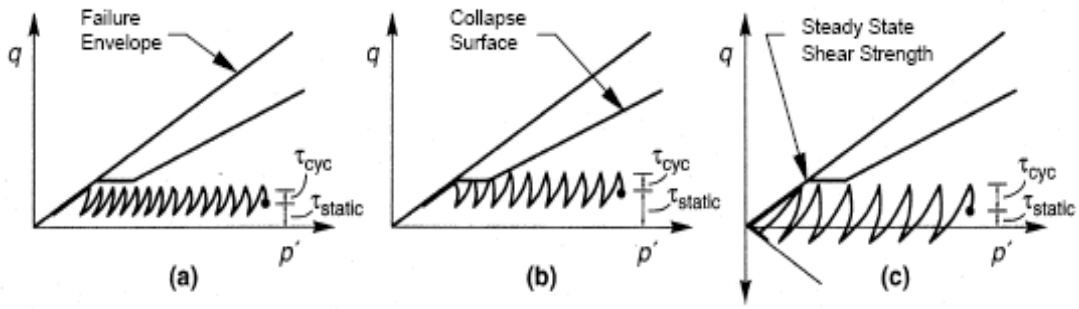

Figure 1.10 Three cases of cyclic mobility shown in stress path space: (a) no stress reversal and combined static and cyclic shear stress less than the steady state strength; (b) no stress reversal and momentary periods where combined static and cyclic shear stresses exceed the steady state strength; and (c) stress reversal and combined static and cyclic shear stresses less than the steady state strength (Kramer, 1996).

Lateral spreading, a common result of cyclic mobility, can occur on gently slope and on flat ground close to rivers and lakes. An example of lateral spreading induced by seismic loading is the Moss Landing liquefaction during the 1989 Loma Prieta earthquake (Boulanger et al., 1997).

1.3 OBJECTIVES AND METHODOLOGY OF THE STUDY

This research study aims to develop probabilistic procedures for analyzing the post-liquefaction stability of future and existing structures constructed of or atop liquefiable soils. The results of this study should help practicing engineers to select appropriate liquefied shear strengths within a risk-based framework. This research study also aims to quantify uncertainties associated with the post-liquefaction residual shear strength of cohesionless soil deposits also termed the liquefied shear strength. By accounting for the variability involved in the stability computations of liquefiable soils,

engineers will be able to make better decisions when designing structures to resist the devastating effects of earthquakes.

The study will quantify the uncertainties involved in available case histories of liquefaction failure using probabilistic techniques and to provide improved procedures for estimating the liquefied shear strength of susceptible soil deposits. Reliability-based stability procedures have been developed to perform back-analysis of the various failures using a spreadsheet.

Liquefaction case histories from the 1999 Kocaeli/Duzce, Turkey earthquake are analyzed to illustrate the use of the reliability based procedure. The Ishihara et al. (1990) slope stability method is employed to back-calculate flow failure case histories. This study is utilized the Seed and Harder (1990) undrained shear strength versus equivalent clean sand SPT blowcount $(S_{us}\text{-}(N_1)_{60\text{-}CS})$ relationship. The computations are performed with Microsoft Excel and @Risk computer programs. The probabilistic back analysis is performed with Monte Carlo Simulations (MCS). The First Order Reliability Method (FORM) as presented by Low and Tang (2004) is implemented into the previously described stability analyses. FORM provides a measurement of the uncertainty involved in the liquefied shear strength by modeling material properties and geometric parameters with probabilistic distributions rather than deterministic values. The MCS is performed to verify the reliability computations with FORM. Lastly, the data from this study are compared with the previous data from Seed and Harder (1990).

1.4 ORGANIZATION AND SCOPE

This thesis is organized as follows. Chapter 2 describes the concept of probability/reliability methods for slope stability analysis. Chapter 3 presents the information from the 1999 Kocaeli/Duzce, Turkey earthquake. Chapter 4 presents the back analyses of the case histories. Lastly, conclusions are presented in Chapter 5.

CHAPTER 2
PROBABILITY/RELIABILITY METHODS FOR SLOPE STABILITY ANALYSIS

2.1 INTRODUCTION TO SLOPE STABILITY ANALYSIS

The evolution of slope stability analyses in geotechnical engineering has followed closely the developments in soil and rock mechanics as a whole. Slopes either occur naturally or are engineered by humans. The increasing demand for engineered cut and fill slopes on construction projects has only increased the need to understand analytical methods, investigative tools, and stabilization methods to solve stability problems. Slope stabilization methods involve specialty construction techniques that must be understood and modeled in realistic ways.

An understanding of geology, hydrology, and soil properties is central to applying slope stability principles properly. Analyses must be based upon a model that accurately represents site subsurface conditions, ground behavior, and applied loads. Judgments regarding acceptable risk or safety factors must be made to assess the result of analyses (Whitman, 1984).

2.2 LIMIT EQUILIBRIUM METHOD

The geotechnical engineer frequently uses limit equilibrium methods of analysis when studying slope stability problems. The method can be approached with single free-body procedures or method of slices. Duncan and Wright (2005) include infinite slope, logarithmic spiral, and Swedish slip circle methods as single free-body procedures.

The methods of slices have become the most common methods due to their ability to accommodate complex geometries and variable soil and water pressure conditions. Some methods of slices accommodate circular slip surfaces, while others accommodate noncircular slip surfaces. There are several commonly used methods, including:

- Ordinary Method of Slices (Fellenius, 1927)
- Janbu's Simplified Method (Janbu, 1954)
- Janbu's Generalized Method (Janbu, 1954)
- Bishop's Simplified Method (Bishop, 1955)
- Bishop's Rigorous Method (Bishop, 1955)
- Lowe and Karafiath's Method (Lowe and Karafiath, 1960)
- Morgenstern-Price Method (Morgenstern and Price, 1965)
- Spencer's Method (Spencer, 1967)
- Sarma's Method (Sarma, 1973)
- Corps of Engineer's Method (1982)

Duncan (1992) showed stability methods that satisfy all conditions of equilibrium (horizontal and vertical force equilibrium and moment equilibrium) result in a factor of safety with an accuracy of ±5 percent. As a result, stability methods that satisfy all conditions of equilibrium can be considered to yield an accurate estimate of the factor of safety.

2.3 THE ISHIHARA ET AL. SIMPLIFIED METHOD (1990)

Ishihara et al. (1990a) and Ishihara et al. (1990b) proposed an infinite slope stability analysis particularly suited to slopes which failed by flow liquefaction. This method was utilized to analyze four failure case histories in Japan: Mochikoshi Tailings Dam (1978), Hokkaido Tailings Dam (1968), Metoki Road Embankment (1968), and Chonan Sand Fills (1987) which failed following an earthquake. All of the case histories

were flow failure cases. The method was also utilized to analyze case histories of flow slide in the collapsible loess deposit in Soviet Tajik following 1989 earthquake.

The Ishihara et al. simplified method (1990) is appropriate when the failure mass is very large in lateral extent as compared the depth to the failure surface. The simplified method is slightly modified to account for the depth to the water table. Figure 2.1 shows the assumed free body diagram of the failed soil mass; it is assumed that the side forces are equal in magnitude and opposite in direction and the ground surface is parallel to the failure surface. The water table is assumed to be parallel to the ground/failure surface.

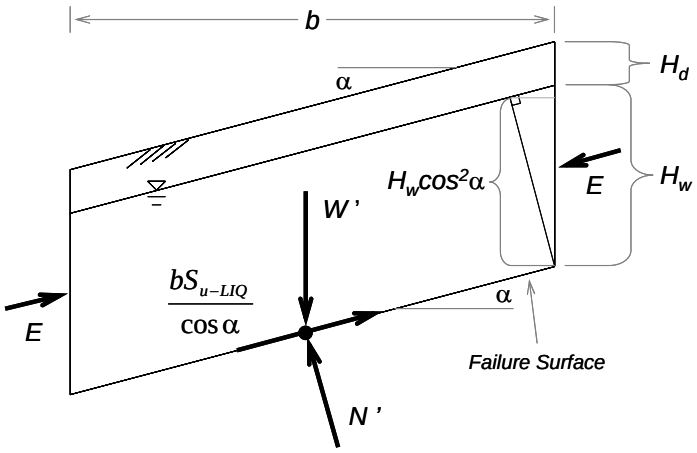

Figure 2.1 Simplified slope stability analysis (after Ishihara et al., 1990a)

Factor of safety, *FS*, is given by Equation 2.1. Expressions used to compute the liquefied shear strength with the simplified method, are shown in Equation 2.2 and Equation 2.3. Equation 2.1 and Equation 2.2 are derived through equilibrium of forces analysis along the failure surface.

$$FS = \frac{S_{u-LIQ}}{(W')\sin\alpha\cos\alpha} \tag{2.1}$$

$$S_{u-LIQ} = FS(W')\sin\alpha\cos\alpha \tag{2.2}$$

Where $S_{u\text{-}LIQ}$ is the liquefied shear strength, FS is factor of safety, α is the angle of the ground/failure surface and W' is the effective weight of the soil above the failure surface, defined as:

$$W' = H_d \gamma_d + H_w \gamma_{sat} - H_w \gamma_w \cos^2 \alpha \qquad (2.3)$$

H_d is the depth to the water table, H_w is the height of the water table above the failure surface, γ_d is the dry unit weight of the soil above the water table, γ_{sat} is the saturated unit weight of the soil above the failure surface, and γ_w is the unit weight of water.

2.4 INTRODUCTION TO RELIABILITY METHODS FOR SLOPE STABILITY ANALYSIS

Geotechnical engineers deal with uncertainties by recognizing that risk and uncertainty are inevitable and by applying the observational method. However, the observational method is applicable only when the design can be changed during construction on the basis of observed behavior. In those cases in which the critical behavior cannot be observed until too late to make changes, the designer must rely on a calculated risk. Recently, several studies of risk analysis for slopes and embankment have been conducted.

Slope stability analysis involves several uncertainties, including computational accuracy, soil unit weight, slope geometry, pore-water pressures, and soil shear strength. These uncertainties are the reasons for a lack of confidence in deterministic analyses (Alonso, 1976). Extensive research has been conducted to evaluate the computational accuracy of two-dimensional limit equilibrium slope stability methods.

Because the uncertainty in computational accuracy is small for methods that satisfy all conditions of equilibrium, it is necessary to consider possible uncertainties in the other previously mentioned parameters. Soil unit weight can be readily measured in the laboratory, slope geometry can be ascertained via elevation surveys and subsurface

techniques, and pore-water pressures can be estimated from boreholes and or/ piezometer installations. However, a large source of uncertainty can be introduced during the selection of the soil shear strength parameters.

2.5 VARIABILITY OF SOIL PARAMETERS

As a natural material, soil contains a large source of uncertainty of soil parameters. Soil parameters are usually measured in the laboratory using special apparatus. Accuracy of the apparatus and human error during the measurement add more uncertainty to measure soil parameters. Figure 2.2 demonstrates one concept of the source of uncertainty in soil parameters (Christian et al., 1994). Systematic error can result from statistical error in mean values arising from limited numbers of measurements, as well as from bias in measurement procedures. Data scatter, on the other hand, includes nonsystematic (random) testing errors and actual spatial variation in the soil profile.

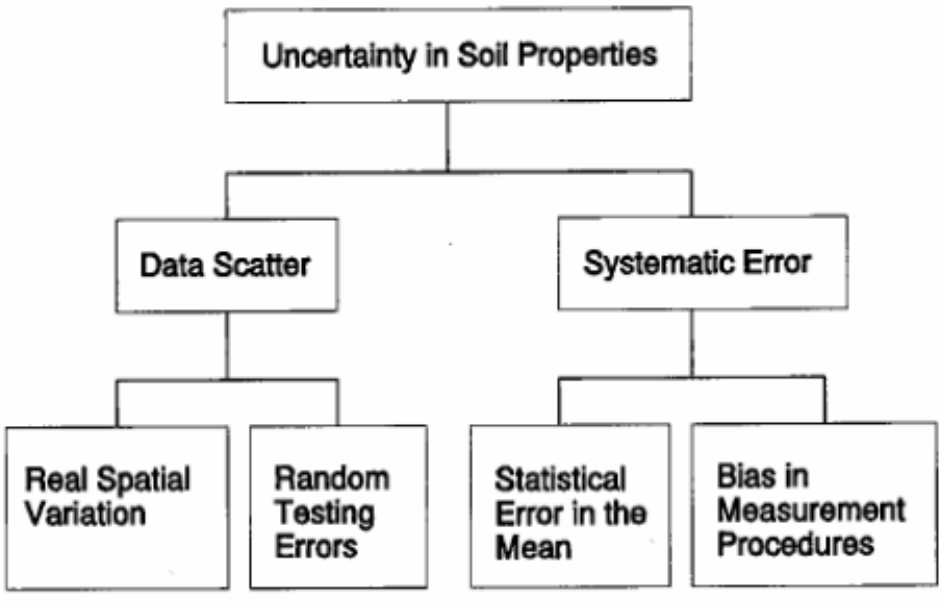

Figure 2.2 Uncertainty in soil properties (from Christian et al., 1994)

Several researchers have collected coefficient of variations of commonly used soil parameters (Chowdhury, 1984; Harr, 1987; Kulhawy, 1992; Lacasse and Nadim, 1997; Duncan, 2000). Table 2.1 presents data of coefficient of variation of soil parameters as summarized by Duncan (2000). Table 2.2 and Table 2.3 present data of coefficient of variation of dry, moist, and buoyant unit weight of soils from recent study (Gutierrez et. al., 2003).

Table 2.1 Coefficient of variation of soil parameters (Duncan, 2000)

Property or in situ test result (1)	Coefficient of variation —V (%) (2)	Source (3)
Unit weight (γ)	3–7%	Harr (1984), Kulhawy (1992)
Buoyant unit weight (γ_b)	0–10%	Lacasse and Nadim (1997), Duncan (2000)[a]
Effective stress friction angle (ϕ')	2–13%	Harr (1984), Kulhawy (1992)
Undrained shear strength (S_u)	13–40%	Harr (1984), Kulhawy (1992), Lacasse and Nadim (1997), Duncan (2000)[a]
Undrained strength ratio (S_u/σ'_v)	5–15%	Lacasse and Nadim (1997), Duncan (2000)[a]
Compression index (C_c)	10–37%	Harr (1984), Kulhawy (1992), Duncan (2000)[a]
Preconsolidation pressure (p_p)	10–35%	Harr (1984), Lacasse and Nadim (1997), Duncan (2000)[a]
Coefficient of permeability of saturated clay (k)	68–90%	Harr (1984), Duncan (2000)[a]
Coefficient of permeability of partly saturated clay (k)	130–240%	Harr (1984), Benson et al. (1999)
Coefficient of consolidation (c_v)	33–68%	Duncan (2000)[a]
Standard penetration test blow count (N)	15–45%	Harr (1984), Kulhawy (1992)
Electric cone penetration test (q_c)	5–15%	Kulhawy (1992)
Mechanical cone penetration test (q_c)	15–37%	Harr (1984), Kulhawy (1992)
Dilatometer test tip resistance (q_{DMT})	5–15%	Kulhawy (1992)
Vane shear test undrained strength (S_v)	10–20%	Kulhawy (1992)

Table 2.2 COVs for dry and moist unit weights of soils (Gutierrez et al., 2003)

Material	*COV* for γ_d	*COV* for γ_m
GP – GW	7-13%	7-9%
SM – ML	5-10%	6-12%
SP – SW	6%	9%

Table 2.3 COVs for buoyant unit weight (Gutierrez et al., 2003)

Material	Buoyant Unit Weight
GP - GW	14.0-18.0%
SM - ML	14.0-35.0%
SP - SW	20.0%

The coefficient of variation is defined in Equation 2.4:

$$COV = \frac{\sigma}{\mu} \tag{2.4}$$

Where *COV* is coefficient of variation, μ is mean value, and σ is standard deviation respectively.

2.6 METHOD OF PROBABILISTIC ANALYSIS

There are several techniques of probabilistic method that are commonly used in Geotechnical Engineering. First Order Reliability Method (FORM) and Monte Carlo Simulation are utilizing in this study. The following paragraphs describe each of these methods in more detail.

2.6.1 First Order Reliability Method (FORM)

The First Order Reliability Method (FORM) was introduced for the first time by Hasofer and Lind (1974). This approach is based on independent, normal variable. For other situation, it will not give correct information on the probability of failure. Several

study corrected and included information on the probability of the random variables (e.g., Rackwitz and Fiessler, 1978; Chen and Lind, 1983).

The First Order Reliability Method (FORM) is not commonly used for slope stability analyses. Low and Tang (1997a) were pioneering the use of FORM for slope stability analyses. They were conducting various studies utilizing the FORM (Low and Tang, 1997a, 1997b; Low, 2003).

In this study, the reliability of each case history is measured with the Hasofer-Lind reliability index, β (Hasofer and Lind, 1974). This study adopts a convenient spreadsheet approach proposed by Low and Tang (2004), where object-oriented constrained optimization is used to obtain a solution for reliability index, β, with Equation 2.5:

$$\beta = \min_{\underline{x} \in F} \sqrt{\left[\frac{x_i - \mu_i^N}{\sigma_i^N}\right]^T [\underline{R}]^{-1} \left[\frac{x_i - \mu_i^N}{\sigma_i^N}\right]} \qquad (2.5)$$

where $\underline{x}$ is a vector representing the random variables, F is the failure domain, $\underline{R}$ is the correlation matrix, and μ_i^N and σ_i^N are the mean and standard deviation computed from Rackwitz-Fiessler (1978) two-parameter equivalent normal transformations. By using the equivalent normal parameters, model properties with different probability distributions (i.e. normal, lognormal, uniform, beta, etc.) can easily be used in the same analysis.

2.6.2 Monte Carlo Simulation

The name ``Monte Carlo" was coined by Stanislaw Ulam and Nicholas Metropolis (Metropolis, 1987) during the Manhattan Project of World War II. Monte Carlo simulation encompasses any technique of statistical sampling employed to approximate solutions to quantitative problems. The simulation is useful for obtaining numerical solutions to problems which are too complicated to solve analytically.

The first step of the simulation is to choose an appropriate deterministic performance function. Next step is to define the input variables for the performance function and the probability distribution for each variable (e.g., beta, gamma, normal, lognormal, uniform). Monte Carlo simulation uses a pseudo random generator to select a random value for each input variable based on the corresponding probability distribution. The selected values are then used to solve the performance function. The process is repeated a large number of times to build up a statistical distribution of the performance variable.

Monte Carlo simulation has been adopted in many studies of slope stability analysis (e.g., Tobutt, 1982; Chandler, 1996; Greco, 1996; Malkawi et al., 2001). The simulation makes it possible to deal multiple input variable problems. In the context of reliability analysis, the simulation provides the distribution of factor of safety and the distribution of probability of failure.

CHAPTER 3

THE 1999 KOCAELI/DUZCE, TURKEY EARTHQUAKE

3.1 INTRODUCTION

Two destructive earthquakes hit Turkey on August 17, 1999 and November 12, 1999. The August 17, 1999 (M_W=7.4) occurred in Kocaeli, while the November 12, 1999 (M_W=7.2) occurred in Duzce. These large magnitude events affected a highly urbanized and industrialized region of Turkey. Damaging ground shaking intensities covered a 2,000 km^2 area in the provinces of Izmit and Istanbul in northwestern Turkey (USGS, 2000).

The epicenters of the earthquakes are located along the North Anatolian Fault zone (Figure 3.1). The study of the North Anatolian Fault zone shows that major earthquake sequences with faulting have been periodically occurring in the zone. The fault zone is a broad belt of crushed rocks a few kilometers wide rather than a single continuous rupture (Ambraseys, 1970). The North Anatolian Fault forms extensional bends and oversteps in the area. The blocks on both sides of the main fault follow the changing directions and adapt their margins to the deflected course (Neugebauer, 1995).

In the aftermath of the earthquake, search and rescue teams brought thousands of bodies out from the wreckage of collapsed buildings. More than 17,000 deaths have been confirmed and another 20,000 people were declared missing and presumed dead. Figure 3.2 showed the locations of earthquake casualties and injuries. The August 17, 1999 earthquake struck at three o'clock in the morning when the buildings were filled with sleeping residents (USGS, 2000).

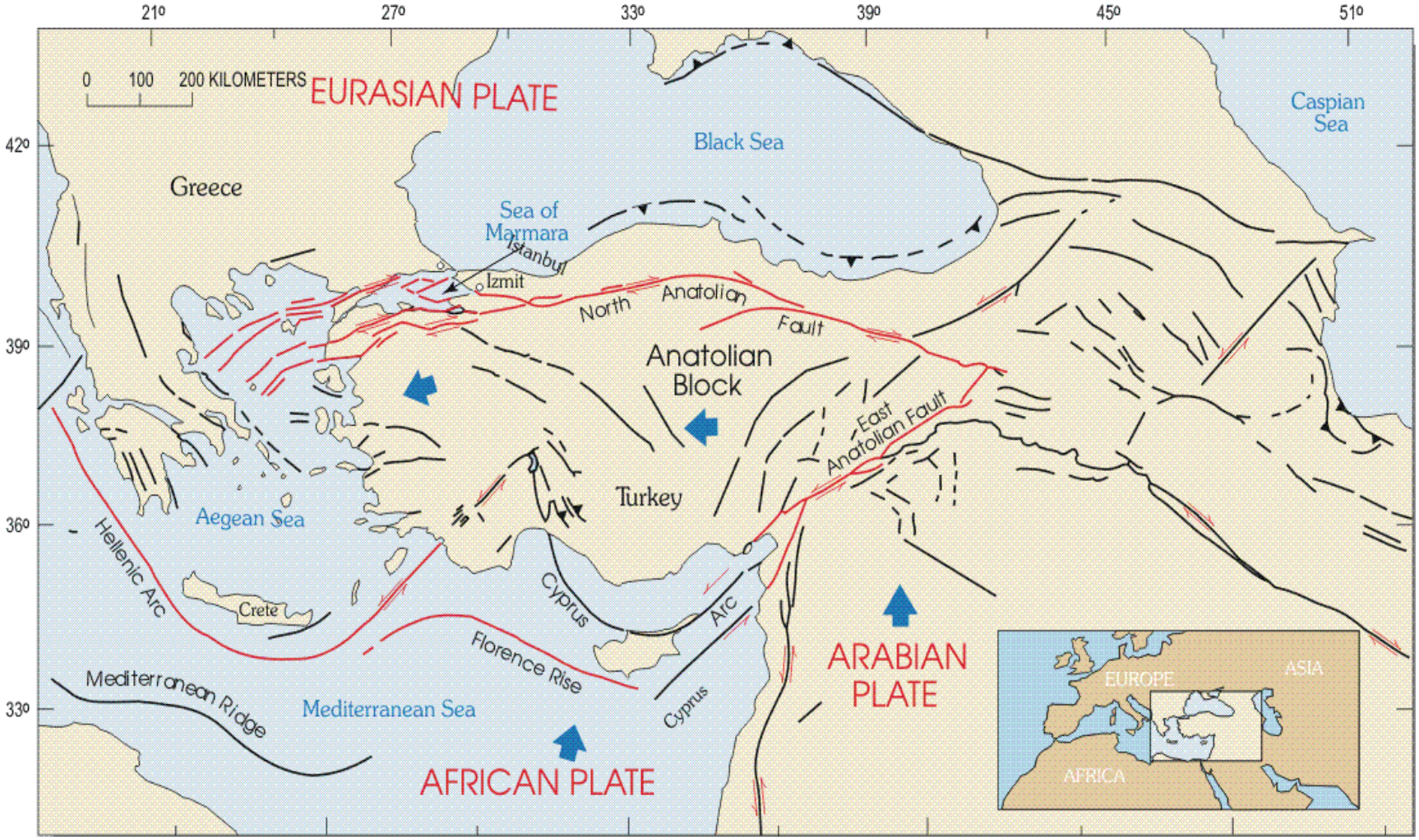

Figure 3.1 Map of active faults in Turkey (www.neis.usgs.gov)

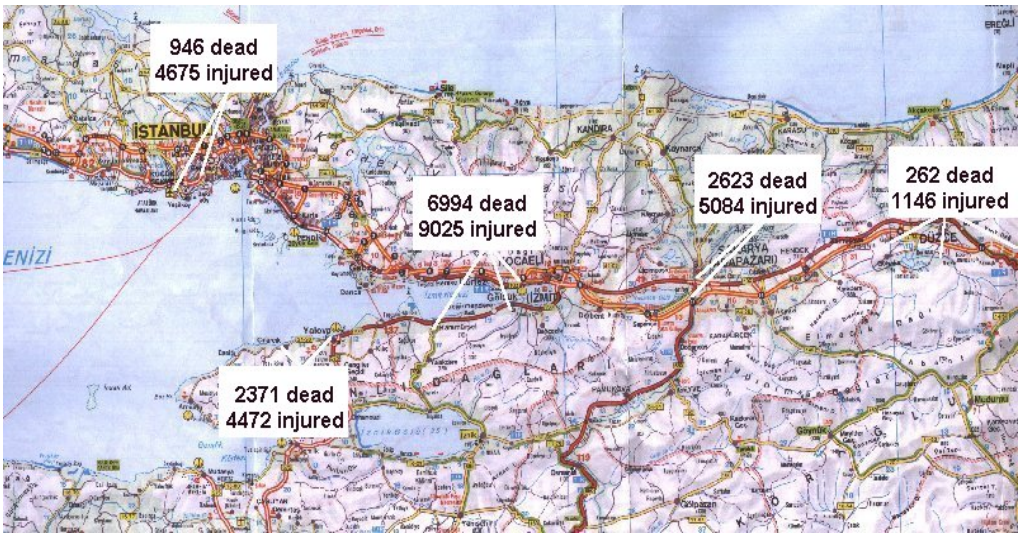

Figure 3.2 Locations of earthquakes casualties and injuries
of the 1999 Kocaeli/Duzce, Turkey earthquake (USGS, 2000)

The earthquakes caused considerable damage to residential and commercial buildings, public facilities and infrastructure. The pervasive building collapses in the earthquakes caused a substantial number of casualties. More than 120,000 housing units were heavily damaged or collapsed, leaving 400,000 to 600,000 people homeless (Erdik, 2000).

Erdik (2000) reported that the earthquake ripped through the industrial corridor of Turkey, affecting manufacturing plants and production facilities along the transportation corridor that links Istanbul with its capital, Ankara. Development in the region is concentrated in the alluvial plains between the hills and mountain ranges surrounding Izmit Bay and the Marmara Sea. Forty percent of the country's annual manufacturing production comes from this region.

The earthquake also damaged the country's largest refinery (Figure 3.3). Telecommunication facilities were severed when the fault rupture cut the main fiber optic cable that runs between Istanbul and Ankara, and damage to two substations initially interrupted power across much of northwestern Turkey. The Istanbul-Ankara motorway and the railroad also sustained heavy damage, including a collapsed overpass, which

impeded transportation into and out of the region during the first week of the disaster (Bendimerad et al., 2000).

Figure 3.3 Damaged refineries after the 1999 Kocaeli earthquake (USGS, 2000)

3.2 GEOLOGY OF TURKEY

Campbell (1971) described that Turkey's varied landscapes are the product of complex earth movements that have shaped Anatolia over thousands of years and have manifested themselves in fairly frequent earthquakes and occasional volcanic eruptions. Except for a relatively small portion of its territory along the Syrian border that is a continuation of the Arabian Platform, Turkey's geologically is part of the great Alpine belt that extends from the Atlantic Ocean to the Himalaya Mountains. This belt was formed during the Tertiary Period (about 65 million to 1.6 million B.C.) as the Arabian, African, and Indian continental plates began to collide with the Eurasian plate, and the sedimentary layers lay down by the prehistoric Tethyan Sea buckled, folded, and contorted. The intensive folding and uplifting of this mountain belt were accompanied by strong volcanic activities and intrusions of igneous rock material, followed by extensive faulting during the Quaternary Period, which began about 1.6 million B.C. These folding

and faulting processes are still at work, as the Turkish and Aegean plates, moving south and southwest, respectively, continue to collide. As a result, Turkey is one of the world's more active earthquake and volcano regions (Ambraseys, 1970). Figure 3.4 shows extension of Anatolia slab toward Hellenic-Greek slab and African plate (Doglioni et al., 2002).

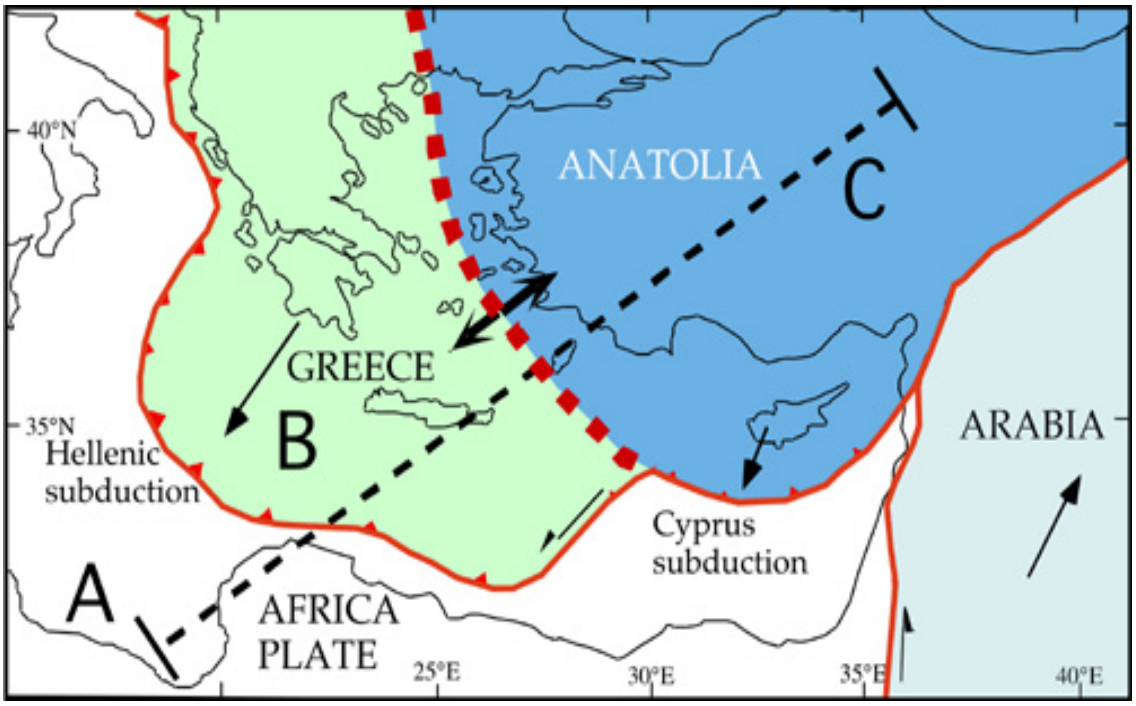

Figure 3.4 Extension movement of Anatolia slab toward Hellenic-Greek slab and African plate (Doglioni et al., 2002).

Turkey's most severe earthquake in the twentieth century occurred in Erzincan on the night of December 26, 1939; it devastated most of the city and caused an estimated 160,000 deaths. Earthquakes of moderate intensity often continue with sporadic aftershocks over periods of several days or even weeks. The most earthquake-prone part of Turkey is an arc-shaped region stretching from the general vicinity of Kocaeli to the area north of Lake Van on the border with Armenia and Georgia (Bozkurt et al., 2000).

Brinkmann (1976) described that most of Turkeys' land surface is located on the Anatolia region, a peninsula with the coast of the Black sea to the north and the

Mediterranean Sea to the west and south. This area is mountainous, composed of mostly sedimentary rocks folded and fractured during the Alpine Orogeny. The country is part of the Alpine orogenic belt, which marks the border between the African and the European plate.

3.3 GEOTECHNICAL EFFECT

Ground failure and ground deformations were significant features of the Kocaeli/Duzce earthquakes and occurred throughout much of the heavily shaken zone. Liquefaction, landslide, and subsidence cases occurred in various areas.

Erdik (2000) reported that along the southwestern shore of the Gulf of Izmit, large scale ground subsidence has occurred due to combination of vertical tectonic motion associated with pull-apart structures and landslides. Many buildings located near the surface fault were torn apart by the fault rupture and collapsed, although there were similar buildings near the fault with no apparent damage.

In Adapazari, located over young riverbed sediments with soft and liquefiable soil layer, hundred of buildings sank. Some area of the main street in Adapazari's city center was completely destroyed. Buildings punched through the soil layer that liquefied in the earthquakes, sinking by more than one meter, and often collapsing as a result (Bendimerad et al., 2000).

Liquefaction also occurred in the areas that ring Izmit bay, causing damaged to the industrial facilities around Yalova, Golcuk, and Kocaeli. Liquefaction also was the main cause of dock and port related damages in the city of Yalova (USGS, 2000).

Liquefaction, coastal subsidence, and landslide movement occurred at Esme, a small town on the north side of Sapanca Lake. Extensional cracks extended inland 140 meters from the shoreline (Erdik, 2000). The same phenomena also occurred in the city

of Degirmendere. Extensional cracks extended inland 75 meters inland, pushed a large section of coastline failed into Izmit Bay (USGS, 2000).

Bendimerad et al. (2000) reported that ground movement and landslide were observed extensively at locations in the countryside between Akyazi and Golkaya. These were observed along rural roads east of Akyazi as well as west of Golkaya.

CHAPTER 4

CASE STUDIES BACK ANALYSIS

4.1 INTRODUCTION

The Kocaeli/Duzce, Turkey earthquakes of 1999 triggered a number of flow failure cases. There are 10 cases that are analyzed in this study presented in Table 4.1.

Table 4.1 Location of case histories

Location	Reference
Cark Canal	PEER (2000)
Cumruhiyet Avenue	PEER (2000)
Degirmendere Nose	PEER (2000); Cetin et al. (2004)
Esme Nose	Rathje et al. (2004)
Hotel Sapanca	PEER (2000); Cetin et al. (2002)
Police Station	PEER (2000)
Seymen Tea Garden	Rathje et al. (2004)
Soccer Field	PEER (2000)
Yakin Street	PEER (2000)
Yalova Harbor	PEER (2000)

Figure 4.1 contains the commonly used chart from Seed and Harder (1990) to estimate the liquefied shear strength, $S_{u\text{-}LIQ}$, of a cohesionless soil deposit based on the equivalent clean sand SPT blowcount, $(N_1)_{60\text{-}cs}$. The fines content, *FC*, corrections for SPT $(N_1)_{60}$ blowcount used in liquefaction evaluations are also shown in Figure 4.1. This

fines content correction is based on the results of back-analyses of liquefaction failure cases conducted by Dr. Harry Seed (1987).

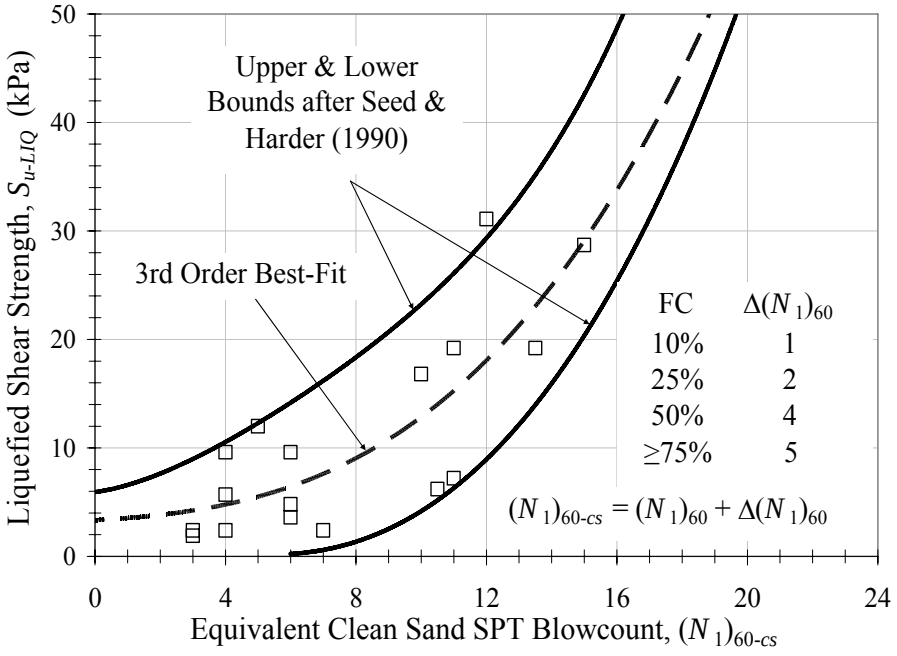

Figure 4.1 Liquefied shear strength relationship (after Seed and Harder, 1990)

Equation 4.1 is the best-fit third-order polynomial through the data presented by Seed and Harder (1990).

$$S_{u-LIQ} = p(N_1)^3_{60-cs} + q(N_1)^2_{60-cs} + r(N_1)_{60-cs} + s \qquad (4.1)$$

Where p, q, r, and s are regression coefficients (p = 0.0050; q = 0.0277; r = 0.1697; s = 3.3376) with an R^2 value of 0.652. Detailed discussion of Figure 4.1 is presented in Chapter 1.

4.2 HOTEL SAPANCA LIQUEFACTION FAILURE

The Hotel Sapanca liquefaction failure occurred during the 1999 Kocaeli Earthquake. The failure and extensive field testing program performed after the earthquake is documented and discussed in further detail by Cetin et al. (2002). Figure 4.2 shows a photograph of the Hotel Sapanca site, located along the southern shores of Lake Sapanca, shortly after the earthquake. The site is located approximately 2.0 kilometers from the fault rupture and experienced maximum horizontal accelerations in the range of 0.35 to 0.40g. The subsurface conditions and parameters used in subsequent stability analyses are inferred from the results of 5 SPT logs and 11 CPT logs. Figure 4.3 and Figure 4.4 show representative soil profiles and logs.

Figure 4.2 Hotel Sapanca after the 1999 Kocaeli Earthquake (Olgun, 2005)

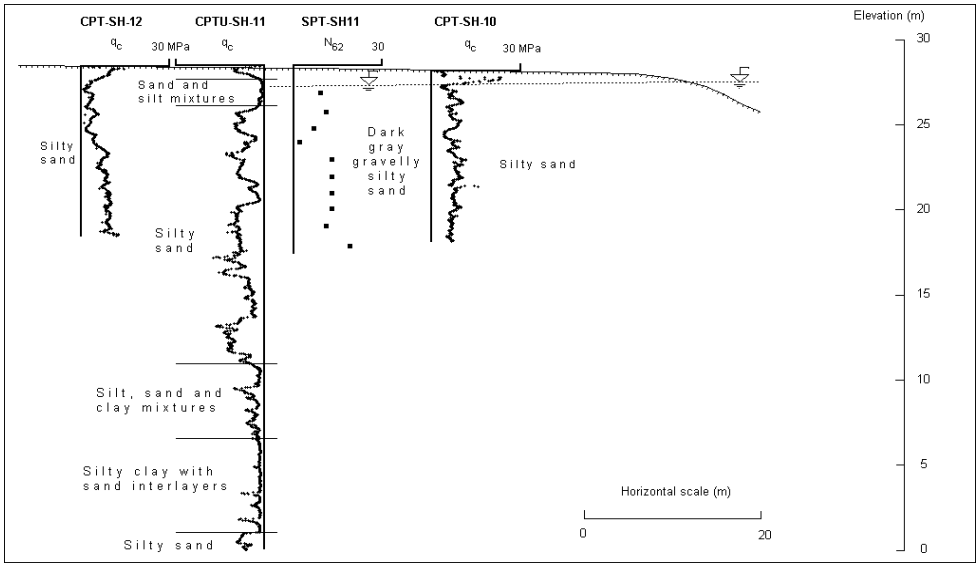

Figure 4.3 Cross Section 1 (PEER, 2000)

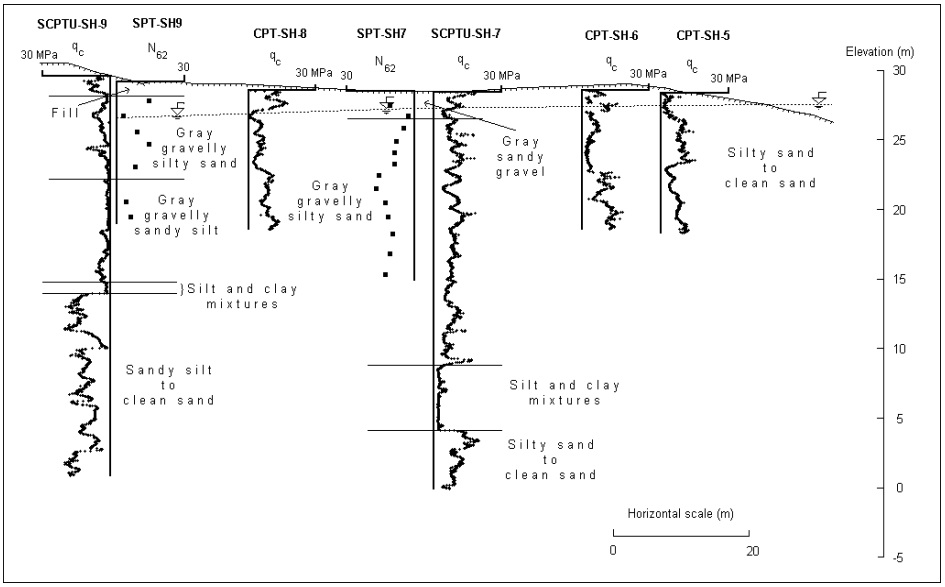

Figure 4.4 Cross Section 2 (PEER, 2000)

4.2.1 Slope Stability Computation

The Ishihara et al. (1990) simplified slope stability analysis is used to estimate the liquefied shear strength of cohesionless soils at the Hotel Sapanca liquefaction failure. Detailed description of the method is presented in Chapter 2.

4.2.2 Parameter Uncertainty

Probability distribution functions (PDF) representative of the various parameters involved in the simplified slope stability analysis are developed through available data from each case history or from historical catalogs of parameter uncertainty. For those case histories where site-specific data is limited or insufficient, probabilistic parameters are estimated from other case histories. Table 2.1 (Duncan, 2000), Table 4.2, and Table 4.3 (Gutierrez et al., 2003) provide ranges for the coefficient of variation, *COV*, of various soil properties commonly used in slope stability computations, including in-situ testing parameters.

Table 4.2 contains probabilistic parameters from the Hotel Sapanca liquefaction failure for the five inputs involved in the slope stability back-analysis; all inputs are assumed to follow a normal (Gaussian) PDF. Detailed description of the data is presented in Appendix A.

Table 4.2 - Normal PDF parameters for Hotel Sapanca

Property	μ	σ
γ_d	21.0 kN/m^3	1.05 kN/m^3
γ_{sat}	22.0 kN/m^3	1.1 kN/m^3
H_d	1.2 m	0.12 m
H_w	6.0 m	1.80 m
α	0.8^O	0.08^O

Figures 4.5 and 4.6 contain distribution functions for the corrected SPT blowcount, $(N_1)_{60}$, and the fines content from the in-situ testing program performed at Hotel Sapanca. The distributions are developed using @RISK program. The distribution of $(N_1)_{60\text{-}cs}$ for the Hotel Sapanca site is obtained through Monte Carlo Simulation using @RISK program with fines content corrections as described by Seed and Harder (1990). Figure 4.7 shows the PDF of $(N_1)_{60\text{-}cs}$ obtained through 10,000 iterations and Latin Hypercube sampling.

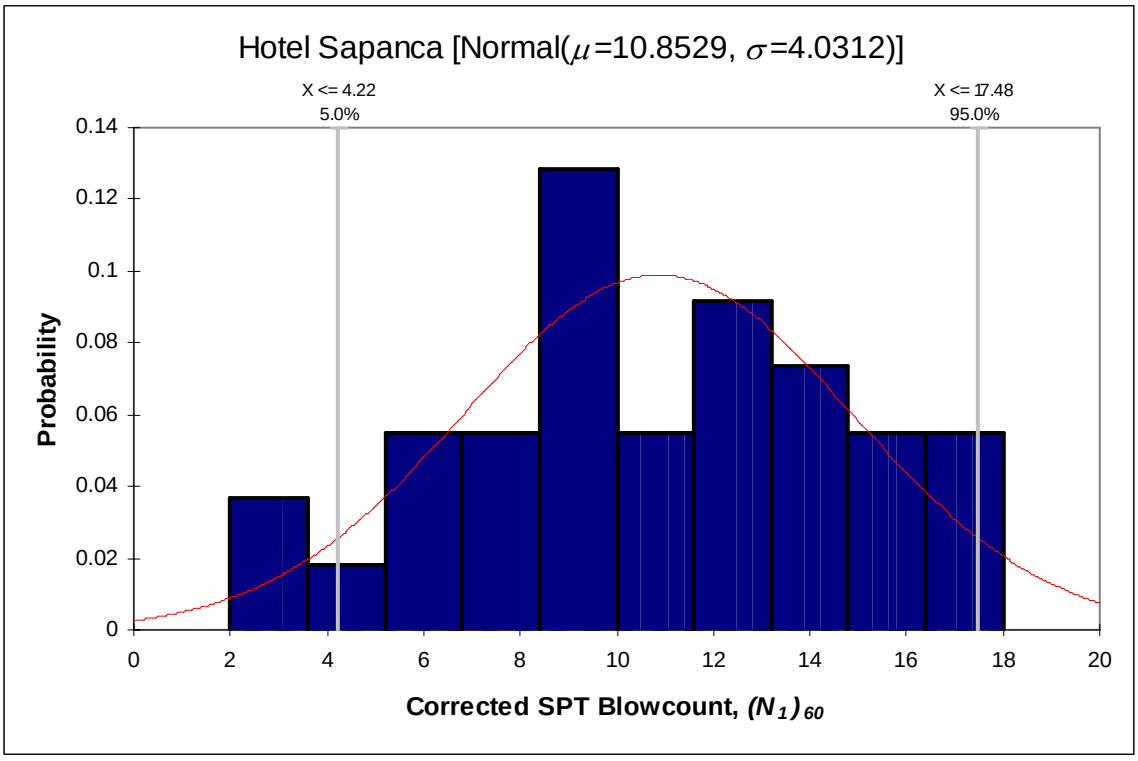

Figure 4.5 Normal PDF of corrected SPT blowcount from Hotel Sapanca

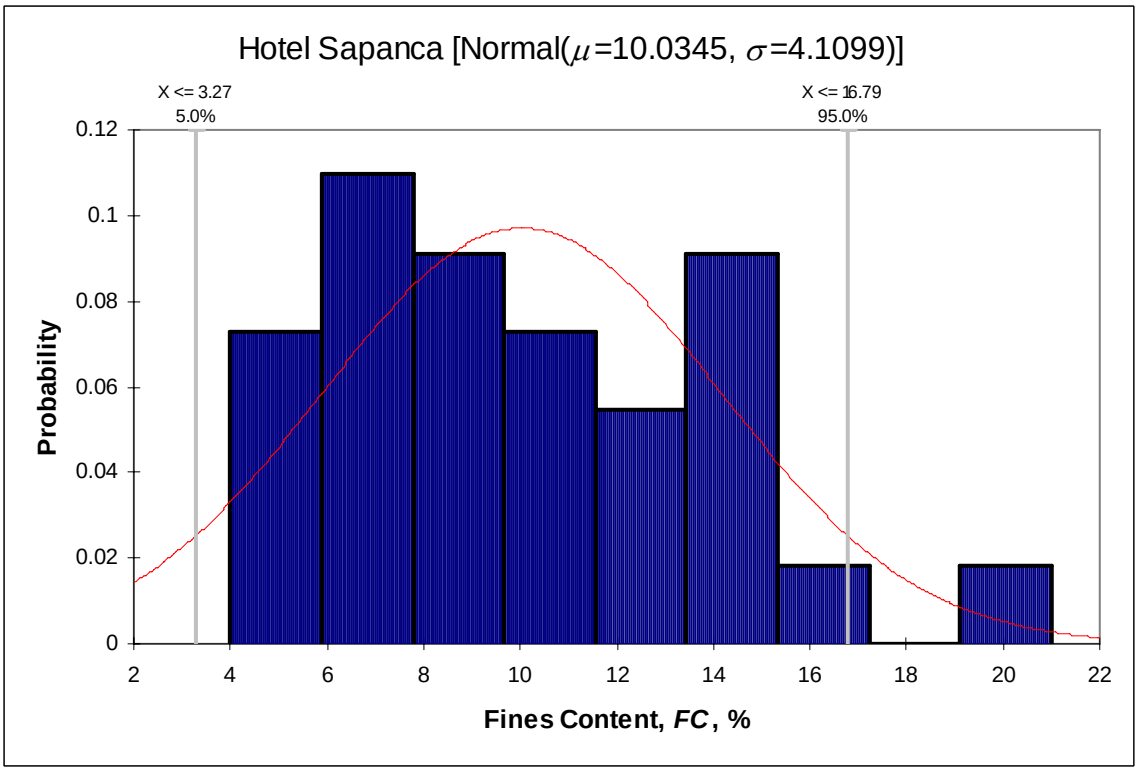

Figure 4.6 Normal PDF of fines content from Hotel Sapanca

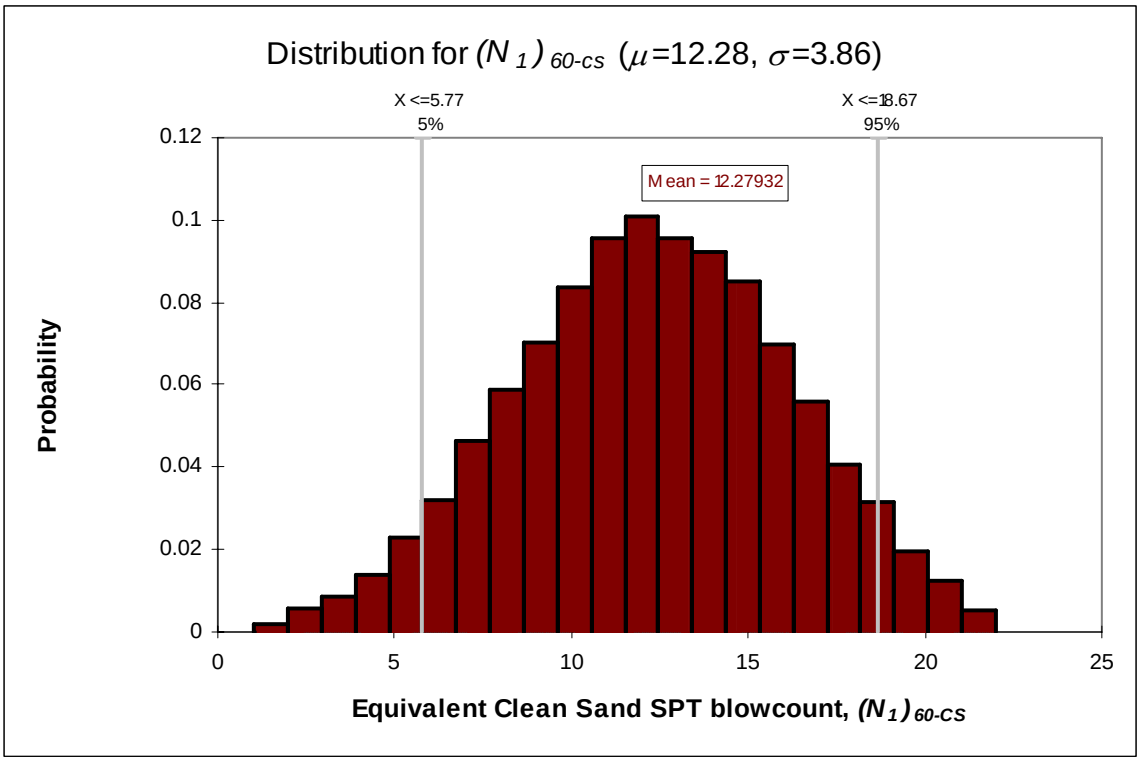

Figure 4.7 Normal PDF of equivalent clean sand SPT blowcount from Hotel Sapanca

When performing probability and reliability computations, the input parameters can be correlated. If the correlations are not accounted for in further estimates, the results can be misleading. The correlation matrix of input parameters for the simplified slope stability analysis is shown in Figure 4.8. All variables in the correlation matrix are variables in slope stability computations, as described in Equation 2.1, 2.2 and 2.3. It is assumed that the dry and saturated unit weights are positively correlated and the depth to the water table and height of the water table above the failure surface are negatively correlated.

	γ_d	γ_{sat}	H_d	H_w	α
γ_d	1	0.9	0	0	0
γ_{sat}	0.9	1	0	0	0
H_d	0	0	1	−0.5	0
H_w	0	0	−0.5	1	0
α	0	0	0	0	1

Figure 4.8 Correlation matrix used for probabilistic infinite slope analysis

4.2.3 Probabilistic Slope Stability Computations

Monte Carlo Simulations are performed to obtain the PDF for the liquefied shear strength using the simplified slope stability procedure described earlier. A total of 10,000 simulations were carried out to generate the liquefied undrained shear strength, $S_{u\text{-}Liq}$, probability density function (PDF). The probabilistic parameters for all input parameters along with the correlation matrix result in a lognormal distribution of liquefied shear strength with a mean, λ, of 3.39kPa and a standard deviation, ζ, of 0.35kPa shown in Figure 4.9.

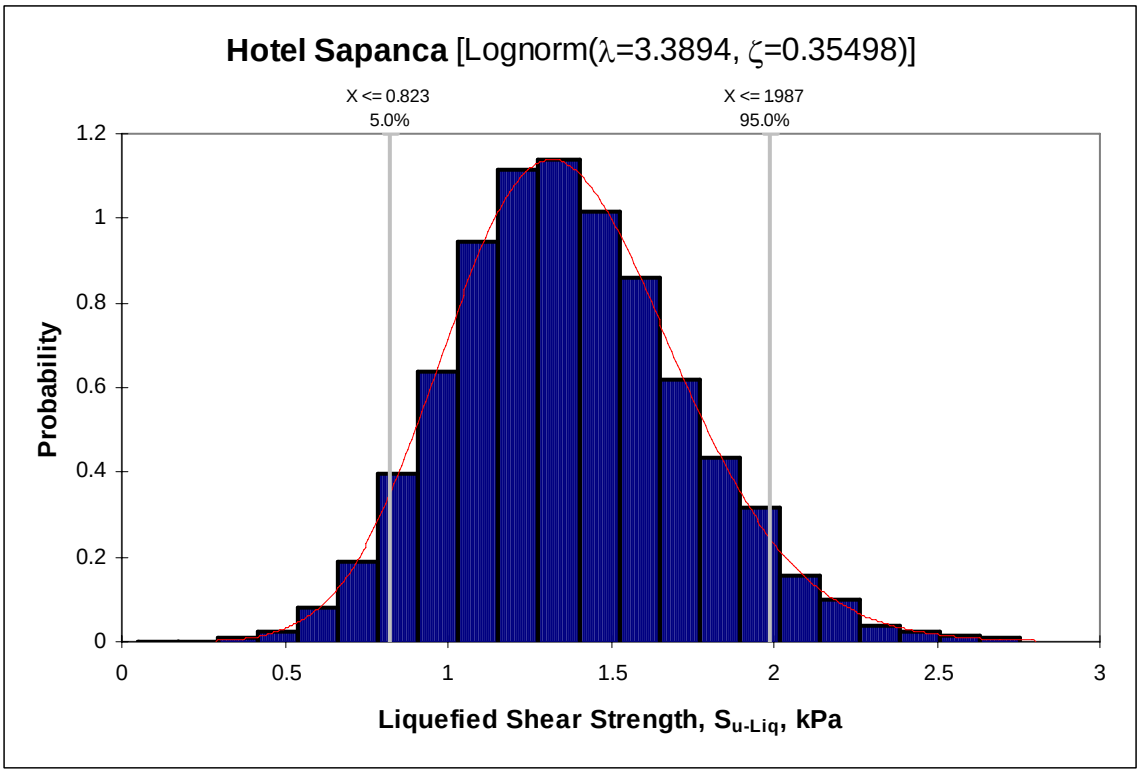

Figure 4.9 Lognormal PDF of Liquefied Shear Strength from Hotel Sapanca

4.2.4 Reliability Computations

The underlying goal of the reliability analysis is to determine how probability of failure and a computed factor of safety against slope instability are related for a particular $S_{u\text{-}LIQ}$-$(N_1)_{60\text{-}cs}$ relationship. The performance function used to assess the reliability is shown in Equation 4.2 and Equation 4.3, where the factor of safety is a function of all parameters involved in the slope stability analysis and the equivalent clean sand SPT blowcount, $(N_1)_{60\text{-}CS}$. Equation 4.3 is derived from Equation 2.1, 2.2, 2.3, and 4.1.

$$G(x) = FS - 1 \tag{4.2}$$

$$FS = \frac{C_1\left[p(N_1)_{60-cs}^3 + q(N_1)_{60-cs}^2 + r(N_1)_{60-cs} + s\right]}{\left(H_d\gamma_d + H_w\gamma_{sat} - H_w\gamma_w\cos^2\alpha\right)\sin\alpha\cos\alpha} \tag{4.3}$$

When the factor of safety, *FS*, is greater than 1.0 the $S_{u\text{-}LIQ}$ relationship from Equation 4.1 is not predicting failure, therefore the probability that the *FS* is greater than 1.0 corresponds to the probability that the strength relationship is inaccurately predicting failure. When the *FS* from Equation 4.3 is less than or equal to 1.0, the $S_{u\text{-}LIQ}$ relationship is accurately predicting failure. The C_1 term in Equation 4.3 accounts for variability in the liquefied shear strength computed from Equation 4.1, the nominal term is defined with a mean of 1.0 and an assumed standard deviation of 0.3.

The reliability of the each case history is measured with the Hasofer-Lind reliability index, β (Hasofer and Lind, 1974). A spreadsheet approach proposed by Low and Tang (2004) are utilized to calculate the reliability index, β. Detailed description of the method is presented in Chapter 2.

The correlation matrix used in the reliability analyses, shown in Figure 4.10, builds upon the correlation matrix in Figure 4.8 incorporating $(N_1)_{60\text{-}cs}$ and C_1.

	γ_d	γ_{sat}	H_d	H_w	α	$(N_1)_{60-cs}$	C_1
γ_d	1	0.9	0	0	0	0	0
γ_{sat}	0.9	1	0	0	0	0	0
H_d	0	0	1	−0.5	0	0	0
H_w	0	0	−0.5	1	0	0	0
α	0	0	0	0	1	0	0
$(N_1)_{60-cs}$	0	0	0	0	0	1	0
C_1	0	0	0	0	0	0	1

Figure 4.10 Correlation matrix used for reliability analyses

The probability distributions for related parameters are determined through statistical analysis when data are available. For those cased histories where site-specific data is not available, parameters can be estimated from the literature. Table 2.1 from Duncan (2000), Table 2.2 and 2.3 from Gutierrez et al. (2003) provide ranges for the

coefficient of variation, *COV*, for various geotechnical engineering parameters commonly used.

The equations are implemented in Microsoft Excel to calculate the reliability index, β. Figure 4.11 showed reliability computations of Hotel Sapanca case using mean value of $(N_1)_{60\text{-}cs}$. The reliability index, β, for Hotel Sapanca case is equal to 3.013. The probability of failure is equals to 0.0013 or 0.13%.

	DistName	Para1	Para2	Para3	Para4	$x_{initial}$	x^*	m^N	s^N	nx
γ_d	Normal	21.00	1.05			21.00	21.11	21.00	1.05	0.10
γ_{sat}	Normal	22.00	1.10			22.00	22.12	22.00	1.10	0.11
H_d	Normal	1.20	0.12			1.20	1.19	1.20	0.12	-0.11
H_w	Normal	6.00	1.80			6.00	6.50	6.00	1.80	0.28
α	Normal	0.80	0.08			0.80	0.81	0.80	0.08	0.14
$(N_1)_{60cs}$	Normal	12.28	3.86			12.28	8.64	12.28	3.86	-0.94
C_1	Normal	1.00	0.30			1.00	0.15	1.00	0.30	-2.84

	γ_d	γ_{sat}	H_d	H_w	α	$(N_1)_{60cs}$	C_1
γ_d	**1.00**	0.90	0.00	0.00	0.00	0.00	0.00
γ_{sat}	0.90	**1.00**	0.00	0.00	0.00	0.00	0.00
H_d	0.00	0.00	**1.00**	-0.50	0.00	0.00	0.00
H_w	0.00	0.00	-0.50	**1.00**	0.00	0.00	0.00
α	0.00	0.00	0.00	0.00	**1.00**	0.00	0.00
$(N_1)_{60cs}$	0.00	0.00	0.00	0.00	0.00	**1.00**	0.00
C_1	0.00	0.00	0.00	0.00	0.00	0.00	**1.00**

reset design points, x^*

Options	Para1	Para2	Para3	Para4
None	value			
Normal	mean	StDev		
Lognorm	mean	StDev		
ExtValue1	mean	StDev		
Uniform	Use BetaDist (1,1,min,max)			
Expo	mean			
Gamma	α	λ		
Weibull	α	λ		
Triang	min	mode	max	
BetaDist	α	λ	min	max
PERTdist	min	mode	max	

	Min.	Max.
γ_d	16.00	26.00
γ_{sat}	17.00	27.00
H_d	0.00	10.00
H_w	0.00	25.00
α	0.00	1.60
$(N_1)_{60cs}$	0.00	25.00
C_1	0.00	2.00

FS
1.00
β
3.013
Pf
0.0013

UNITS ARE IN KILOPASCALS & METERS

Stability computations are based on Ishihara et al (1990).

Reliability computations are based on Low and Tang (2004).

A best-fit line through the Seed and Harder (1990) data is used to estimate the liquefied shear strength based on the input $(N_1)_{60}$

Figure 4.11 Reliability computations of Hotel Sapanca case using mean value of $(N_1)_{60\text{-}cs}$

Monte Carlo Simulations are performed to verify the Hasofer-Lind reliability index. Probability density function of factor of safety is developed using Equation 4.3. Figure 4.12 shows the results of the simulations, where the probability that the factor of safety, *FS*, is less than 1.0 equals to 0.16%. These results verify that the Hasofer-Lind reliability index can be used in-place of Monte Carlo Simulations.

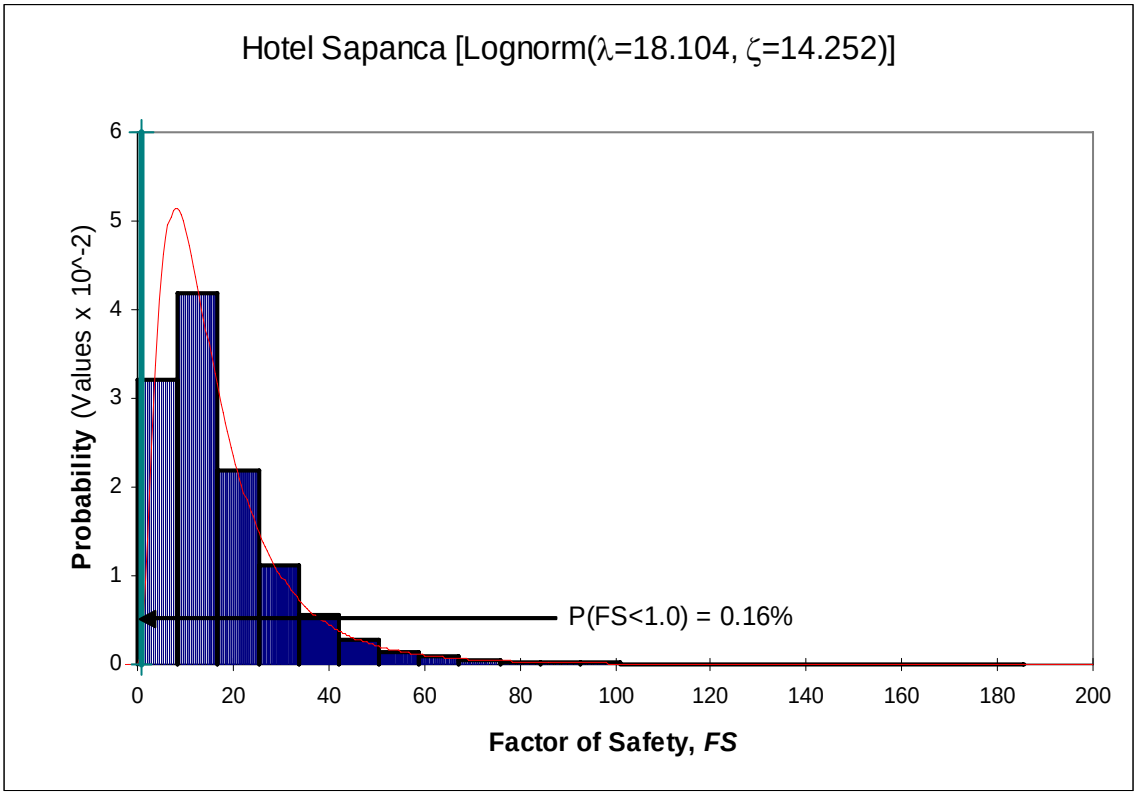

Figure 4.12 Lognormal PDF of factor of safety for the Hotel Sapanca failure

The reliability index, β, is also computed using minimum value of $(N_1)_{60\text{-}cs}$. Figure 4.13 showed reliability computations of Hotel Sapanca case using mean value of $(N_1)_{60\text{-}cs}$. The reliability index, β, for Hotel Sapanca case is equals to 2.039. The probability of failure is equals to 0.021 or 2.1%.

	DistName	Para1	Para2	Para3	Para4	$x_{initial}$	x^*	m^N	s^N	nx
γ_d	Normal	21.00	1.05			21.00	21.21	21.00	1.05	0.20
γ_{sat}	Normal	22.00	1.10			22.00	22.23	22.00	1.10	0.21
H_d	Normal	1.20	0.12			1.20	1.17	1.20	0.12	-0.21
H_w	Normal	6.00	1.80			6.00	6.93	6.00	1.80	0.51
α	Normal	0.80	0.08			0.80	0.82	0.80	0.08	0.26
$(N_1)_{60cs}$	Normal	2.00	0.63			2.00	1.91	2.00	0.63	-0.15
C_1	Normal	1.00	0.30			1.00	0.42	1.00	0.30	-1.94

	γ_d	γ_{sat}	H_d	H_w	α	$(N_1)_{60cs}$	C_1
γ_d	**1.00**	0.90	0.00	0.00	0.00	0.00	0.00
γ_{sat}	0.90	**1.00**	0.00	0.00	0.00	0.00	0.00
H_d	0.00	0.00	**1.00**	-0.50	0.00	0.00	0.00
H_w	0.00	0.00	-0.50	**1.00**	0.00	0.00	0.00
α	0.00	0.00	0.00	0.00	**1.00**	0.00	0.00
$(N_1)_{60cs}$	0.00	0.00	0.00	0.00	0.00	**1.00**	0.00
C_1	0.00	0.00	0.00	0.00	0.00	0.00	**1.00**

reset design points, x*

Options	Para1	Para2	Para3	Para4
None	value			
Normal	mean	StDev		
Lognorm	mean	StDev		
ExtValue1	mean	StDev		
Uniform	Use BetaDist (1,1,min,max)			
Expo	mean			
Gamma	α	λ		
Weibull	α	λ		
Triang	min	mode	max	
BetaDist	α	λ	min	max
PERTdist	min	mode	max	

	Min.	Max.
γ_d	16.00	26.00
γ_{sat}	17.00	27.00
H_d	0.00	10.00
H_w	0.00	25.00
α	0.00	1.60
$(N_1)_{60cs}$	0.00	25.00
C_1	0.00	2.00

FS
1.00
β
2.039
Pf
0.021

UNITS ARE IN KILOPASCALS & METERS

Stability computations are based on Ishihara et al (1990).

Reliability computations are based on Low and Tang (2004).

A best-fit line through the Seed and Harder (1990) data is used to estimate the liquefied shear strength based on the input $(N_1)_{60}$

Figure 4.13 Reliability computations of Hotel Sapanca case using minimum value of $(N_1)_{60\text{-}cs}$

4.3 OTHER CASE HISTORIES

All nine other case histories are analyzed with the same procedure that is applied for Hotel Sapanca failure case. Table 4.3 contains parameters used in the analyses. Detailed description of the parameters is presented in Appendix A.

Table 4.3 Parameters used in the analyses

Case	Mean/ St. Dev.	γ_d (kN/m^3)	γ_{sat} (kN/m^3)	H_d (m)	H_w (m)	α (^{O})	FC (%)	$(N_1)_{60}$ (blows/30cm)
Cark Canal	μ	17.500	20.500	2.60	1.80	1.0000	72.60	5.20
	σ	0.875	1.025	0.26	0.54	0.1000	23.00	1.92
Cumruhiyet Avenue	μ	15.000	16.000	1.10	3.60	0.1720	84.60	5.83
	σ	0.750	0.800	0.11	1.08	0.0172	21.20	4.58
Degirmendere Nose	μ	21.000	22.000	1.70	1.70	8.9000	16.70	14.43
	σ	1.050	1.100	0.17	0.51	0.8900	11.00	3.10
Esme Nose	μ	21.000	22.000	1.00	7.00	3.0000	45.00	10.60
	σ	1.050	1.100	0.10	2.10	0.3000	11.25	3.60
Police Station	μ	20.000	21.500	1.10	1.40	0.7000	42.00	6.33
	σ	1.000	1.075	0.11	0.42	0.0700	33.40	3.21
Seymen Tea Garden	μ	20.000	21.500	1.00	12.00	2.0000	30.00	9.73
	σ	1.000	1.075	0.10	3.60	0.2000	3.00	2.94
Soccer Field	μ	20.000	21.500	0.80	1.60	0.1000	44.70	3.67
	σ	1.000	1.075	0.08	0.48	0.0100	25.80	1.53
Yakin Street	μ	15.000	16.000	0.80	3.70	0.1700	89.65	7.10
	σ	0.750	0.800	0.08	0.51	0.0170	8.65	4.63
Yalova Harbor	μ	21.000	22.000	0.80	3.60	0.2860	15.93	10.75
	σ	1.050	1.100	0.08	0.48	0.0286	8.51	3.24

Figure 4.14 to Figure 4.22 show the liquefied shear strength distribution of each case. Table 4.4 shows the summary of probabilistic slope stability computations of all the cases. The mean of liquefied shear strength, μ, ranged from 0.06kPa to 8.68kPa. The standard deviation of liquefied shear strength, σ, ranged from 0.01kPa to 1.53kPa. The coefficient of variation of liquefied shear strength, *COV*, is ranged from 16.18% to 29.65%.

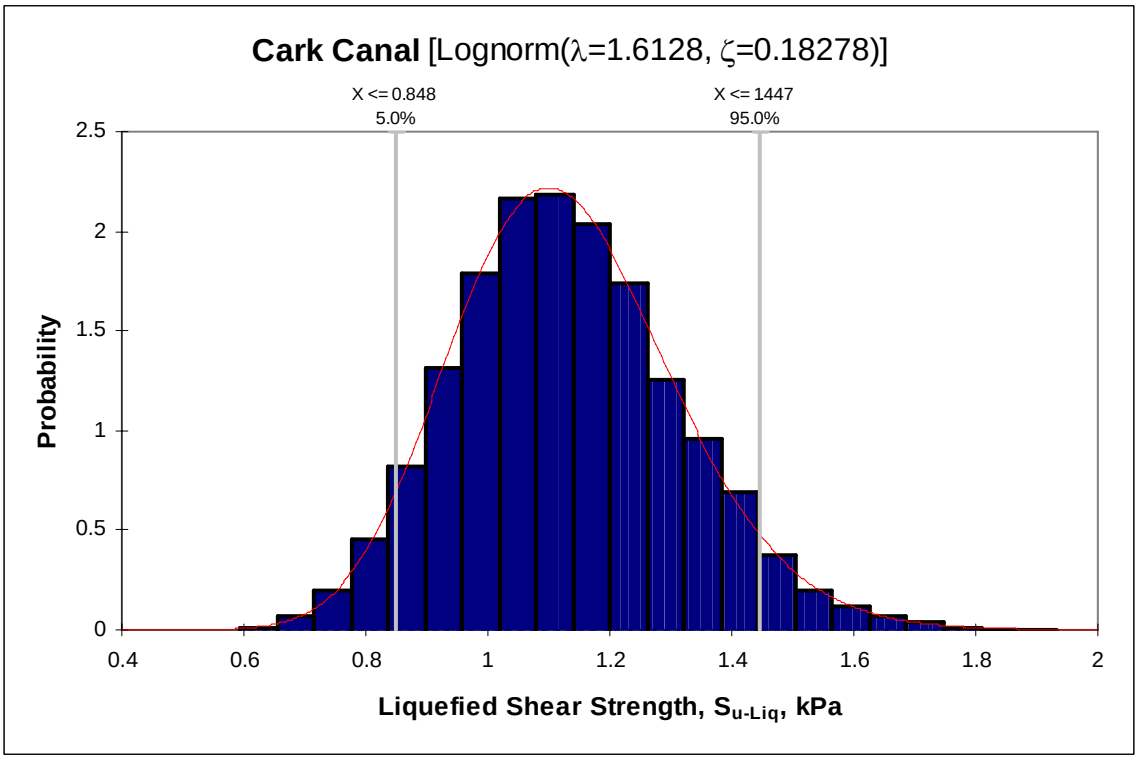

Figure 4.14 Lognormal PDF of Liquefied Shear Strength from Cark Canal

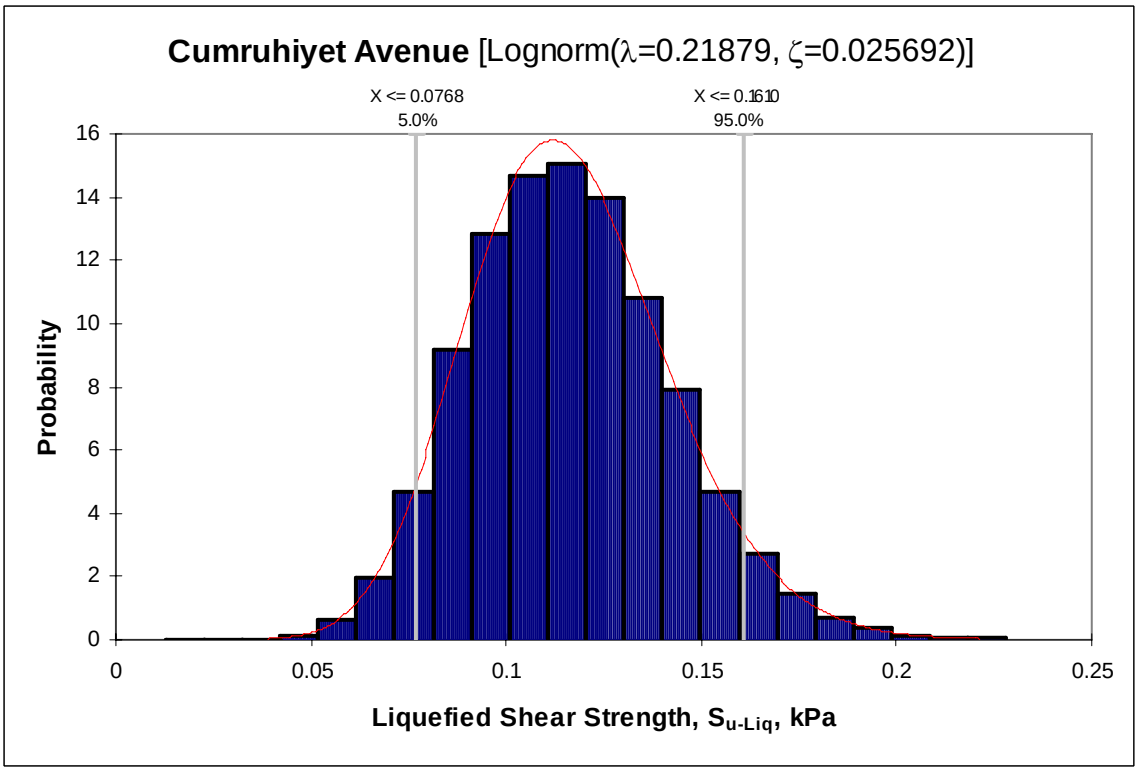

Figure 4.15 Lognormal PDF of Liquefied Shear Strength from Cumruhiyet Avenue

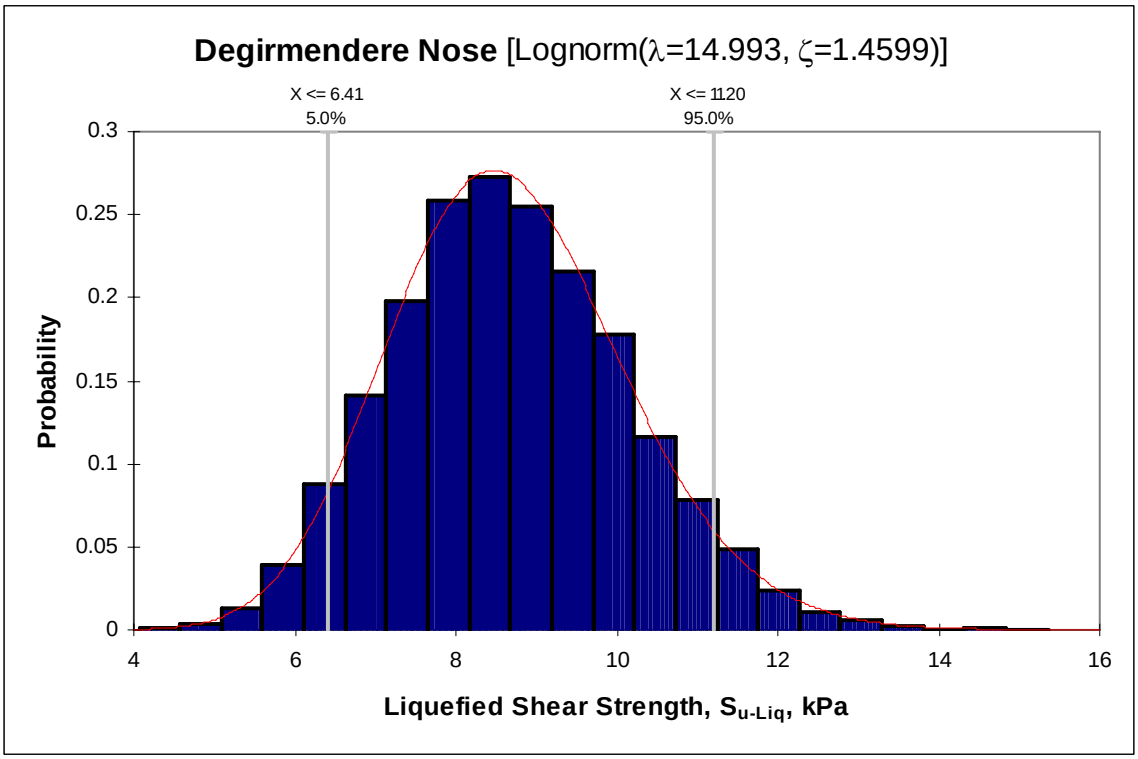

Figure 4.16 Lognormal PDF of Liquefied Shear Strength from Degirmendere Nose

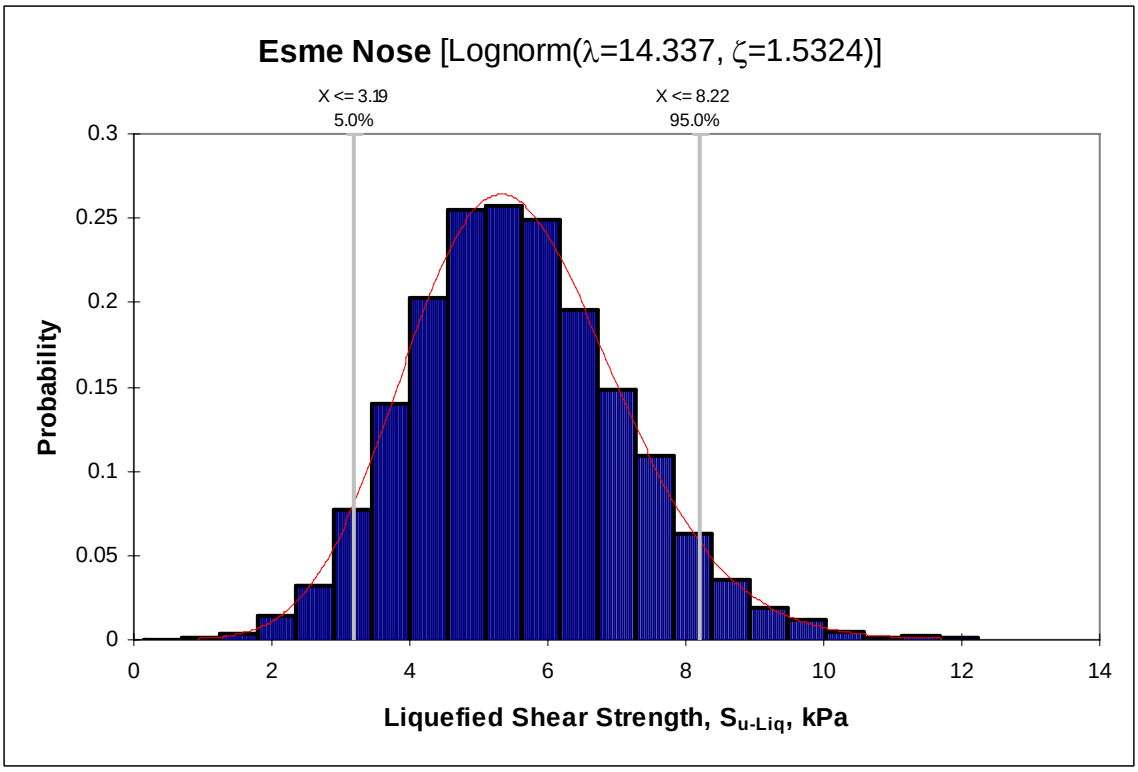

Figure 4.17 Lognormal PDF of Liquefied Shear Strength from Esme Nose

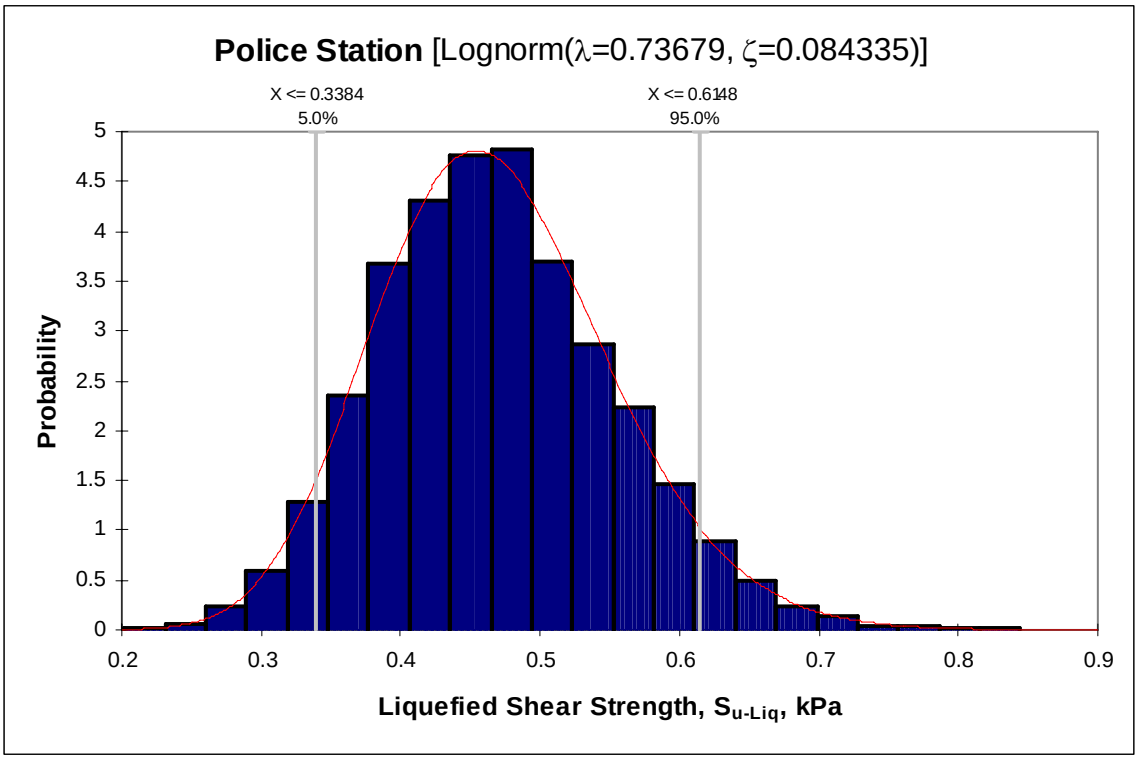

Figure 4.18 Lognormal PDF of Liquefied Shear Strength from Police Station

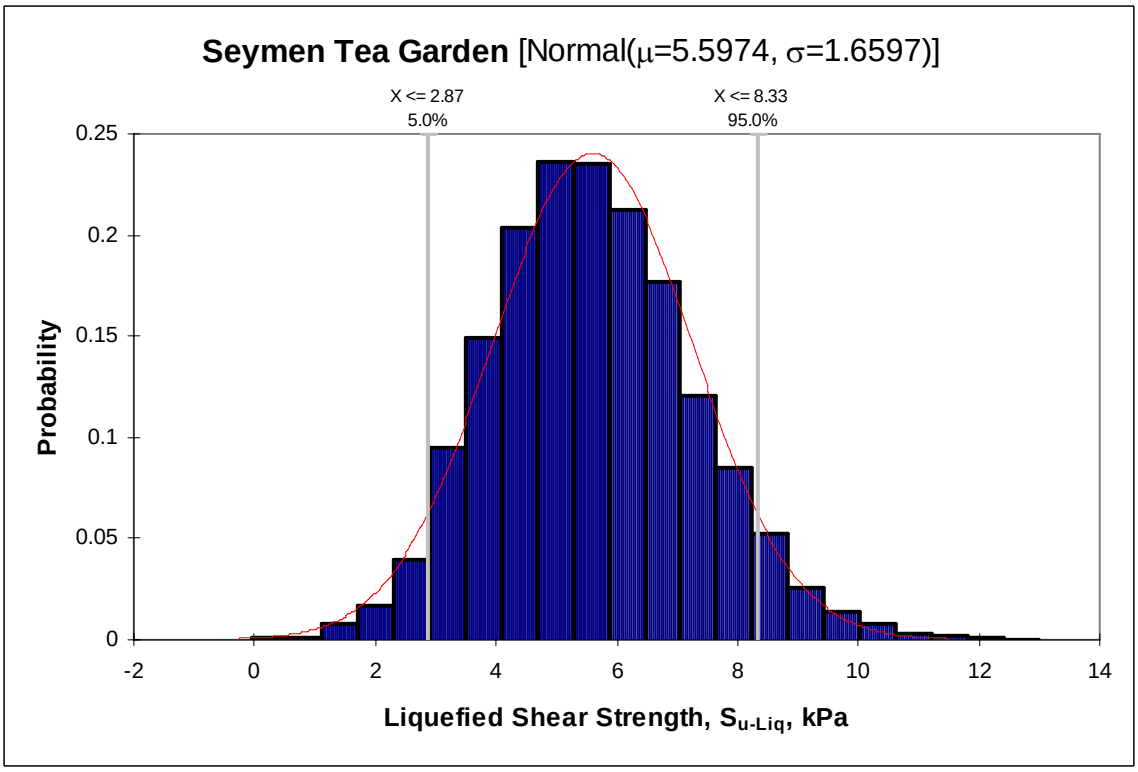

Figure 4.19 Normal PDF of Liquefied Shear Strength from Seymen Tea Garden

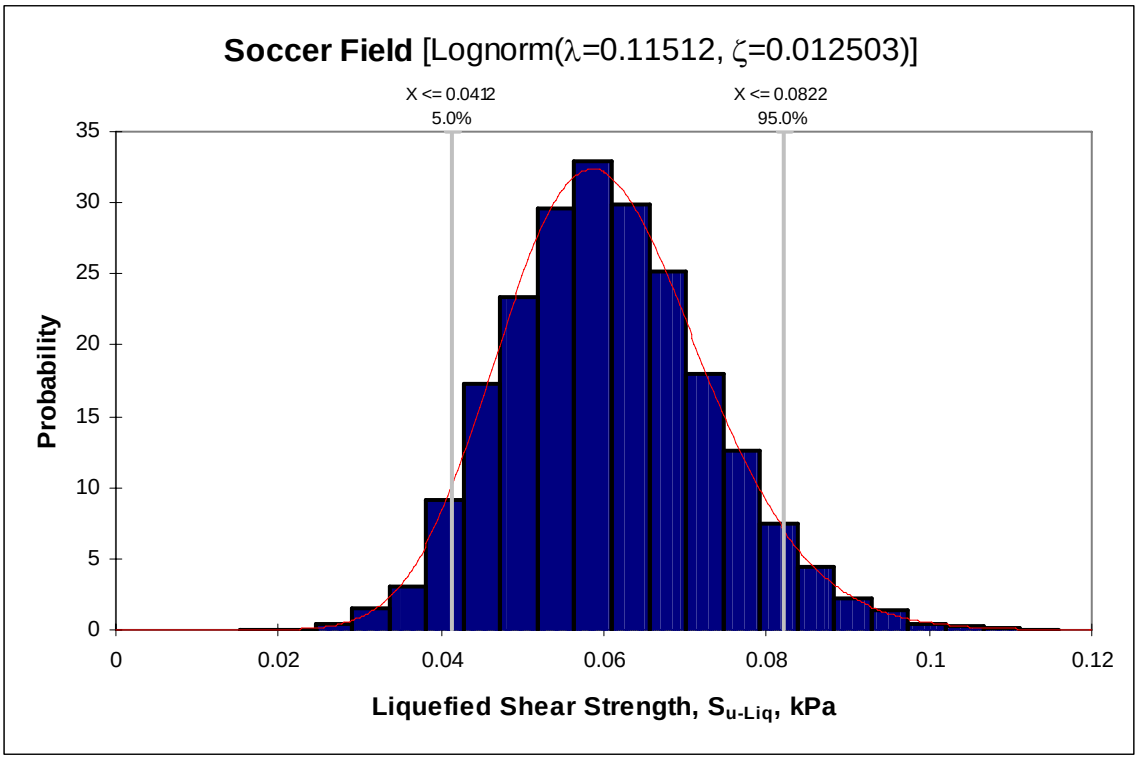

Figure 4.20 Lognormal PDF of Liquefied Shear Strength from Soccer Field

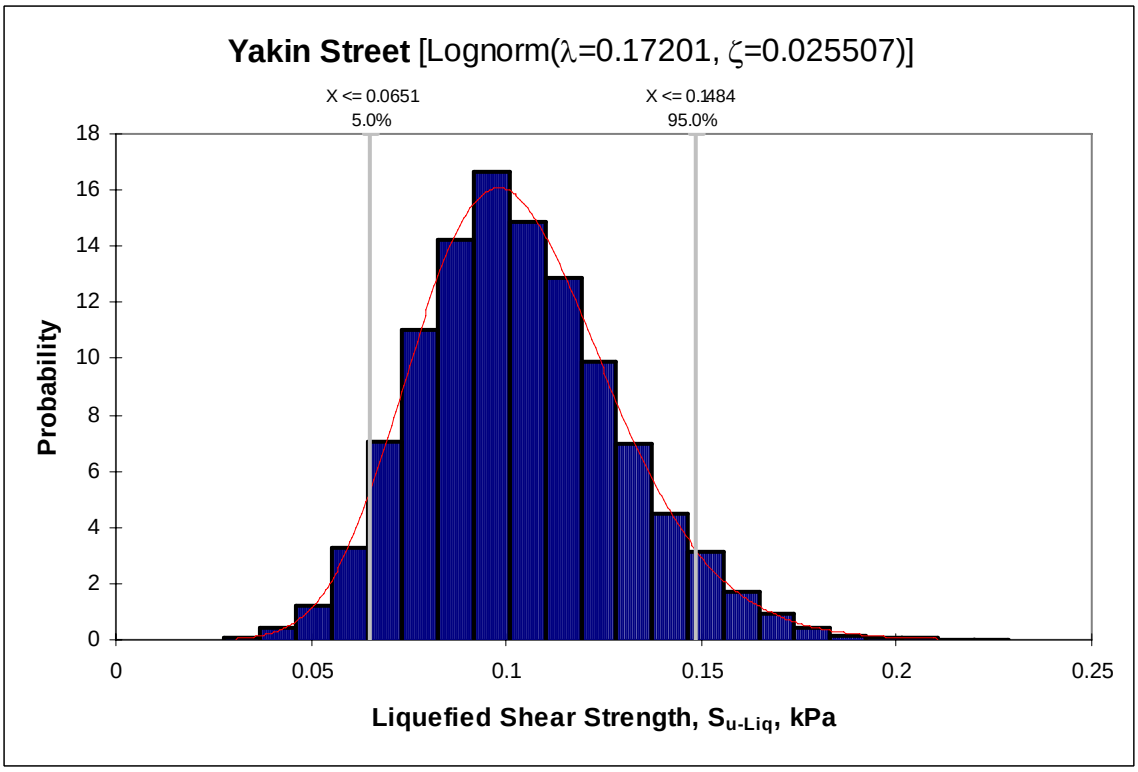

Figure 4.21 Lognormal PDF of Liquefied Shear Strength from Yakin Street

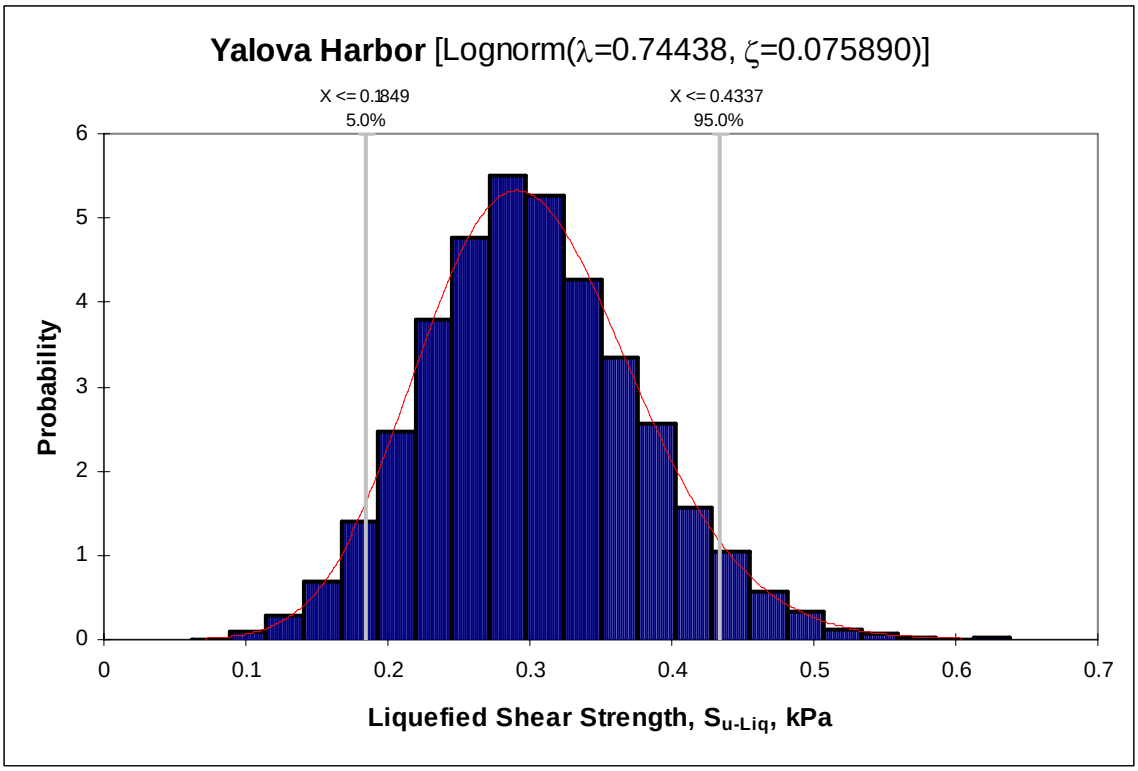

Figure 4.22 Normal PDF of Liquefied Shear Strength from Yalova Harbor

Table 4.4 Summary of the probabilistic slope stability analyses

Case History	$S_{u\text{-}LIQ}$		*COV*
	μ (kPa)	σ (kPa)	(%)
Cark Canal	1.13	0.18	16.18
Cumhuriyet Avenue	0.12	0.03	22.08
Degirmendere Nose	8.68	1.46	16.82
Esme Nose	5.57	1.53	27.53
Hotel Sapanca	1.37	0.35	25.85
Police Station	0.47	0.08	18.00
Seymen Tea Garden	5.60	1.66	29.65
Soccer Field	0.06	0.01	20.64
Yakin Street	0.12	0.03	25.83
Yalova Harbor	0.30	0.08	25.07

Table 4.5 shows the summary of the reliability computations of all the cases. Each case is analyzed for factor of safety equal to one, using mean values of $(N_1)_{60\text{-}cs}$. The reliability index, β, is ranged from 2.110 to 3.314. The probability of failure, *Pf*, is ranged from 0.0005 to 0.0174 or 0.05% to 1.74%. Reliability computations for each case are presented in Appendix B. Figure 4.23 shows the normal CDF of reliability index from all of the cases. The mean of reliability index, μ, is equal to 2.90. The standard deviation of reliability index, σ, is equal to 0.52.

Table 4.5 Summary of the reliability computations using mean values of $(N_1)_{60\text{-}cs}$

No.	Location	*FS*	β	*Pf*
1	Cark Canal	1.00	3.021	0.0013
2	Cumruhiyet	1.00	3.303	0.0005
3	Degirmendere Nose	1.00	2.200	0.0139
4	Esme Nose	1.00	2.190	0.0143
5	Hotel Sapanca	1.00	3.013	0.0013
6	Police Station	1.00	3.208	0.0007
7	Seymen Tea Garden	1.00	2.110	0.0174
8	Soccer Field	1.00	3.310	0.0005
9	Yakin Street	1.00	3.314	0.0005
10	Yalova Harbor	1.00	3.283	0.0005

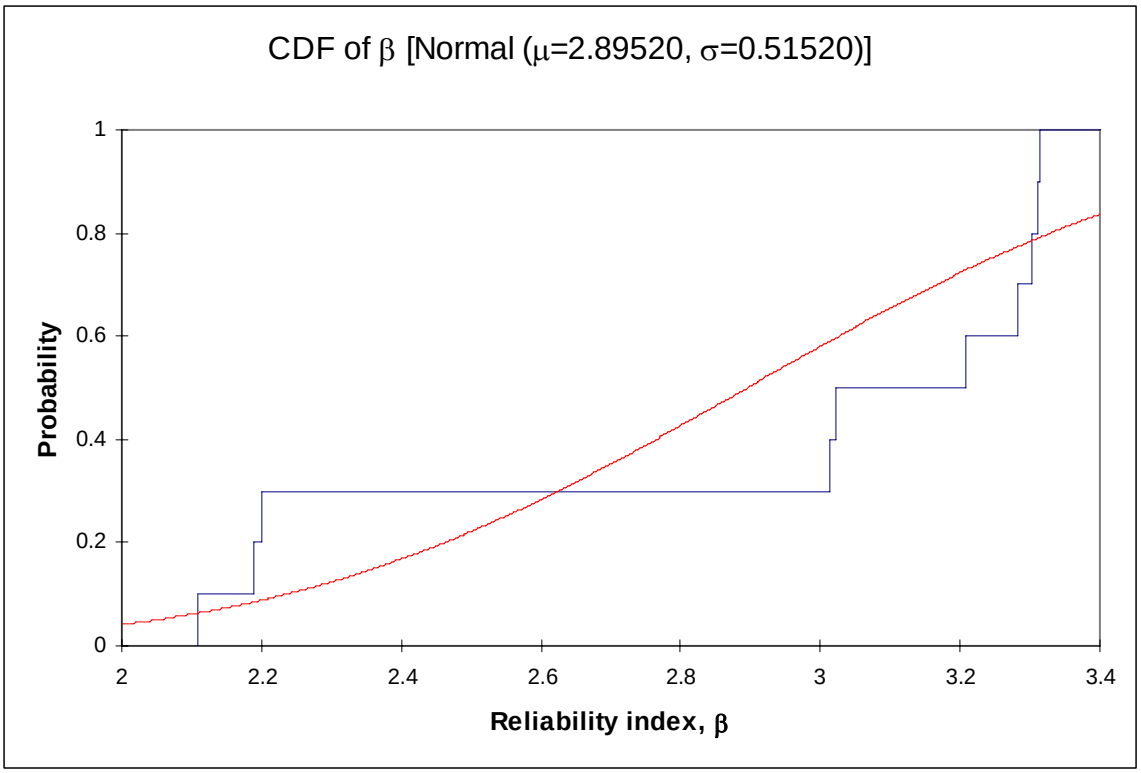

Figure 4.23 Normal CDF of reliability index using mean values of $(N_1)_{60\text{-}cs}$

Figure 4.24 shows relationship between reliability index, β, and probability of failure, *Pf*. Equation 4.6 is the best-fit logarithmic equation through the data, with an R^2 value of 0.9757.

$$Pf = -0.0362 Ln(\beta) + 0.0429 \qquad (4.6)$$

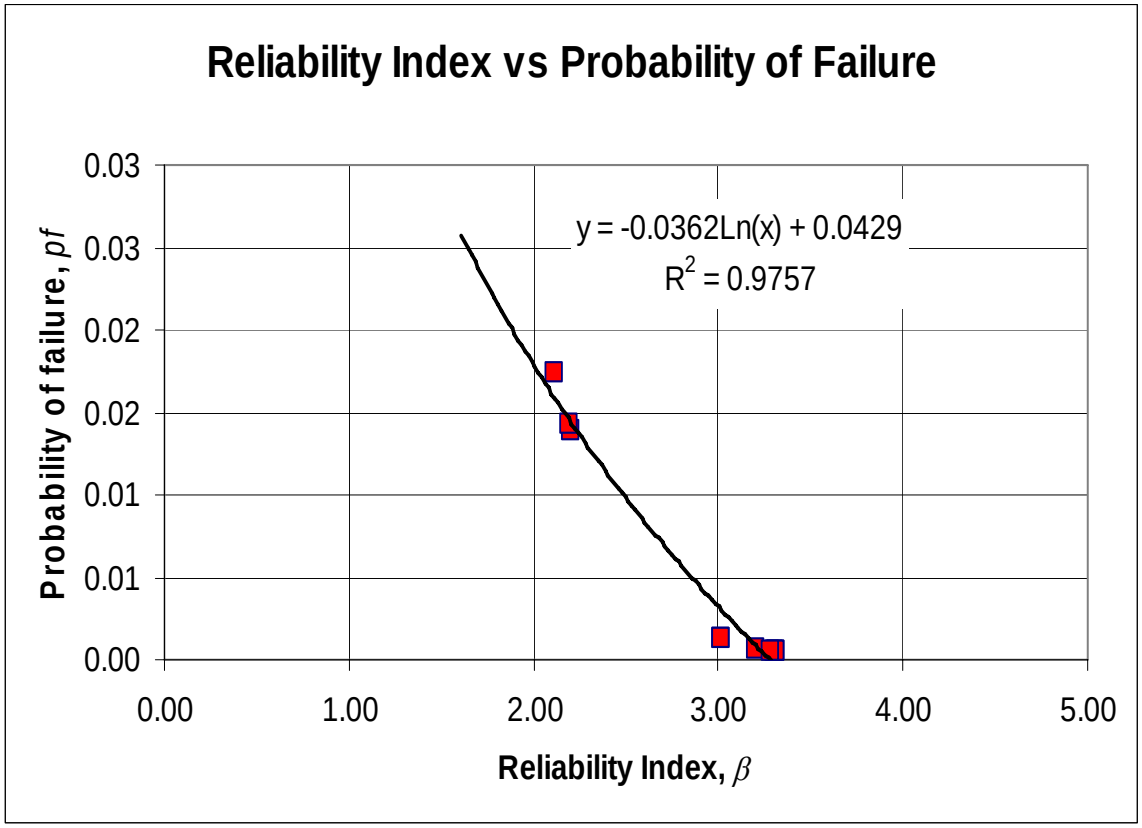

Figure 4.24 Relationship between reliability index, β, and probability of failure, *Pf*.

Monte Carlo Simulations are performed to verify the Hasofer-Lind reliability index for all of nine cases. Figure 4.25 to Figure 4.33 show the results of the simulations. The probability of the factor of safety, *FS*, is less than 1.0 is ranged from 0.01% to 1.90%.

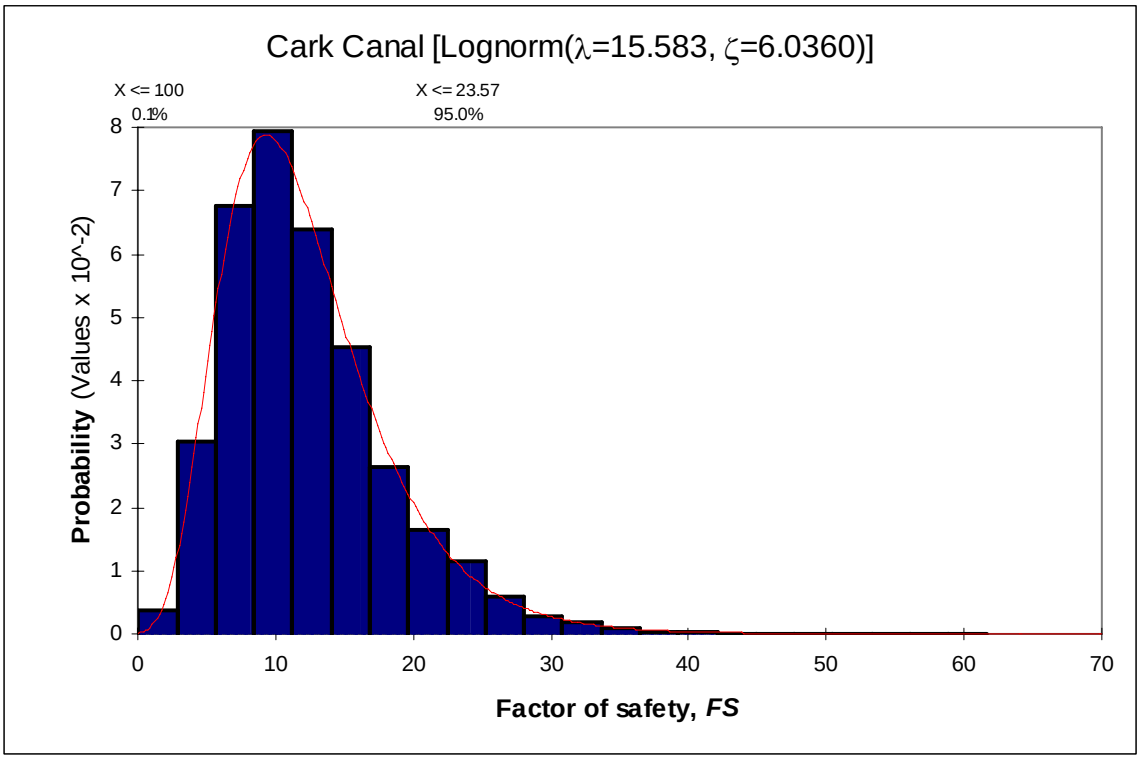

Figure 4.25 Lognormal PDF of factor of safety for the Cark Canal failure

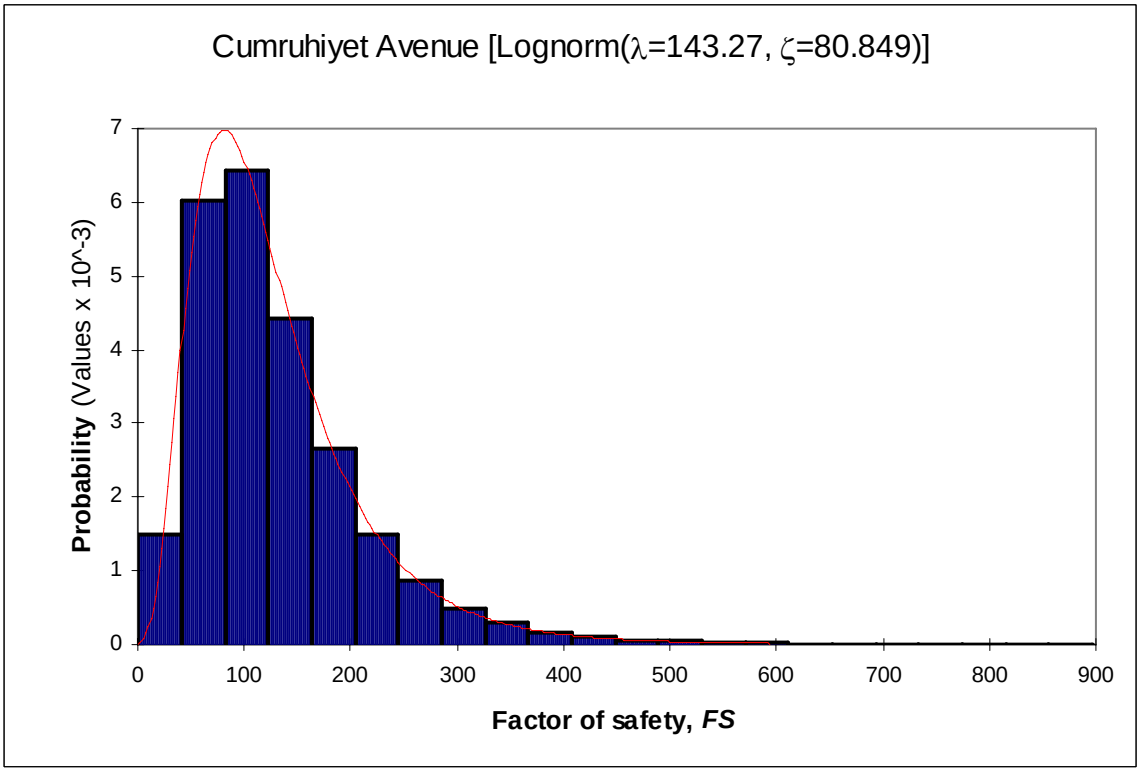

Figure 4.26 Lognormal PDF of factor of safety for the Cumruhiyet Avenue failure

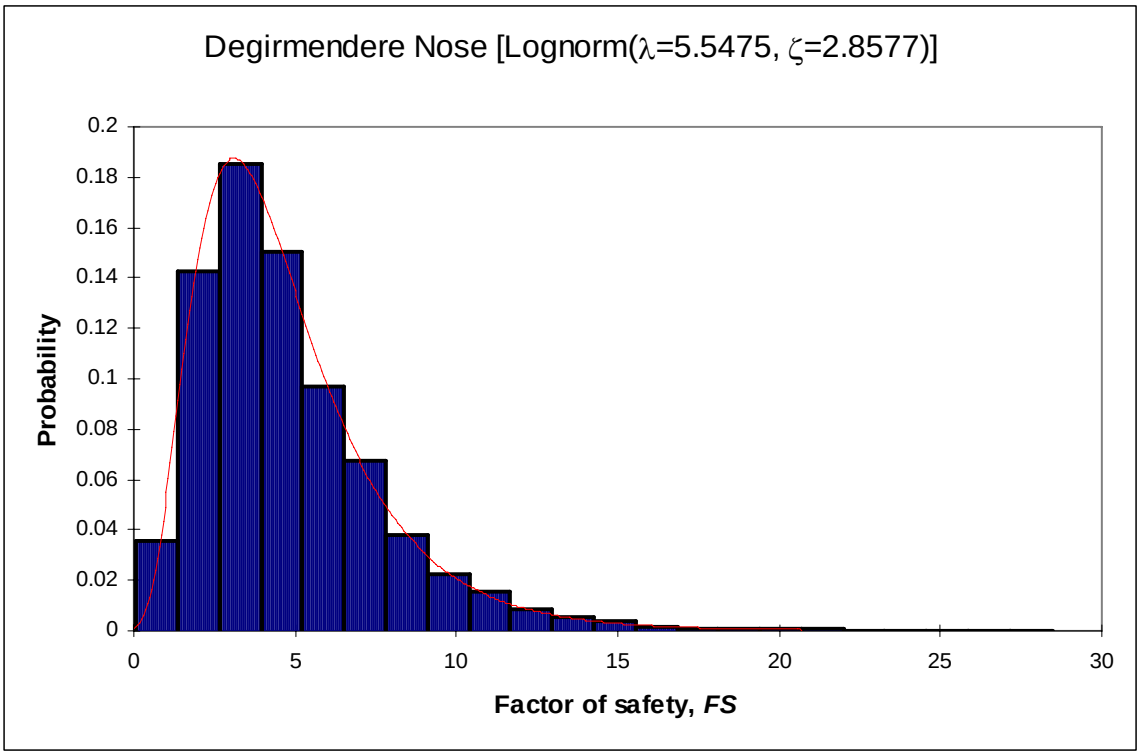

Figure 4.27 Lognormal PDF of factor of safety for the Degirmendere Nose failure

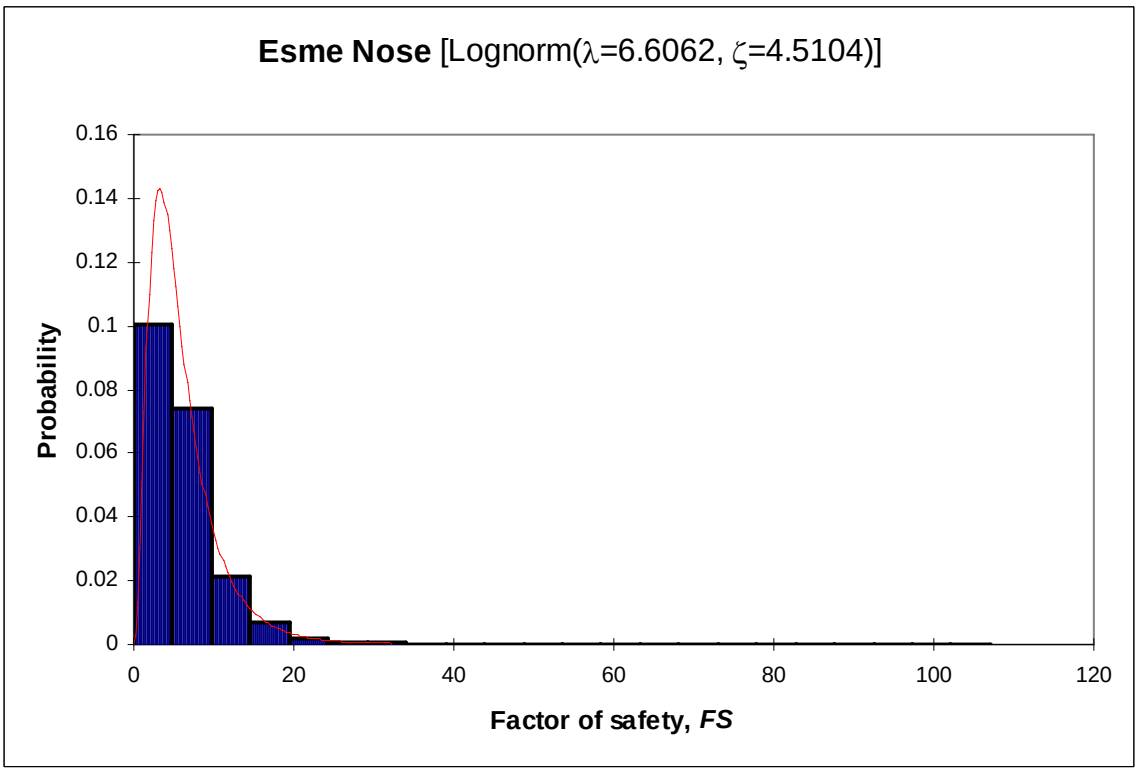

Figure 4.28 Lognormal PDF of factor of safety for the Esme Nose failure

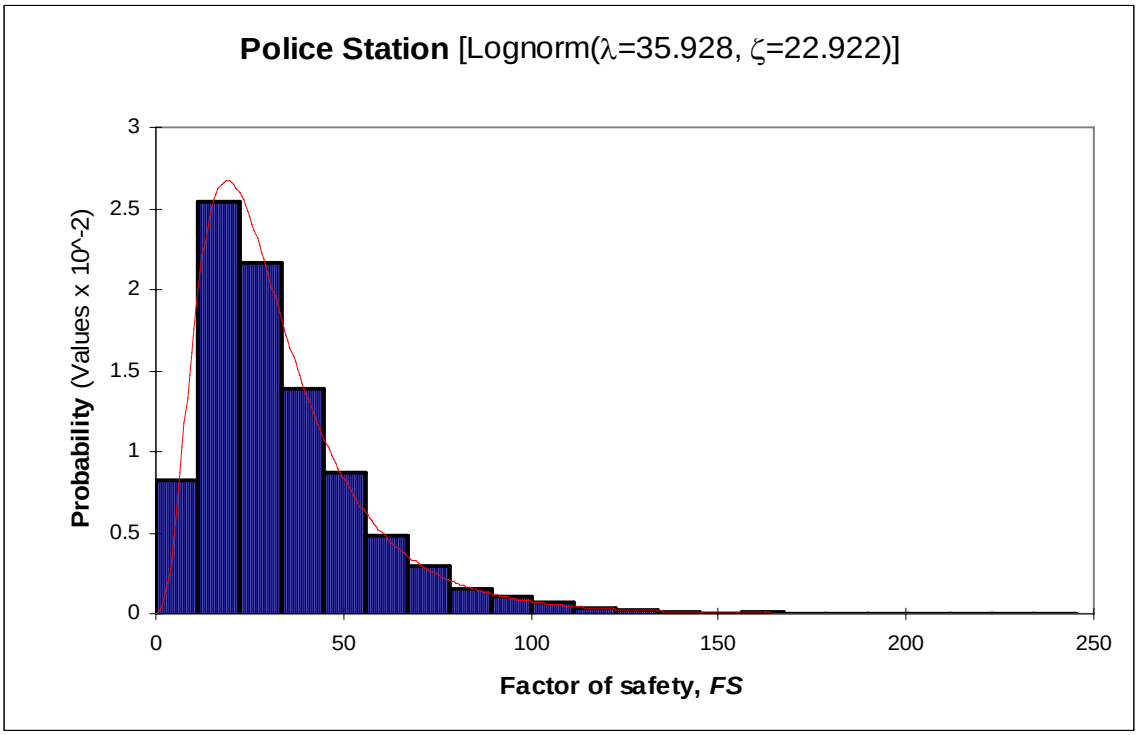

Figure 4.29 Lognormal PDF of factor of safety for the Police Station failure

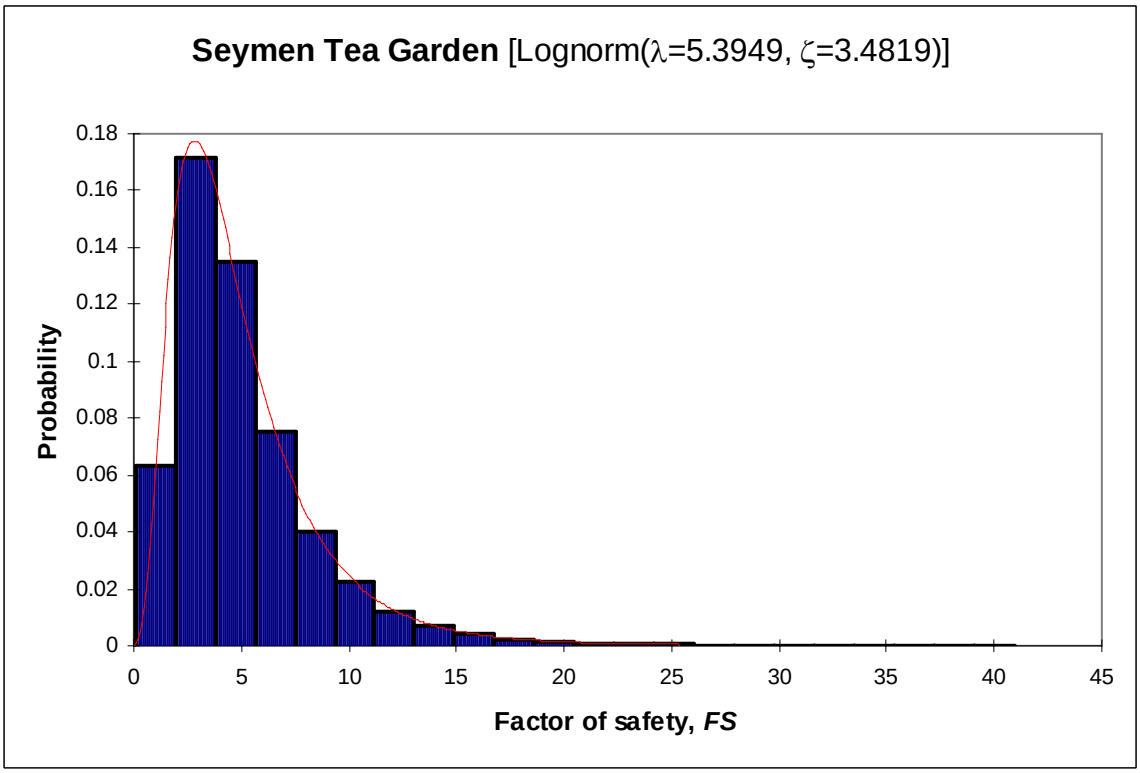

Figure 4.30 Lognormal PDF of factor of safety for the Seymen Tea Garden failure

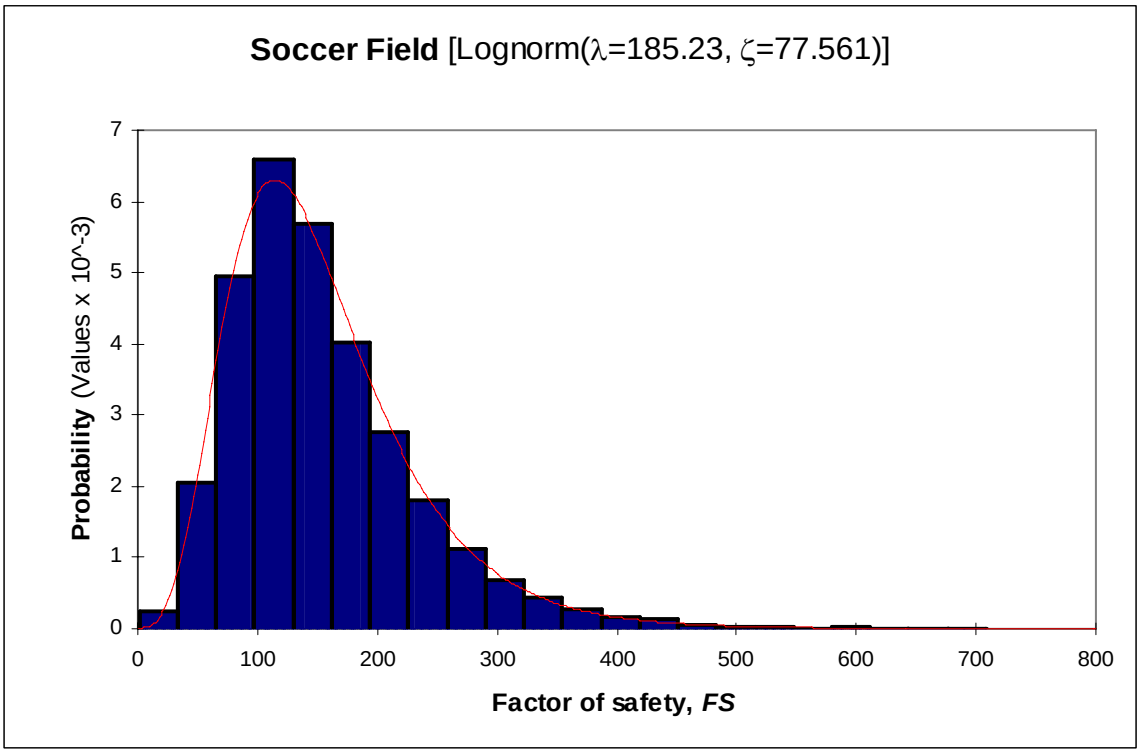

Figure 4.31 Lognormal PDF of factor of safety for the Soccer Field failure

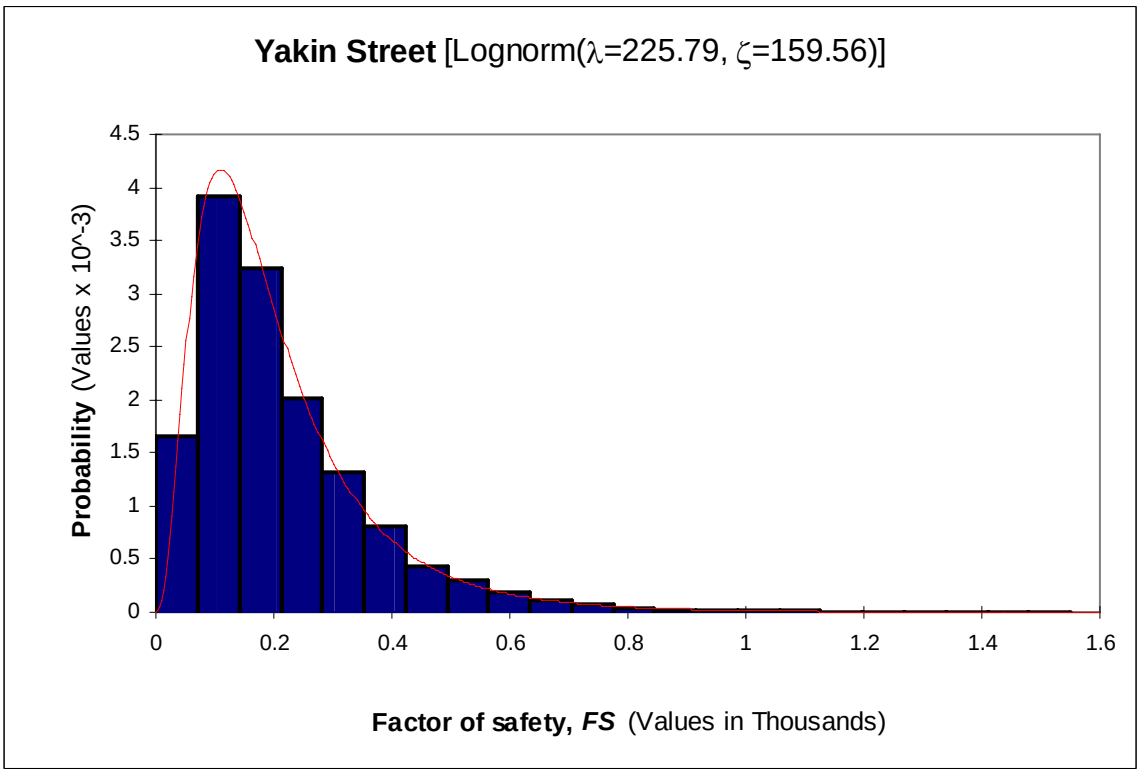

Figure 4.32 Lognormal PDF of factor of safety for the Yakin Street failure

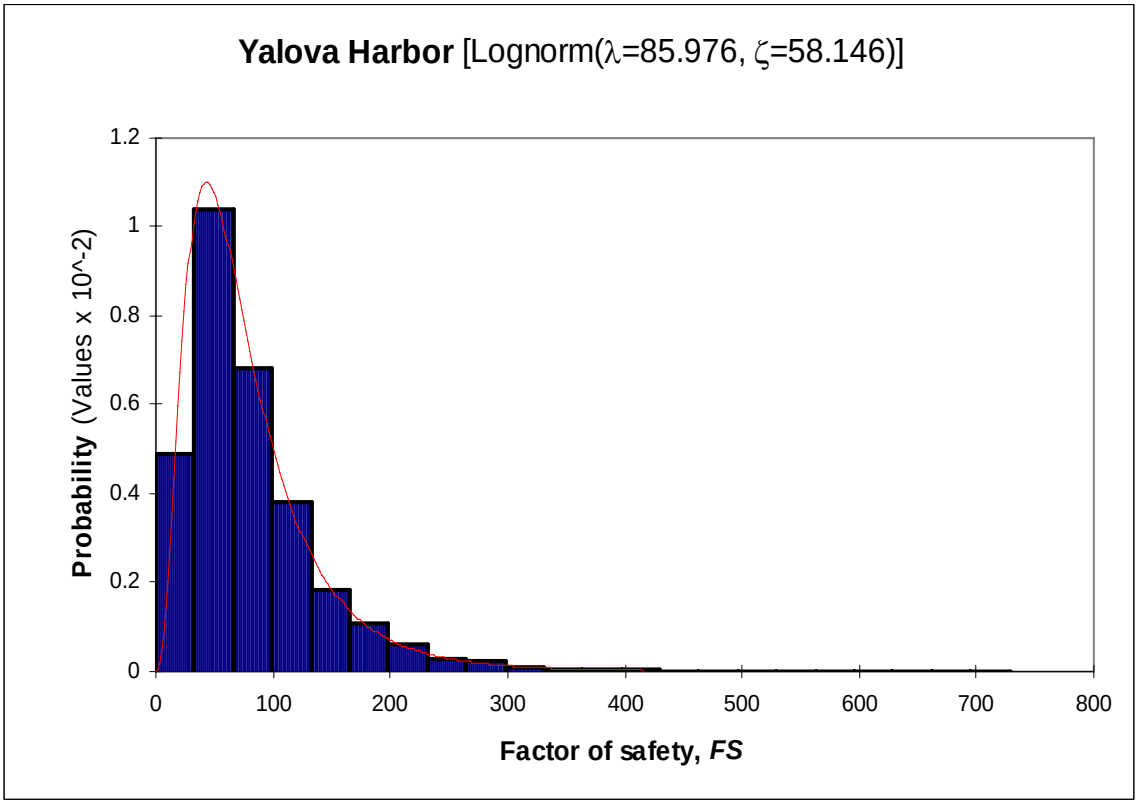

Figure 4.33 Lognormal PDF of factor of safety for the Yalova Harbor failure

Table 4.6 shows comparison of probability of failure from First Order Reliability Method analyses (FORM) and Monte Carlo Simulations (MCS). The results verify that FORM can be used in-place of MCS. Figure 4.34 is the plot of probability of failure from FORM analyses versus probability of failure from MCS. The plot shows that MCS will lead to higher probability of failure.

Table 4.6 Comparison of probability of failure from FORM and Monte Carlo Simulation

Location	Probability of Failure	
	FORM	Monte Carlo Simulation
Cark Canal	0.13%	0.08%
Cumruhiyet	0.05%	0.01%
Degirmendere Nose	1.39%	1.90%
Esme Nose	1.43%	1.77%
Hotel Sapanca	0.13%	0.16%
Police Station	0.07%	0.03%
Seymen Tea Garden	1.74%	2.14%
Soccer Field	0.05%	0.01%
Yakin Street	0.05%	0.01%
Yalova Harbor	0.05%	0.01%

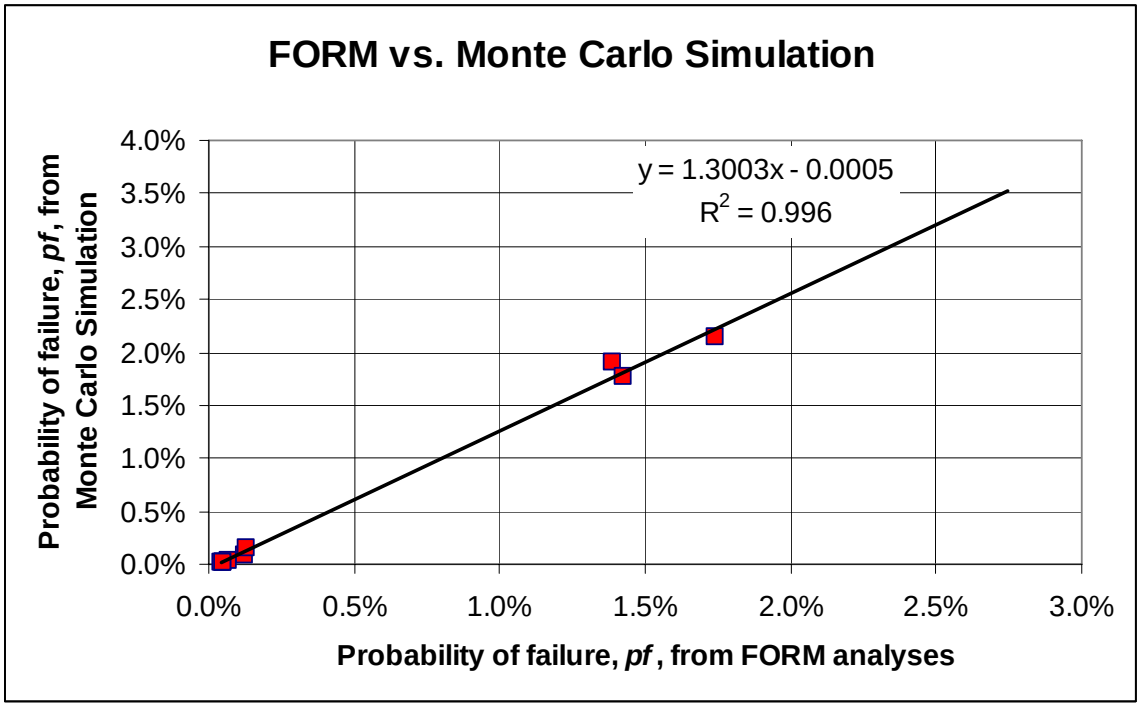

Figure 4.34 Probability of failure from FORM analyses versus probability of failure from Monte Carlo Simulation

The reliability computations are also performed using minimum values of $(N_1)_{60\text{-}cs}$. Table 4.7 shows the summary of the reliability computations of all the cases. Each case is analyzed for factor of safety equal to one, using minimum values of $(N_1)_{60\text{-}cs}$. The reliability index, β, is ranged from 0.089 to 3.280. The probability of failure, *Pf*, is ranged from 0.1% to 46.5%. Reliability computations for each case are presented in Appendix B. Figure 4.35 shows the normal CDF of reliability index from all of the cases. The mean of reliability index, μ, is equal to 2.14. The standard deviation of reliability index, σ, is equal to 1.31.

Table 4.7 Summary of the reliability computations using minimum values of $(N_1)_{60\text{-}cs}$

No.	Location	*FS*	β	*Pf*
1	Cark Canal	1.00	2.520	0.6%
2	Cumruhiyet	1.00	3.241	0.1%
3	Degirmendere Nose	1.00	0.089	46.5%
4	Esme Nose	1.00	0.310	37.8%
5	Hotel Sapanca	1.00	2.039	2.1%
6	Police Station	1.00	2.956	0.2%
7	Seymen Tea Garden	1.00	0.617	26.9%
8	Soccer Field	1.00	3.280	0.1%
9	Yakin Street	1.00	3.242	0.1%
10	Yalova Harbor	1.00	3.117	0.1%

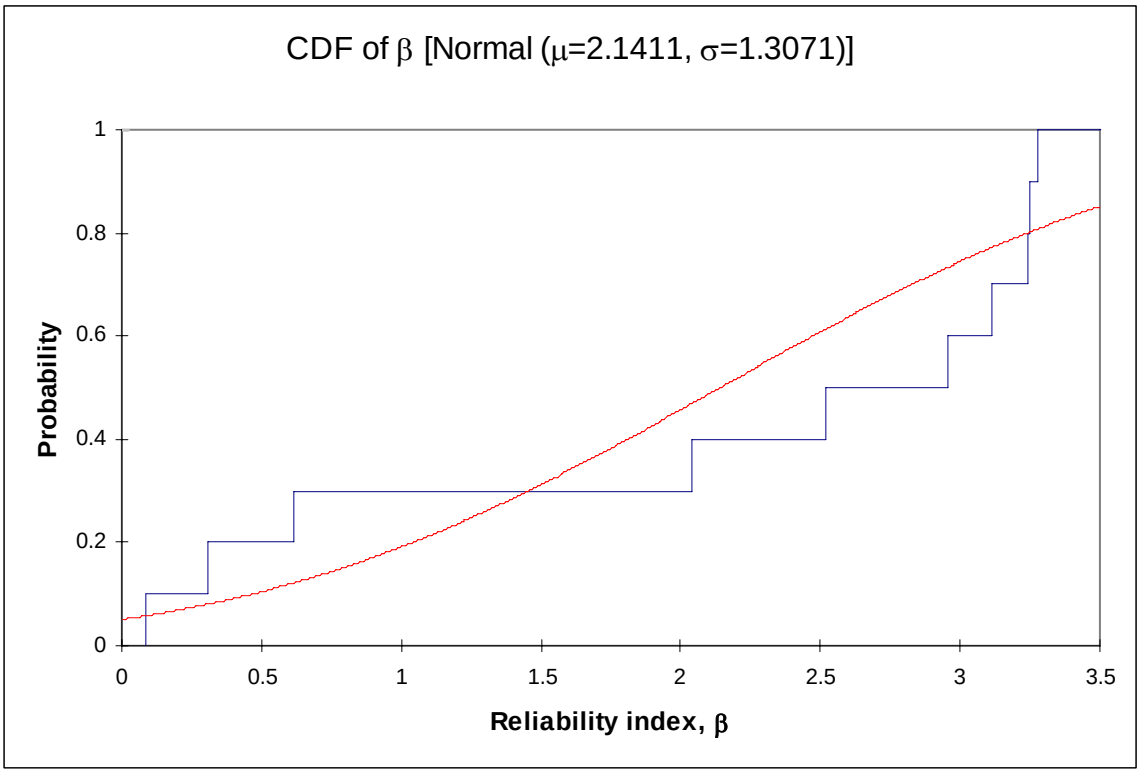

Figure 4.35 Normal CDF of reliability index using minimum values of $(N_1)_{60\text{-}cs}$

4.4 COMPARISON OF DATA FROM THIS STUDY AND PREVIOUS DATA FROM SEED AND HARDER (1990)

Figure 4.36 contains the commonly used relationship from Seed and Harder (1990) to estimate the liquefied shear strength, $S_{u\text{-}LIQ}$, of a cohesionless soil deposit based on the equivalent clean sand SPT blowcount, $(N_1)_{60\text{-}cs}$. This relationship is utilized in this study.

All the corresponding values of liquefied shear strength-SPT blowcounts ($S_{u\text{-}LIQ}$-$(N_1)_{60\text{-}CS}$) from each case of this study are plotted in the Seed and Harder (1990) relationship. The data from this study are represented with red dots. All the data plot between upper bound and lower bound of the Seed and Harder (1990) relationship. The minimum blowcounts are used in this plot. If the mean value are used the data will plot to the right of Seed and Harder (1990) relationship.

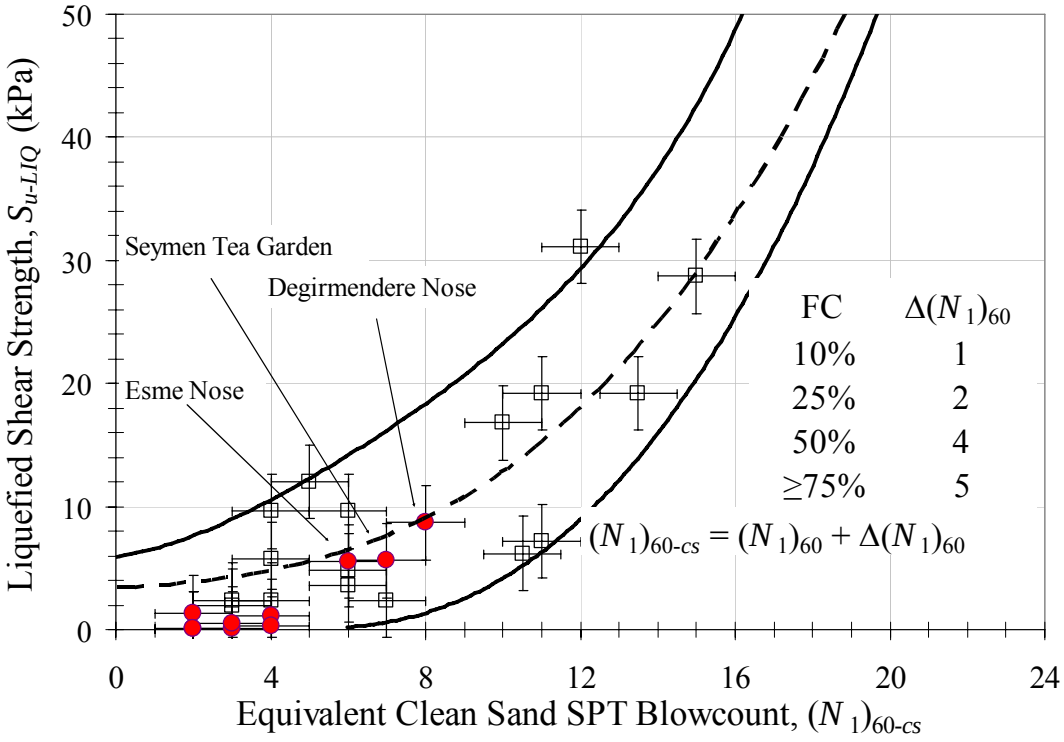

Figure 4.36 Comparison of data from this study and data from Seed and Harder (1990)

CHAPTER 5
CONCLUSIONS

5.1 CONCLUSIONS

Ten case histories were analyzed in this study. The back analyses of the case histories yield liquefied shear strengths, $S_{u\text{-}Liq}$, with mean, μ, ranged from 0.06kPa to 8.68kPa. The standard deviation of liquefied shear strengths, σ, ranged from 0.01kPa to 1.53kPa. The coefficient of variation of liquefied shear strengths, *COV*, ranged from 16.18% to 29.65%. Cases with higher surface slope angle (i.e., Esme Nose, $\alpha = 3.0^{O}$; Seymen Tea Garden, $\alpha = 2.0^{O}$; Degirmendere Nose $\alpha = 8.9^{O}$), yield to significantly high values of liquefied shear strength, ranged from 5.57kPa to 8.68kPa. Other cases with lower surface angle ($\alpha \leq 1.0^{O}$), yield to low values of liquefied shear strength, ranged from 0.06kPa to 1.37kPa.

By implementing Ishihara et al. (1990) slope stability method and Seed and Harder (1990) relationship in a spreadsheet (Low and Tang, 2004), the reliability index computations of all the cases were performed. Each case is analyzed for a factor of safety equal to one, using mean values of $(N_1)_{60\text{-}cs}$. The reliability index, β, ranged from 2.110 to 3.314. The probability of failure, *Pf*, ranged from 0.0005 to 0.0174 (0.05% to 1.74%). The plots between reliability index, β, and probability of failure, *Pf*, resulted in a simple logarithmic relationship, $Pf = -0.0362Ln(\beta) + 0.0429$, with an R^2 value of 0.9757.

Monte Carlo Simulations are performed to verify the reliability index, β, from FORM analyses. The simulations are performed to develop the probability density function of factor of safety for each case. The probability of the factor of safety, *FS*, is less than 1.0 ranged from 0.01% to 1.90%. The results confirm that FORM can be used as an alternative to Monte Carlo Simulation. Plots of probability of failure from FORM

analyses versus probability of failure from Monte Carlo Simulation, show a tendency that Monte Carlo Simulation yields probability of failure slightly higher than from FORM analysis. This is attributed to the truncation of PDFs used in MCS.

The probability of failure calculated using mean values of $(N_1)_{60\text{-}cs}$ ranged from 0.05% to 1.74% which are very low. Therefore, it is not recommended to use mean values of $(N_1)_{60\text{-}cs}$ for design.

The reliability index computations are also performed using minimum values of $(N_1)_{60\text{-}cs}$. The reliability index, β, ranged from 0.089 to 3.280. The probability of failure, *Pf*, ranged from 0.1% to 46.5%. There is a correlation between low probability values and low values of $(N_1)_{60\text{-}cs}$ and $S_{u\text{-}Liq}$.

The liquefied shear strengths, $S_{u\text{-}Liq}$, from back analyses with corresponding value of equivalent clean sand SPT blowcount, $(N_1)_{60\text{-}cs}$, are plotted on the Seed and Harder (1990) relationship. The data from this study plot between upper and lower bound (±1 standard deviation) of the Seed and Harder (1990) relationship. The equivalent clean sand SPT blowcount, $(N_1)_{60\text{-}cs}$, are represented by minimum value of blowcount, if the mean value are used the data will plot to the right of the Seed and Harder (1990) relationship.

5.2 FUTURE STUDY

This study shows that the Ishihara et al. (1990) simplified slope stability method is particularly suited to slopes which failed by flow liquefaction. Other flow liquefaction cases may need to be analyzed using different slope stability methods (e.g., Janbu's method; Spencer's method; Newmark's method).

The current relationships between back-calculated undrained liquefied shear strength, $S_{u\text{-}Liq}$, and the equivalent clean sand SPT blowcount, $(N_1)_{60\text{-}cs}$, are based on a limited database. This study adds 10 new data points to the database, but the data remain widely scattered. Therefore, there is a need to expand the database by analyzing additional flow liquefaction case histories triggered by other earthquakes (e.g., the 1990

Luzon earthquake; the 1995 Kobe earthquake; the 1999 Chi-Chi earthquake; the 2001 Nisqually earthquake).

REFERENCES

Alonso, E. (1976). "Risk Analysis of Slopes and Its Application to slopes in Canadian Sensitive Clays." *Geotechnique*, 26, 453-472.

Ambraseys, N. N. (1970). "Some Characteristic Features of the Anatolian Fault Zone." *Tectonophysics*, 9, 143-165.

Anderson, Loren R., Sharp, Kevan D., Bowles, David, S., and Canfield, Ronald. V. (1984). "Application of Methods of Probabilistic Characterization of Soil Properties." *Probabilistic Characterization of Soil Properties: Bridge Between Theory and Practice, Proceedings of a Symposium*, ASCE, Atlanta, Georgia, pp. 90-105.

Ang, A. H. –S., and Tang, W. H. (1975). *Probability Concepts in Engineering Planning and Design, Vol. I, Basic Principles*. John Wiley & Sons, New York.

Ang, A. H. –S., and Tang, W. H. (1984). *Probability Concepts in Engineering Planning and Design, Vol. II, Decision, Risk and Reliability*. John Wiley & Sons, New York.

Baecher, Gregory B., and Christian, John T. (2003). *Reliability and Statistics in Geotechnical Engineering*. John Wiley & Sons, New York.

Baziar, Mohammad H., and Dobry, Ricardo (1995). "Residual Strength and Large-Deformation Potential of Loose Silty Sands." *Journal of Geotechnical Engineering*, ASCE, Vol. 121, No. 12, pp. 896-906.

Bendimerad, F., Johnson, L., Coburn, A., Rahnama, M., and Morrow, G. (2000). *Kocaeli, Turkey Earthquake Event Report*. Risk Management Solutions Inc., Menlo Park, California.

Benjamin, J. R., and Cornell, C. A. (1970). *Probability, Statistics, and Decision for Civil Engineers*. McGraw-Hill, New York.

Bishop, A. W. (1955). "The Use of the Slip Circle in the Stability Analysis of Slopes." *Geotechnique*, Vol. 5, No. 1, pp. 7-17.

Bozkurt, B., Winchester, J. A., and Piper, J. D. A. (2000). *Tectonics and Magmatism in Turkey and the Surrounding Area*. Geological Society, London, Special Publications, **173**.

Boulanger, Ross W., Mejia, Lelio H., and Idriss, Izzat M. (1997). "Liquefaction at Moss Landing during Loma Prieta Earthquake." *Journal of Geotechnical and Geoenvironmental Engineering*, ASCE, Vol. 123, No. 5, pp. 453-467.

Bray, Jonathan D., Sancio, Rodolfo B., Durgunoglu, T., Onalp, A., Youd, T. Leslie, Stewart, Jonathan P., Seed, Raymond B., Cetin, Onder K., Bol, E., Baturay, M. B., Christensen, C., and Karadayilar, T. (2004). "Subsurface Characterization at Ground Failure Sites in Adapazari, Turkey." *Journal of Geotechnical and Geoenvironmental Engineering*, ASCE, Vol. 130, No. 7, pp. 673-685.

Brinkmann, R. (1976). *Geology of Turkey*. Elsevier Scientific Publishing Company, Amsterdam, Netherlands.

Campbell, Angus S. (1971). *Geology and History of Turkey*. The Petroleum Exploration Society of Libya, Tripoli, Libya.

Casagrande, Arthur (1936). "Characteristics of Cohesionless Soils Affecting the Stability of Slopes and Earth Fills." *Journal of the Boston Society of Civil Engineers*, pp. 257-276.

Casagrande, Arthur (1975). "Liquefaction and Cyclic Deformation of Sands, a Critical Review." *Proceedings of the Fifth Pan American Conference on Soil Mechanics and Foundation Engineering*, Buenos Aires, Argentina, Vol. 1, pp. 80-133.

Castro, Gonzalo, Poulos, Steve J., and Leathers, Francis D. (1985). "Re-Examination of Slide of Lower San Fernando Dam." *Journal of Geotechnical Engineering*, ASCE, Vol. 111, No. 9, pp. 1093-1107.

Castro, G., Keller, T. O, and Boynton, S. S. (1989). "Re-Evaluation of the Lower San Fernando Dam: Report 1, an Investigation of the February 9, 1971 Slide." *U.S. Army Corps of Engineers Contract Report GL-89-2*, Vols. 1 and 2, U.S. Army Corps of Engineers Waterways Experiment Station, Vicksburg, Mississippi.

Castro, G., Seed, Raymond B., Keller, Thomas O., and Seed, H. Bolton (1992). "Steady-State Strength Analysis of Lower San Fernando Dam Slide." *Journal of Geotechnical Engineering*, ASCE, Vol. 118, No. 3, pp. 406-424.

Cetin, K.O., Youd, T.L., Seed, R.B., Bray, J.D., Sancio, R., Lettis, W., Yilmaz, M.T., and Durgunoglu, H.T. (2002), "Liquefaction-Induced Deformations at Hotel Sapanca during Kocaeli (Izmit), Turkey Earthquake." *Soil Dynamics and Earthquake Eng*ineering, Vol. 22, pp. 1083-1092.

Cetin, K. Onder, Isik, Nihat, and Unutmaz, Berna (2004). "Seismically Induced Landslide at Degirmendere Nose, Izmit Bay During Kocaeli (Izmit)-Turkey Earthquake." *Soil Dynamics and Earthquake Engineering*, Elsevier, Vol. 24, pp. 189-197.

Chandler, Douglass Scott (1996). "Monte Carlo Simulation to Evaluate Slope Stability." *Uncertainty in the Geologic Environment: From Theory to Practice, Proceedings of Uncertainty '96*, ASCE, Madison, Wisconsin, Vol. 1, pp. 474-493.

Chen, X., and Lind, N. C. (1983). "Fast Probability Integration by Three-Parameter Normal Tail Approximation." *Stuctural Safety*, Vol. 1, pp. 269-276.

Chowdury R. N. (1984). "Recent Developments in Landslide Studies: Probabilistic Methods State-of-the-Art-Report." *Proceedings, IV International Symposium on Landslides*, Toronto, Canada, Vol. 1, pp. 209-228.

Christian, John T., Ladd, Charles C., and Baecher, Gregory B. (1994). "Reliability Applied to Slope Stability Analysis." *Journal of Geotechnical Engineering*, ASCE, Vol. 120, No. 12, pp. 2180-2207.

Coduto, Donald P. (1999). *Foundation Design, Principles and Practices*. Prentice Hall, Englewood Cliffs, New Jersey.

Davis, Alton P., Castro, Gonzalo, and Poulos, Steve J. (1988). "Strengths Backfigured from Liquefaction Case Histories." *Proceedings: Second International Conference on Case Histories in Geotechnical Engineering*, Shamsher Prakash., St. Louis, Missouri, Vol. III, pp. 1693-1701.

Doglioni, C., Agostini, S., Crespi, M., Innocenti, F., Manetti, P., Riguzzi, F., and Savascin, Y. (2002). "On the Extension in Western Anatolia and the Aegean Sea." *Journal of the Virtual Explorer*, Vol. 8, pp. 169-183.

Duncan, J. Michael (1992). "State-of-the-Art Static Stability and Deformation analysis." *Stability and Performance of Slopes and Embankments: II*, Geotechnical Special Publication 31, ASCE, Reston, VA, pp. 222-266.

Duncan, J. Michael (1996). “State of the Art: Limit Equilibrium and Finite-Element Analysis of Slopes.” *Journal of Geotechnical Engineering*, ASCE, Vol. 122, No. 7, pp. 577-596.

Duncan, J. Michael (2000). “Factors of Safety and Reliability in Geotechnical Engineering.” *Journal of Geotechnical and Geoenvironmental Engineering*, ASCE, Vol. 126, No. 4, pp. 307-316.

Duncan, J. M., and Wright, S. G. (2005). *Soil Strength and Slope Stability*. John Wiley & Sons, New York.

Erdik, M. (2000). *Report on 1999 Kocaeli and Duzce (Turkey) Earthquakes.* Bogazici University, Istanbul, Turkey.

Finn, W. D. L. (1981). “Liquefaction Potential: Developments Since 1976.” *1st International Conference on Recent Advances in Geotechnical Earthquake Engineering and Soil Dynamics*. St. Louis, Missouri, pp. 655-681.

Greco, V. R. (1996). “Efficient Monte Carlo Technique for Locating Critical Slip Surface.” *Journal of Geotechnical Engineering*, ASCE, Vol. 122, No. 7, pp. 517-525.

Gu, W. H., Morgenstern, N. R., and Robertson, P. K. (1993). “Progressive Failure of Lower San Fernando Dam.” *Journal of Geotechnical Engineering*, ASCE, Vol. 119, No. 2, pp. 333-349.

Gutierrez, M., Duncan, J. M., Woods, C., and Eddy, M. (2003). Development of a Simplified Reliability-Based Method for Liquefaction Evaluation. Final Technical Report. Virginia Polytechnic Institute and State Institute. Blacksburg, Virginia.

Harr, Milton E. (1987). *Reliability-Based Design in Civil Engineering*. McGraw-Hill, New York.

Hasofer, Abraham M., and Lind, Niels C. (1974). “Exact and Invariant Second-Moment Code Format.” *Journal of Engineering Mechanics*, ASCE, Vol. 100, No. EM1, pp. 111-121.

Ishihara, K., Yasuda, S., and Yoshida, Y. (1990). “Liquefaction-Induced Flow Failure of Embankments and Residual Strength of Silty Sands.” *Soils and Foundations*, Vol. 30, No. 3, pp. 69-80.

Ishihara, K., Okusa, S., Oyagi, N., and Ischuk, A. (1990). "Liquefaction-Induced Flow Slide in the Collapsible Loess Deposit in Soviet Tajik." *Soils and Foundations*, Vol. 30, No. 4, pp. 73-89.

Ishihara, K., Verdugo, R., and Acacio, A. A. (1991). "Characterization of Cyclic Behavior of Sand and Post-Seismic Stability Analyses." *Proc., 9th Asian Regional Conf. Soil Mech. Found. Eng.*, Vol. 2, Bangkok, Thailand, pp. 45-67.

Ishihara, K. (1993). "Liquefaction and Flow Failure during Earthquakes." *Geotechnique*, The Institution Of Civil Engineers, Vol. 43, No. 3, pp. 351-415.

Ishihara, K. (2002). "Failure of Slopes and Soil Property Characterization." *The Second Lumb Lecture*, Hong Kong, pp. 1-31.

Janbu, Nilmar (1968). "Slope Stability Computations." *Soil Mech. And Found. Engrg. Rep.*, The Technical University of Norway, Trondheim, Norway.

Konrad, J. M., and Watts, B. D. (1995). "Undrained Shear Strength for Liquefaction Flow Failure Analysis." *Canadian Geotechnical Journal*, Vol. 32, No. 5, pp. 783-794.

Kramer, Steven L. (1996). *Geotechnical Earthquake Engineering*. Prentice Hall, Upper Saddle River, New Jersey.

Kulhawy, Fred H. (1992). "On the Evaluation of Static Soil Properties." *Stability and Performance of Slopes and Embankments-II, Proceedings of a Specialty Conference*, ASCE, Berkeley, California, Vol. 1, pp. 95-115.

Lacasse, Suzanne, and Nadim, Farrokh (1996). "Uncertainties in Characterizing Soil Properties." *Uncertainty in the Geologic Environment: From Theory to Practice, Proceedings of Uncertainty '96*, ASCE, Madison, Wisconsin, Vol. 1, pp. 49-75.

Low, B. K., and Tang, Wilson H. (1997). "Reliability Analysis of Reinforced Embankments on Soft Ground." *Canadian Geotechnical Journal*, Vol. 34, No. 5, pp. 672-685.

Low, B. K., and Tang, Wilson H. (1997). "Probabilistic Slope Stability Analysis Using Janbu's Generalized Procedure of Slices." *Computers and Geotechnics*, Vol. 21, No. 2, pp. 121-142.

Low, B. K., and Tang, W. H. (2004). "Reliability Analysis Using Object-Oriented Constraint Optimization." *Stuctural Safety*, Vol. 26, pp. 69-89.

Low, B. K. (2003). "Practical Probabilistic Slope Stability Analysis." *Proceedings, Soil and Rock America 2003, 12th Panamerican Conference on Soil Mechanics and Geotechnical Engineering and 39th U.S. Rock Mechanics Symposium*, M.I.T., Cambridge, Massachusetts, Vol. 2, pp. 2777-2784.

Malkawi, A. I. H., Hassan, W. F., and Sarma, S. K. (2001). "An Efficient Search Method for Finding the Critical Circular Slip Surface using the Monte Carlo Technique." *Canadian Geotechnical Journal*, Vol. 38, No. 5, pp. 1081-1089.

Metropolis, N. (1987). "The Beginning of the Monte Carlo Method." *Los Alamos Science*, Special Issue.

Ming, H. Y., and Li, X. S. (2003). "Fully Coupled Analysis of Failure and Remediation of Lower San Fernando Dam." *Journal of Geotechnical and Geoenvironmental Engineering*, ASCE, Vol. 129, No. 4, pp. 336-349.

Morgenstern, N. R., and Price, V. E. (1965). "The Analysis of the Stability of General Slip Surfaces." *Geotechnique*, Vol. 15, No. 1, pp. 79-93.

Neugebauer, J. (1995). "Structures and Kinematics of the North Anatolian Fault Zone, Adapazari-Bolu Region, Northwest Turkey." *Tectonophysics*, 243, 119-134.

Olgun, C. G. (2005). *Documentation of 1999 Kocaeli/Duzce, Turkey Earthquake*. Virginia Polytechnic Institute & State University, Blacksburg, VA.

Olson, Scott M., and Stark, Timothy D. (2002). "Liquefied Strength Ratio from Liquefaction Flow Failure Case Histories." *Canadian Geotechnical Journal*, Vol. 39, No. 3, pp. 629-647.

Olson, Scott M., and Stark, Timothy D. (2003). "Yield Strength Ratio and Liquefaction Analysis of Slopes and Embankments." *Journal of Geotechnical and Geoenvironmental Engineering*, ASCE, Vol. 129, No. 8, pp. 727-737.

Palisade Corporation (1996). *@RISK: Risk Analysis and Simulation add-in of Microsoft Excel or Lotus 1-2-3*. Palisade Corporation, Newfield, N.Y.

PEER (2000). Documneting Incidents of Ground Failure Resulting from the August 17, 1999 Kocaeli, Turkey Earthquake. PEER, Berkeley, CA. (http://peer.berkeley.edu/turkey/adapazari/).

Poulos, Steve J., Castro, Gonzalo, and France, John W. (1985). "Liquefaction Evaluation Procedure." *Journal of Geotechnical Engineering*, ASCE, Vol. 111, No. 6, pp. 772-792.

Rackwitz, R., and Fiessler, B. (1978). "Structural Reliability Under Combined Random Load Sequences." *Computers & Structures*, 9, pp. 484-494.

Rathje, Ellen M., Karatas, I., Wright, Stephen G., and Bachhuber, J. (2004). "Coastal Failures during the 1999 Kocaeli Earthquake in Turkey." *Soil Dynamics and Earthquake Engineering*, Elsevier, Vol. 24, pp. 699-712.

Robertson, Peter K. (1994). "Suggested Terminology for Liquefaction." *47th Canadian Geotechnical Conference*, Halifax, Nova Scotia, pp. 277-286.

Robertson, P. K., and Fear, C. E. (1995). "Liquefaction of Sands and Its Evaluation." *Proceedings of the 1st International Conference on Earthquake Geotechnical Engineering*. Edited by K. Ishihara. A. A. Balkema, Amsterdam, pp. 1253-1289.

Sancio, R.B., Bray, J.D., Stewart, J.P., Youd, T.L., Durgunoglu, H.T., Onalp, A. Seed, R.B., Christensen, C., Baturay, M.B., and Karadayilar, T. (2002), "Correlation Between Ground Failure and Soil Conditions in Adapazari, Turkey," *Soil Dynamics and Earthquake Engineering*. Vol. 22, no. 9-12, pp. 1093-1102.

Seed, H. B., Lee, K. L., and Idriss, I. M. (1973). "Analysis of the Slide in the San Fernando Dams during the Earthquake of February 9, 1971." *Earthquake Engineering Research Center* 73-2, University of California, Berkeley, California.

Seed, H. B. (1979). "Considerations in the Earthquake-Resistant Design of Earth and Rockfill Dams." *Geotechnique*, The Institution Of Civil Engineers, Vol. 29, No. 3, pp. 215-263.

Seed, H. Bolton (1987). "Design Problems in Soil Liquefaction." *Journal of Geotechnical Engineering*, ASCE, Vol. 113, No. 8, pp. 827-845.

Seed, H. B., Seed, R. B., Harder, L. F. Jr., and Jong, H.-L. (1989). "Re-Evaluation of the Lower San Fernando Dam: Report 2, Examination of the Post-Earthquake Slide of February 9, 1971." *U.S. Army Corps of Engineers Contract Report GL-89-2*, U.S. Army Corps of Engineers Waterways Experiment Station, Vicksburg, Mississippi.

Seed, Raymond B., and Harder, Leslie F. Jr. (1990). “SPT-Based Analysis of Cyclic Pore Pressure Generation and Undrained Residual Strength.” *Proceedings of Memorial Symposium for H. Bolton Seed*, J Michael Duncan ed., BiTech Publishers, Vancouver, B. C., Canada, Vol. 2, pp. 351-376.

Spencer, E. (1967). “A Method of Analysis of the Stability of Embankments Assuming Interslice Forces.” *Geotechnique*, Vol. 17, pp. 11-26.

Stark, Timothy D., and Mesri, Gholamreza (1992). “Undrained Shear Strength of Liquefied Sands for Stability Analysis.” *Journal of Geotechnical Engineering*, ASCE, Vol. 118, No. 11, pp. 1727-1747.

Tang, W. H., Yucemen, M. S., and Ang, A. H. S. (1976). “Probability-Based Short Term Design of Slopes.” *Canadian Geotechnical Journal*, Vol. 13, pp. 201-215.

Tobutt, D. C. (1982). “Monte Carlo Simulation Methods for Slope Stability.” *Computer and Geosciences*, Vol. 8, No. 2, pp. 199-208.

USGS (2000). “Implications for Earthquake Risk Reduction in the United States from the Kocaeli, Turkey, Earthquake of August 17, 1999.” *U.S. Geological Survey Circular 1193.*

Whitman, V. W. (1984). “Evaluating Calculated Risk in Geotechnical Engineering.” *Journal of Geotechnical Engineering*, ASCE, Vol. 110, No. 2, pp. 145-188.

Wride, C. E. (Fear), McRoberts, E. C., and Robertson, P. K. (1999). “Reconsideration of Case Histories for Estimating Undrained Shear Strength in Sandy Soils.”

Vasquez-Herrera, A., and Dobry, R. (1989). “Re-Evaluation of the Lower San Fernando Dam: Report 3, the Behavior of Undrained Contractive Sand and Its Effect on Seismic Liquefaction Flow Failures of Earth Structures.” *U.S. Army Corps of Engineers Contract Report GL-89-2*, U.S. Army Corps of Engineers Waterways Experiment Station, Vicksburg, Mississippi.

APPENDIX A

APPENDIX A

Appendix A contains detailed discussions pertaining to the 1999 Kocaeli earthquake and cases of liquefaction instability where detailed site investigations where performed by Zetas Corporation (Sancio et al., 2002). Data and photos in Appendix are from other researchers including PEER (2000), Cetin et al. (2002), Cetin et al. (2004), Rathje et al. (2004), and Olgun (2005).

Cark Canal

The 1999 Kocaeli earthquake triggered extensive liquefaction failure in the city of Adapazari. The failures were observed in the area around Cark Canal. The failures were causing the movement of soil mass toward the canal.

Figure A.1 - Photograph of Cark Canal site (PEER, 2000)

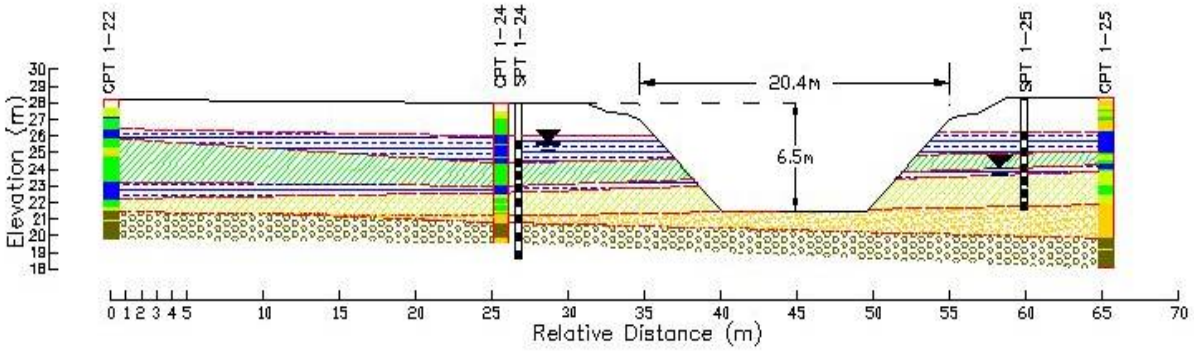

Figure A.2 - Cross section of Cark Canal site (PEER, 2000)

Source of data:

PEER (2000). Documenting Incidents of Ground Failure Resulting from the August 17, 1999 Kocaeli, Turkey Earthquake. Berkeley, CA. (http://peer.berkeley.edu/turkey/adapazari/).

Soil Type/Description:

The site is moderately stratified with alternating strata of loose silts, clays, and sands from a depth of 1.8m to 6.2m. The borings indicate that depths below 6.2m contain fine to medium sand grading into gravel with depth. The top 1.8m at the site contain man-made fill.

Failure modes:

One possible failure mode involves liquefaction of a cohesionless stratum within the loose stratified layer. It is possible that a film of water may have formed along the boundary high and low permeable materials.

Failure surface/ground surface slope angle, α:

The slope angle is estimated from the above diagram. The surface angle is approximately 1.0^{O}, with an assumed coefficient of variation of 10% (standard deviation equals 0.1^{O}).

Depth to water table, H_d:

The depth to the water table at the site is estimated to have a mean of 2.6m, with a standard deviation of 0.26m.

Height of water above the failure surface, H_w:

The failure surface is assumed to go through the middle of the stratified layer (which occurs at a depth of 4.4m). The height of water above the failure surface is therefore 1.8m on average, with an assumed coefficient of variation of 30%.

Saturated unit weight of soil above the failure surface, γ_{sat}:

The saturated unit weight of soil above the failure surface is estimated to be $20.5 kN/m^3$ based on typical unit weights of soils (Coduto, 1999). Assuming a COV of 5%, the standard deviation is equal to $1.025 kN/m^3$.

Dry unit weight of soil above the water table, γ_d:

The dry unit weight of soil above the water table is estimated to be 17.5kN/m^3 based on typical unit weights of soils (Coduto, 1999). Assuming a COV of 5%, the standard deviation is equal to 0.875kN/m^3.

Fines content, FC:

The fines content in the stratified layer range from 33% to 99%. Fines contents were estimated from seven samples within the stratified layer; 33%, 65%, 78%, 80%, 90%, 98%, and 99% (μ = 77.6%, σ = 23.0%, COV = 29.7%). It should be noted that the fines content of 33% corresponds to silty sand located roughly in the middle of the stratified layer.

SPT data:

The uncorrected blowcounts, N_M, in the stratified layer range from 3 to 8 blows per 30cm. Uncorrected blowcounts were obtained from 5 samples within the stratified layer; 3, 4, 5, 6, and 8 (μ = 5.2, σ = 1.9, and COV = 37.0%).

The minimum uncorrected blowcount in the stratified layer occurs within a CL classified material. The lowest uncorrected blowcount occurring in a sandy or silty seam within the stratified layer is 4 at a depth of 2.5m.

Cumhuriyet Avenue

Cumruhiyet Avenue was the other area of the city of Adapazari where liquefaction failure also occurred. This site is in the downtown area of the city Adapazari. The failures were causing damage to buildings in this area.

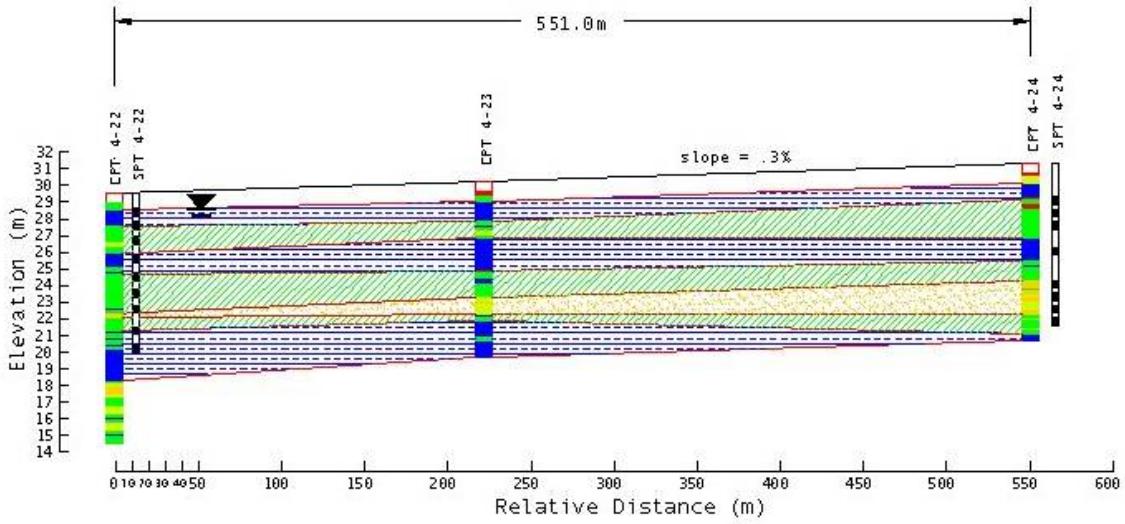

Figure A.3 - Cross section of Cumruhiyet Avenue site (PEER, 2000)

Source of data:

PEER (2000). Documenting Incidents of Ground Failure Resulting from the August 17, 1999 Kocaeli, Turkey Earthquake. Berkeley, CA. (http://peer.berkeley.edu/turkey/adapazari/).

Soil Type/Description:

The top 1.5m at this site contain fill and high plastic silty clays. From 1.5m to 8m the soils are predominately loose ML soils with low plasticity. Below 8m the material consists of high plasticity silty clays (CH).

Failure modes:

One possible failure mode involves liquefaction of the loose cohesionless soils within the ML stratum (1.5m to 8m).

Failure surface/ground surface slope angle, α:

From the cross section shown above, the surface is approximately 0.3% equal to 0.172^{O}. Assuming a COV of 10%, the standard deviation is equal to 0.0172^{O}.

Depth to water table, H_d:

The depth to the water table at the site is estimated to have a mean of 1.1m, with a standard deviation of 0.11m.

Height of water above the failure surface, H_w:

The failure surface is assumed to go through the middle of the stratified layer (which occurs at a depth of 4.7m). The height of water above the failure surface is therefore 3.6m on average, with an assumed coefficient of variation of 30%.

Saturated unit weight of soil above failure surface, γ_{sat}:

The saturated unit weight of soil above the failure surface is estimated to be $16.0kN/m^3$ based on typical unit weights of ML and CH soils (Coduto, 1999). Assuming a COV of 5% the standard deviation is equal to $0.8kN/m^3$.

Dry unit weight of soil above water table, γ_d:

The dry unit weight of soil above the water table is estimated to be $15.0kN/m^3$ based on typical unit weights of soils (Coduto, 1999). Assuming a COV of 5% the standard deviation is equal to $0.75kN/m^3$.

Fines content, FC:

The loose ML stratum has non-plastic fines of 54%, 54%, 89%, 97%, 99, 99%, and 100%. The fines content of the ML stratum has a mean of 84.6% and a standard deviation of 21.2%.

SPT data:

The loose ML stratums with occasional CH and CL material (depths 1.5m to 8m) has uncorrected blowcounts of 3, 3, 4, 4, 4, and 14. The mean uncorrected blowcount is 5.3 with a

standard deviation of 4.3. The CH material below 8m has uncorrected blowcounts of 5 and 8 blowcounts.

The minimum blowcount of 3 within the loose ML stratum occurs at a depth 3.5m to 5.5m.

Degirmendere Nose

The 1999 Kocaeli earthquake triggered liquefaction failures in the city of Degirmendere. The site is located in the north area of the city on the shore of Izmit Bay. The liquefaction failure was causing the movement of a large body of soil into the Izmit Bay.

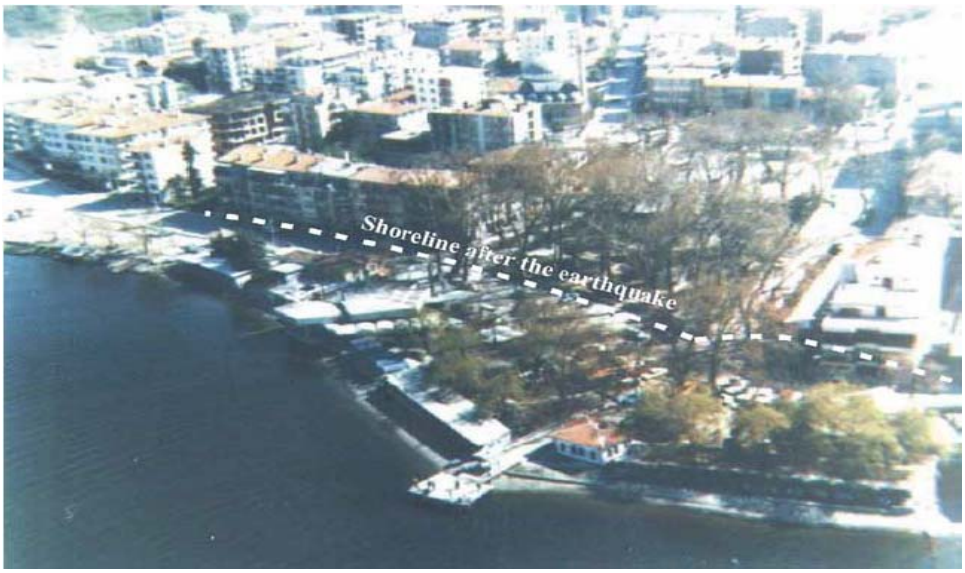

Figure A.4 - Photograph of Degirmendere Nose before the 1999 Kocaeli earthquake (Cetin et al., 2004)

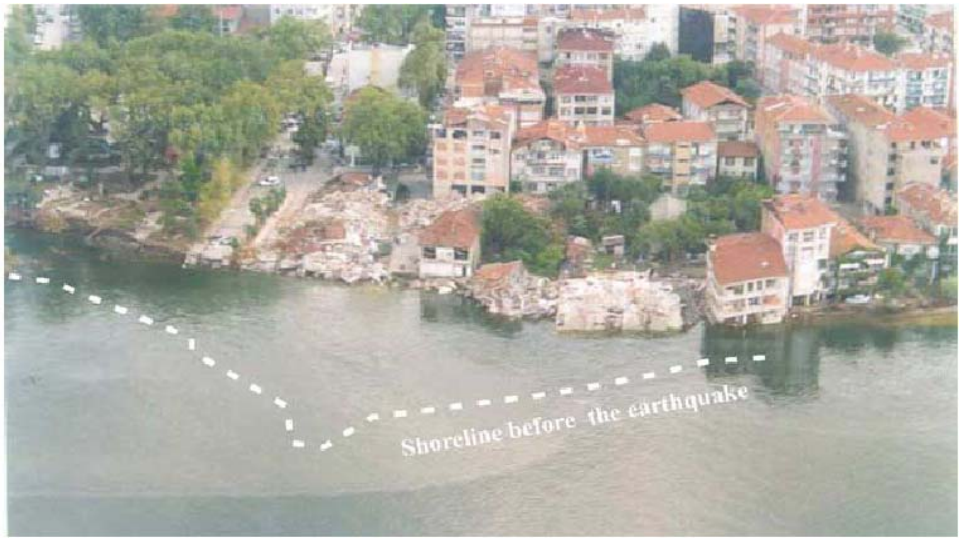

Figure A.5 - Photograph of Degirmendere Nose after the 1999 Kocaeli earthquake (Cetin et al., 2004)

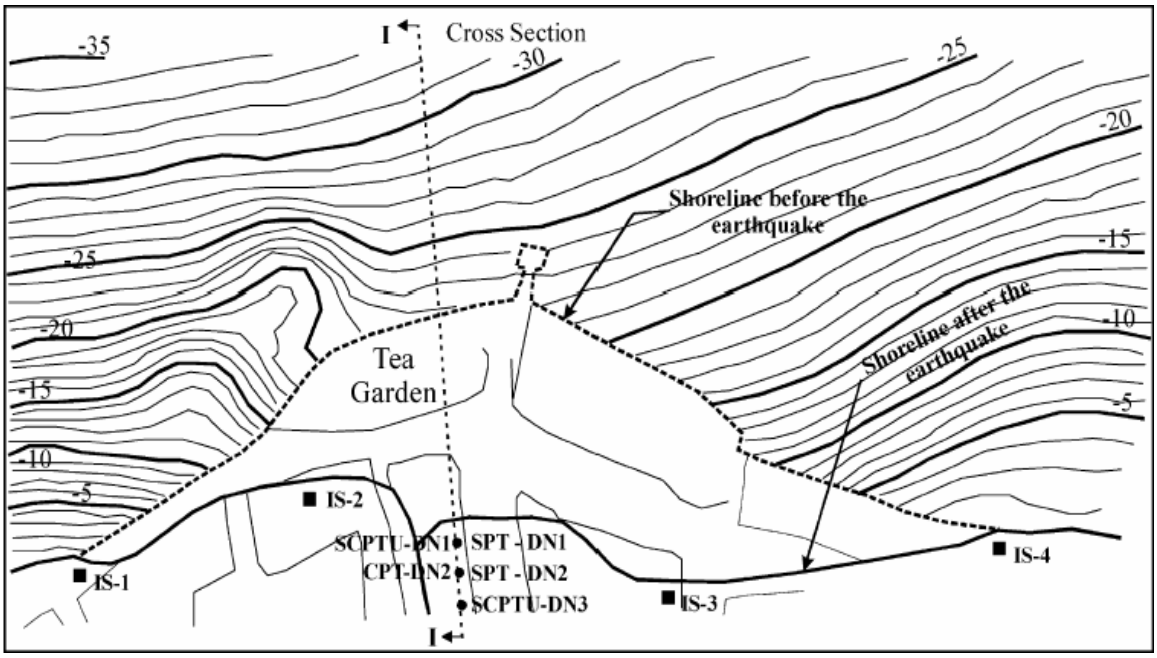

Figure A.6 - Bathymetry map of Degirmendere Nose site (Cetin et al., 2004)

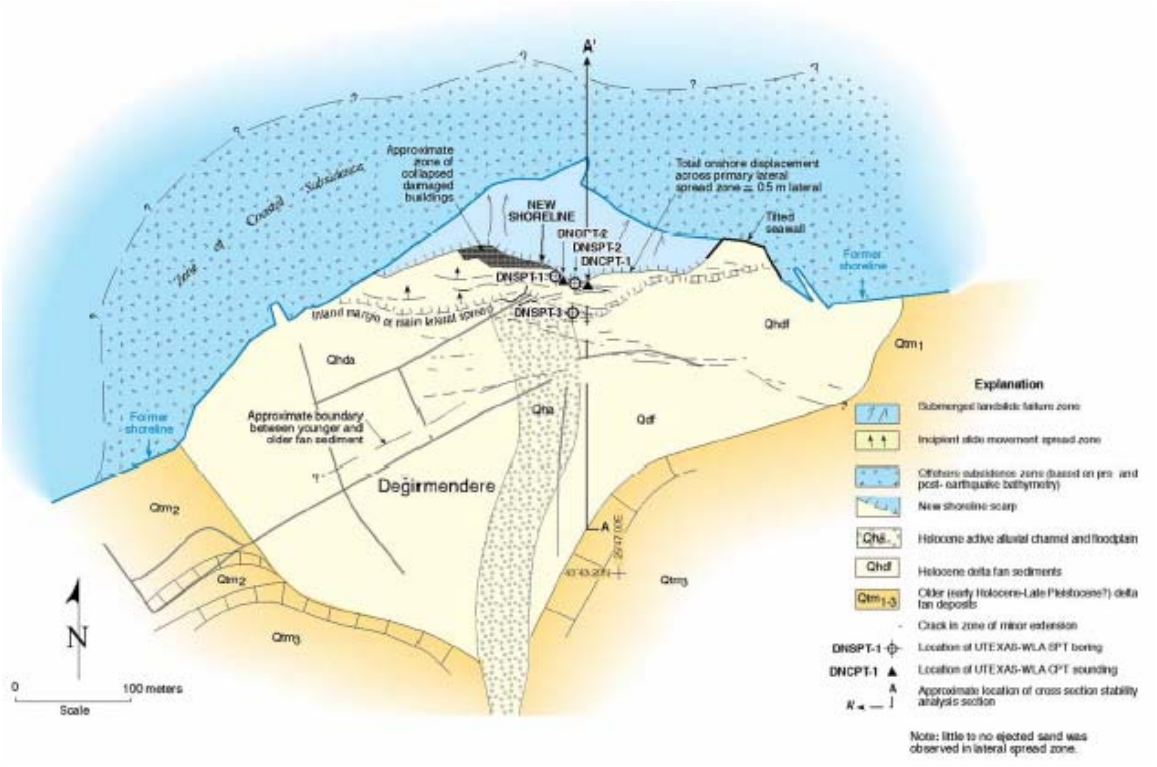

Figure A.7 - Coastal failure and local geology at Degirmendere Nose site (Rathje et al., 2004)

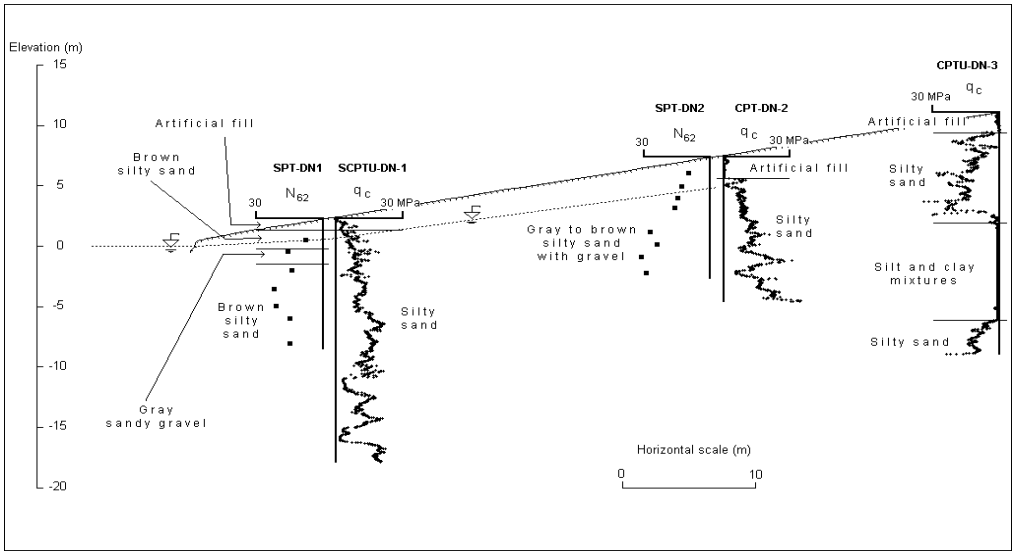

Figure A.8 - Cross section I-I of Degirmendere Nose site (PEER, 2000)

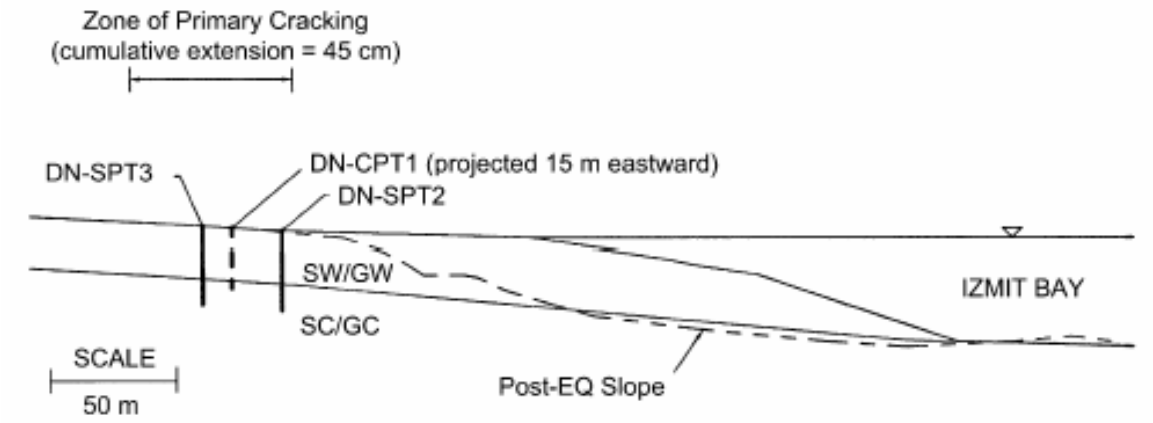

Figure A.9 - Pre and post earthquake geometry of Degirmendere Nose site (Rathje et al., 2004)

Sources of data:

Cetin, K. O., Isik, N., and Unutmaz, B. (2004). "Seismically induced landslide at Degirmendere Nose, Ismit Bay during Kocaeli (Izmit)-Turkey earthquake." *Soil Dynamics and Earthquake Engineering*, Vol. 24, pp 189-197.

PEER (2000). Documenting Incidents of Ground Failure Resulting from the August 17, 1999 Kocaeli, Turkey Earthquake. Berkeley, CA. (http://peer.berkeley.edu/turkey/adapazari/).

Rathje, E. M., Karatas, I., Wright, S. G., and Bachhuber, J. (2004). "Coastal failures during the 1999 Kocaeli earthquake in Turkey." *Soil Dynamics and Earthquake Engineering*, Vol. 24, pp.699-712.

Soil Type/Description:

The site predominately consists of silty sands (SM), well-graded sands (SW), and poorly graded sands (SP). The top 1.0m of boring DN1 at the site contain man-made fill and from 2.5m to 3.8m contain sandy gravel.

Failure modes:

Failure mode of the site is liquefaction of the silty sand layer.

Failure surface/ground surface slope angle, α:

The slope angle is estimated from the above diagram. The surface slope is approximately 8.9^{O}, with an assumed coefficient of variation of 10%.

Depth to water table, H_d:

The depth to the water table at the site is estimated to have a mean of 1.7m with a standard deviation of 0.17m.

Height of water above the failure surface, H_w:

The failure surface is assumed to go through the middle of the liquefiable layer (which occurs at a depth of 3.4m). The height of water above the failure surface is therefore 1.7m on average, with an assumed coefficient of variation of 30%.

Saturated unit weight of soil above failure surface, γ_{sat}:

The saturated unit weight of soil above the failure surface is estimated to be $22.0 kN/m^3$ based on typical unit weights of silty sand (Coduto, 1999). Assuming a COV of 5%, the standard deviation is equal to $1.1 kN/m^3$.

Dry unit weight of soil above water table, γ_d:

The dry unit weight of soil above the water table is estimated to be 21.0kN/m^3 based on typical unit weights of silty sand (Coduto, 1999). Assuming a COV of 5%, the standard deviation is equal to 1.05kN/m^3.

Fines content, FC:

The fines content in the stratified layer range from 7% to 40%. Fines contents were estimated from seven samples within the liquefiable layer; 7%, 11%, 12%, 13%, 14%, 20%, and 40% (μ = 16.7%, σ = 11.0%, COV = 65.7%).

SPT data:

The uncorrected blowcounts, N_M, in the liquefiable layer range from 8 to 16 blows per 30cm. Uncorrected blowcounts were obtained from seven samples within the liquefiable layer; 8, 10, 13, 14, 15, 16, and 16 (μ = 13.1, σ = 3.1, and COV = 23.4%).

The lowest uncorrected blowcount measured in the sandy stratum is equal to 8 at a depth of 2.0m in SPT-DN-1.

Esme Nose

Liquefaction failure was occurred near the city of Esme following the 1999 Kocaeli earthquake. The post earthquake investigation was discovering ground cracking at the failure site. The failure site is located in the south area of the city on the shore of Lake Sapanca.

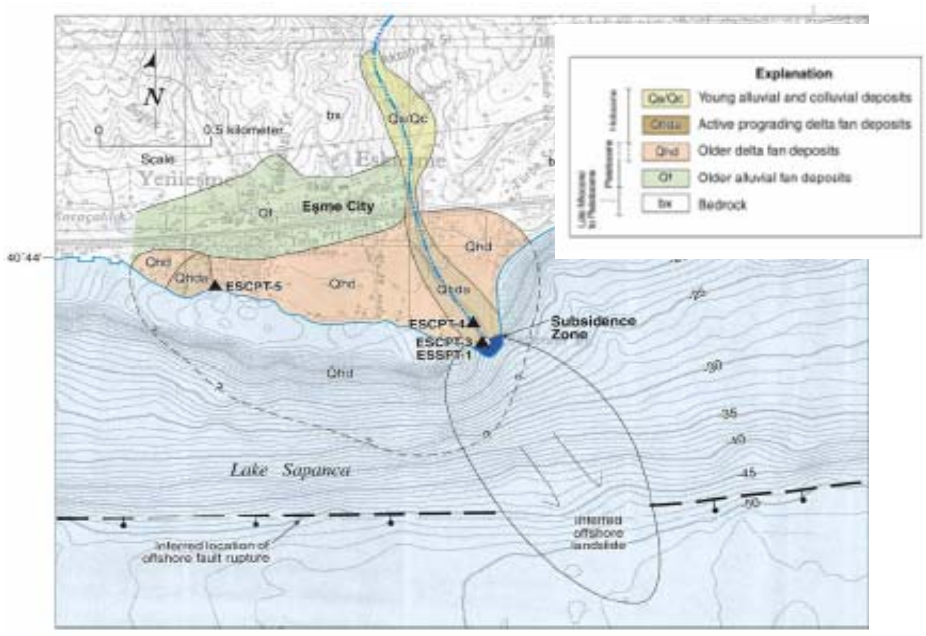

Figure A. 10 - Coastal failure and local geology at Esme Nose site (Rathje et al., 2004)

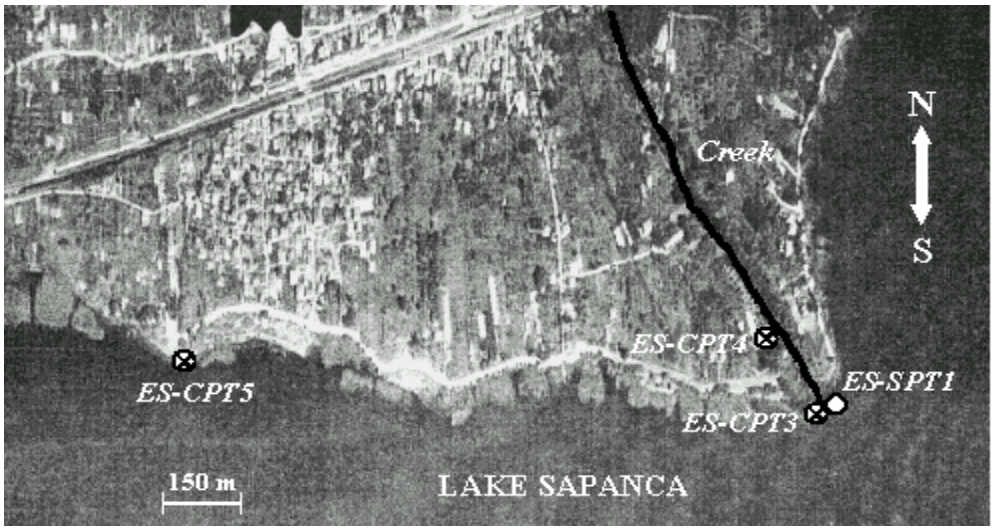

Figure A.11 - Locations of SPT and CPT at Esme Nose site
(http://www.ce.utexas.edu/prof/rathje/research/turkey.html)

Figure A.12 - Post earthquake shoreline at Esme Nose site
(http://www.ce.utexas.edu/prof/rathje/research/turkey.html)

Source of data:

Rathje, E. M., Karatas, I., Wright, S. G., and Bachhuber, J. (2004). "Coastal failures during the 1999 Kocaeli earthquake in Turkey." *Soil Dynamics and Earthquake Engineering*, Vol. 24, pp.699-712.

Soil Type/Description:

The upper 10m consists of sand to silty sand. From 10m to 20m, the material transitions from a non-plastic sandy silt to a silty sand. The material below 20m is silty clay.

Failure modes:

Based on penetration resistance, it appears that the liquefaction within the upper 15m of the site is likely.

Failure surface/ground surface slope angle, α:

Rathje et al. (2004) report that the post earthquake slope of failure surface is approximately 7^{O} increasing to 15^{O} moving away from the shoreline; onshore the slope is

approximately 2^O to 4^O. Regarding only the onshore slope the mean slope angle is 3^O and the standard deviation is equal to 0.3^O.

Depth to water table, H_d:

The depth to the water table is between 0 and 2m from the ground surface. The mean is 1.0m and the standard deviation is 0.1m.

Height of water above the failure surface, H_w:

Assuming that the silty sands and sandy silts in the top 15m are the potentially liquefiable layer, the depth to the middle of this layer is 8.0m; subtracting the mean depth to the water table results in an average height of water above the failure surface of 7.0m, with an assumed coefficient of variation of 30%.

Saturated unit weight of soil above failure surface, γ_{sat}:

The mean saturated unit weight of soil above the failure surface is estimated to be 22.0kN/m^3 based on typical unit weights of silty sand (Coduto, 1999). Assuming a COV of 5%, the standard deviation is equal to 1.1kN/m^3.

Dry unit weight of soil above water table, γ_d:

The mean dry unit weight of soil above the water table is estimated to be 21.0kN/m^3 based on typical unit weights of silty sand (Coduto, 1999). Assuming a COV of 5%, the standard deviation is equal to 1.05kN/m^3.

Fines content, FC:

The fines content in the upper stratum is 10% to 30%. The non-plastic silt layer has fines ranging from 50 to 80%. The silty sand layer has a fines content of about 15%. Regarding only the upper stratum and the non-plastic silt layer, the assumed average fines content is 45% with a standard deviation equal to 11.25%.

SPT data:

The energy corrected blowcounts in the top 15 meters of the site range from 5 to 15 blows per 30cm. The energy corrected blowcounts were obtained from 10 samples within the liquefiable layer; 6, 13, 9, 5, 9, 13, 15, 6, 12, and 12 (μ = 10.0, σ = 3.5, and COV = 35.0%).

The minimum uncorrected blowcount of 6 occurs at a depth of 6m.

Hotel Sapanca

The 1999 Kocaeli earthquake triggered extensive liquefaction failures in the area around Hotel Sapanca. This area located in the shore of Lake Sapanca. The failures were causing the movement of soil mass toward the lake.

Figure A.13 - Aerial photograph of Hotel Sapanca (Olgun, 2005)

Figure A.14 - Ground cracking at Hotel Sapanca site
after the 1999 Kocaeli earthquake (Olgun, 2005)

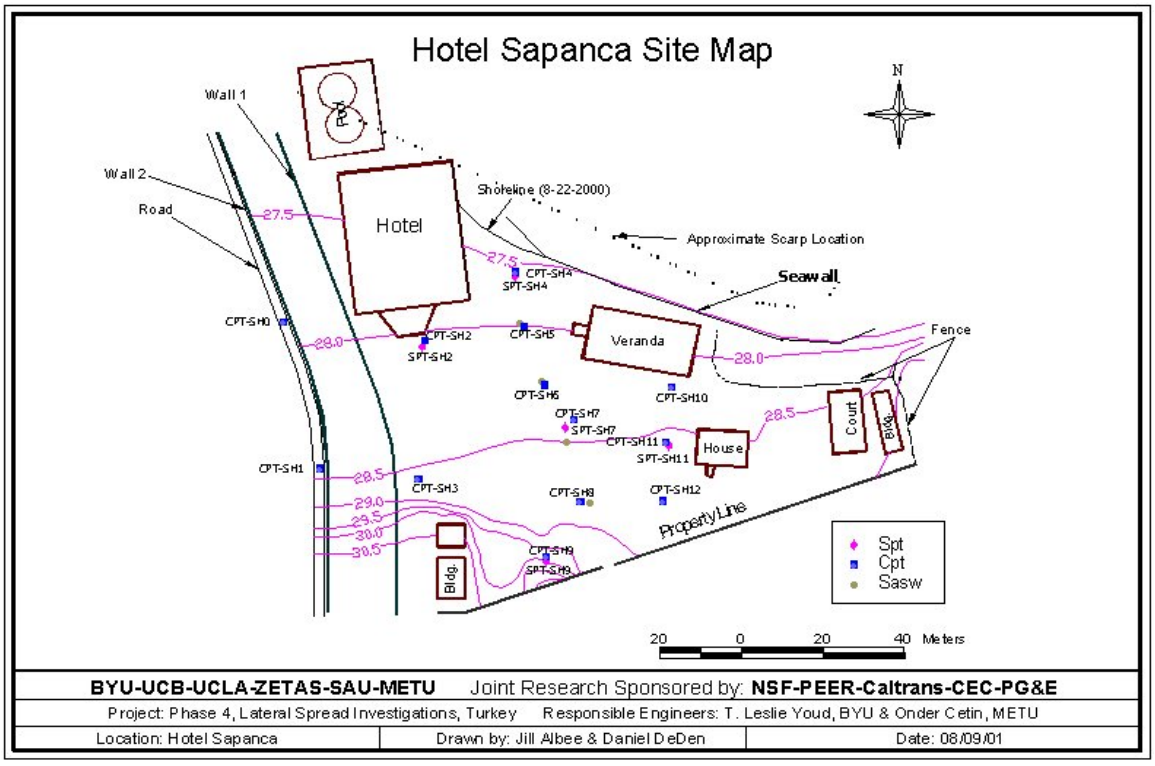

Figure A.15 - Hotel Sapanca site map (PEER, 2000)

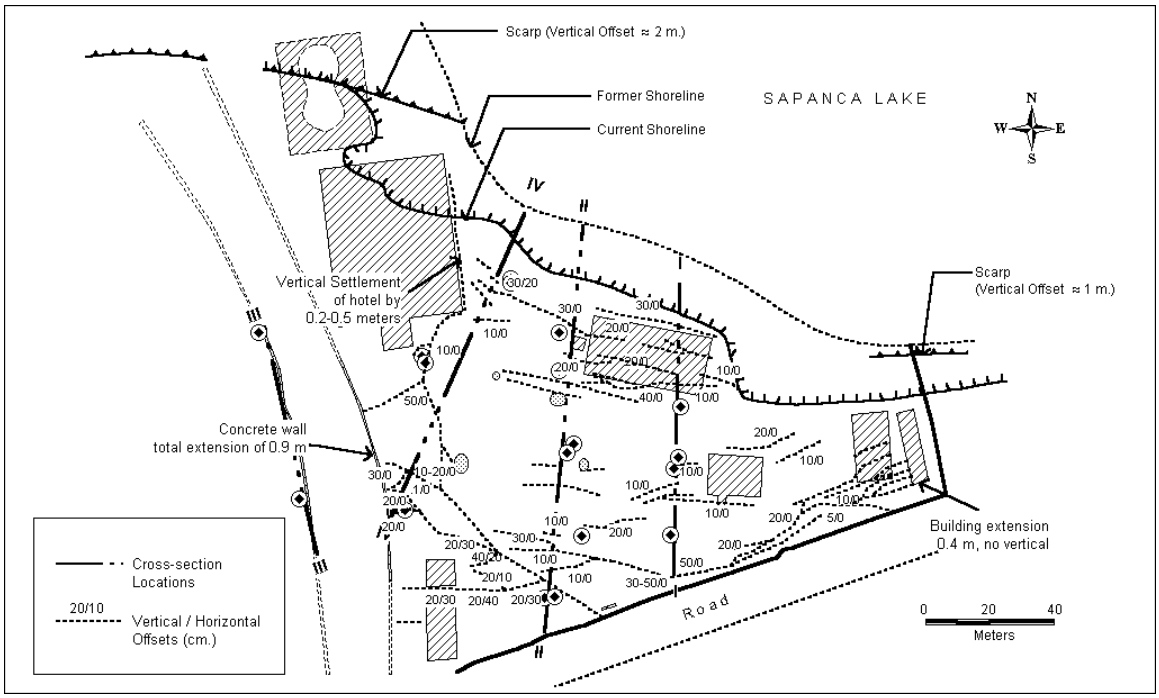

Figure A.16 - Ground deformation map of the Hotel Sapanca site (Cetin et al., 2002)

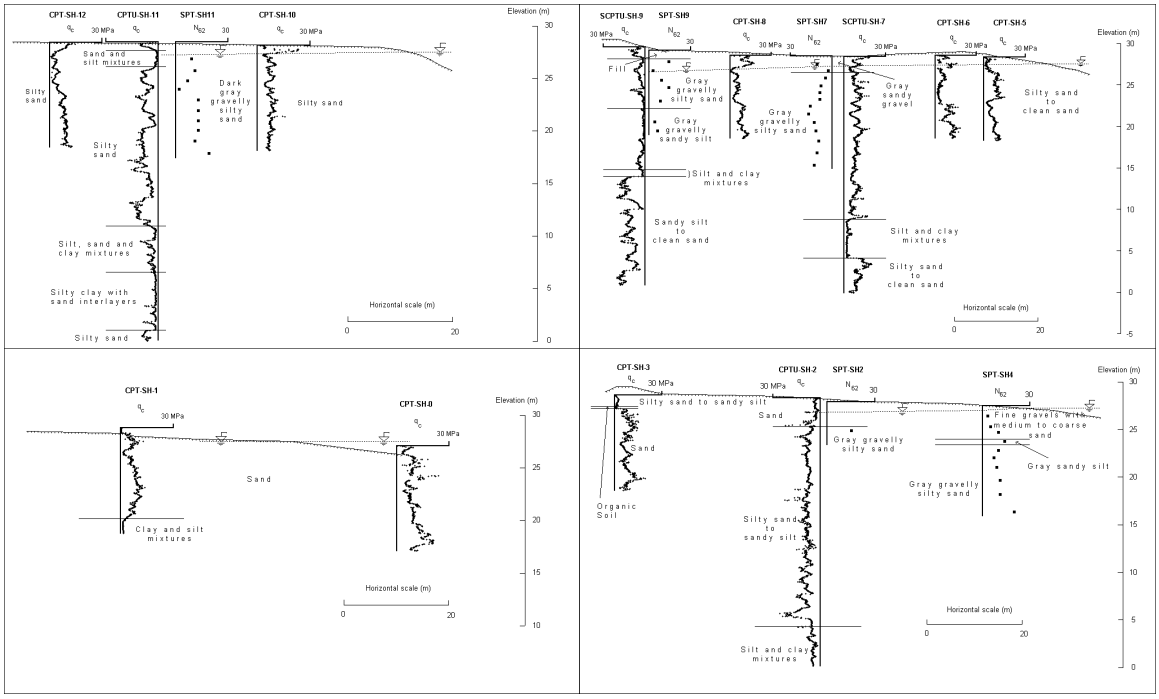

Figure A.17a-d - Cross sections of Hotel Sapanca site (PEER, 2000)

Sources of data:

Cetin, K.O., Youd, T.L., Seed, R.B., Bray, J.D., Sancio, R., Lettis, W., Yilmaz, M.T., and Durgunoglu, H.T. (2002), "Liquefaction-Induced Deformations at Hotel Sapanca during Kocaeli (Izmit), Turkey Earthquake." *Soil Dynamics and Earthquake Eng*ineering, Vol. 22, pp. 1083-1092.

PEER (2000). Documenting Incidents of Ground Failure Resulting from the August 17, 1999 Kocaeli, Turkey Earthquake. Berkeley, CA. (http://peer.berkeley.edu/turkey/adapazari/).

Soil Type/Description:

The site is predominately silty sands. The top 3.5m of boring SH4 and the top 2.0m of boring SH7 contain gravels. Boring SH9 from 2.5m to 3.8m contains sandy silt.

Failure modes:

Failure mode of the site is because of the liquefaction of silty sand layer.

Failure surface/ground surface slope angle, α:

The slope angle is estimated from the above diagram. The surface slope is approximately 0.8^{O}, with an assumed coefficient of variation of 10%.

Depth to water table, H_d:

The depth to the water table at the site is estimated to have a mean of 1.2m with a standard deviation of 0.12m.

Height of water above the failure surface, H_w:

The failure surface is assumed to go through the middle of the liquefiable layer (which occurs at a depth of 7.2m). The height of water above the failure surface is therefore 6.0m on average, with an assumed coefficient of variation of 30%.

Saturated unit weight of soil above failure surface, γ_{sat}:

The saturated unit weight of soil above the failure surface is estimated to be 22.0kN/m^3 based on typical unit weights of silty sand (Coduto, 1999). Assuming a COV of 5%, the standard deviation is equal to 1.1kN/m^3.

Dry unit weight of soil above water table, γ_d:

The dry unit weight of soil above the water table is estimated to be 21.0kN/m^3 based on typical unit weights of silty sand (Coduto, 1999). Assuming a COV of 5%, the standard deviation is equal to 1.05kN/m^3.

Fines content, FC:

The fines content in the liquefiable layer range from 4% to 21%. Fines contents were estimated from 29 samples within the liquefiable layer; 4, 4, 5, 5, 6, 6, 7, 7, 7, 7, 8, 9, 9, 9, 9, 10, 11, 11, 11, 12, 12, 13, 14, 14, 14, 15, 15, 16, and 21 (μ = 10.03%, σ = 4.11%, COV = 40.96%).

SPT data:

The uncorrected blowcounts, N_M, in the liquefiable layer range from 2 to 17 blows per 30cm. Uncorrected blowcounts were obtained from 34 samples within the liquefiable layer; 2, 3, 4, 5, 6, 6, 7, 7, 8, 8, 9, 9, 9, 9, 9, 10, 10, 11, 11, 11, 11, 11, 12, 13, 13, 13, 13, 13, 14, 14, 14, 15, 16, and 17 (μ = 10.01, σ = 3.69, and COV = 36.55%).

The minimum uncorrected blowcount of 2 occurs at a depth of 4.75m in SPT-SH11.

Police Station

The 1999 Kocaeli earthquake also triggered liquefaction failures along the south shore of the Bay of Izmit. The Police Station site was located to the east from the City of Golcuk. The failures were causing extensive ground cracking in the area.

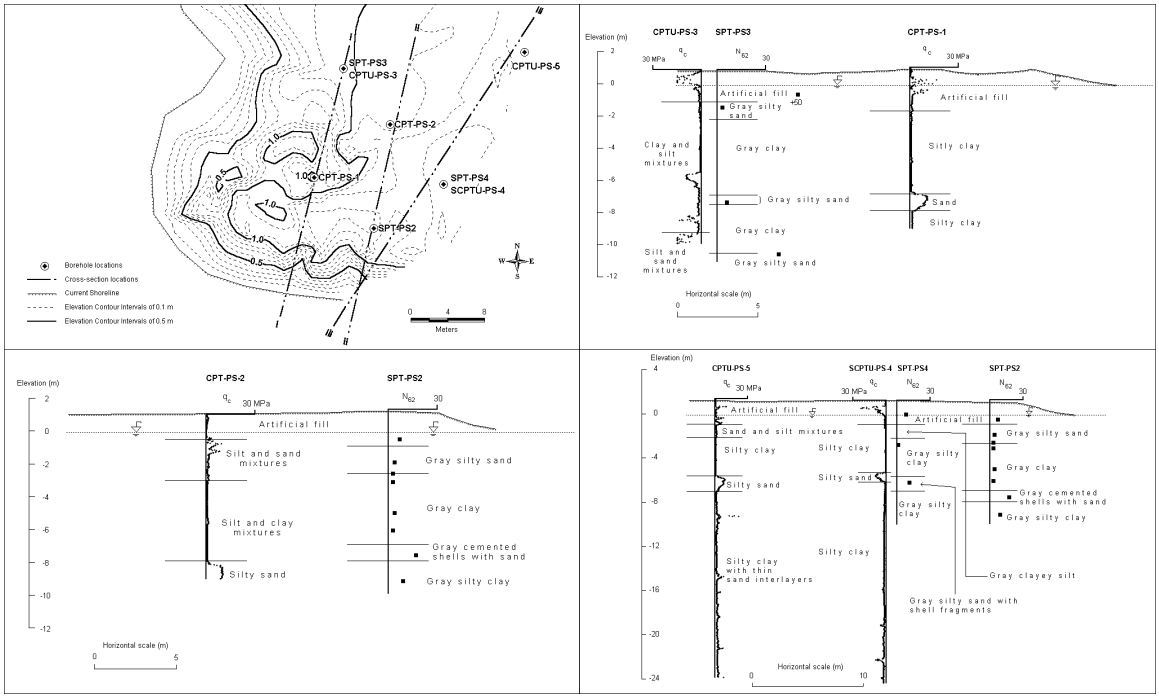

Figure A.18a - Police Station site map (PEER, 2000)

Figure A.18b-c - Cross sections of Police Station site (PEER, 2000)

Source of data:

PEER (2000). Documenting Incidents of Ground Failure Resulting from the August 17, 1999 Kocaeli, Turkey Earthquake. Berkeley, CA. (http://peer.berkeley.edu/turkey/adapazari/).

Soil Type/Description:

The site is stratified with alternating strata of loose silts, clays, and sands. The liquefiable layer consists of sandy silt and silty sand from a depth of 1.1m to 3.9m. The borings indicate that depths below 3.9m contain clay layer. The top 1.1m at the site contain man-made fill.

Failure modes:

Failure mode of the site is because of the liquefaction of liquefiable layer.

Failure surface/ground surface slope angle, α:

The slope angle is estimated from the above cross section. The surface slope is approximately 0.7^{O}, with an assumed coefficient of variation of 10%.

Depth to water table, H_d:

The depth to the water table at the site is estimated to have a mean of 1.1m with a standard deviation of 0.11m.

Height of water above the failure surface, H_w:

The failure surface is assumed to go through the middle of the liquefiable layer (which occurs at a depth of 2.5m). The height of water above the failure surface is therefore 1.4m on average, with an assumed coefficient of variation of 30%.

Saturated unit weight of soil above failure surface, γ_{sat}:

The saturated unit weight of soil above the failure surface is estimated to be 21.5kN/m^3 based on typical unit weights of soils (Coduto, 1999). Assuming a COV of 5%, the standard deviation is equal to 1.075kN/m^3.

Dry unit weight of soil above water table, γ_d:

The dry unit weight of soil above the water table is estimated 20.0kN/m^3 based on typical unit weights of soils (Coduto, 1999). Assuming a COV of 5% the standard deviation is equal to 1.0 kN/m^3.

Fines content, FC:

The fines content in the liquefiable layer range from 12% to 78%. Fines contents were estimated from three samples within the liquefiable layer; 12%, 36%, and 78% (μ = 42.0%, σ = 33.4%, and COV = 79.5%).

SPT data:

The uncorrected blowcounts, N_M, in the liquefiable layer range from 3 to 8 blows per 30cm. Uncorrected blowcounts were obtained from three samples within the liquefiable layer; 3, 4, and 8 ($\mu = 5.0$, $\sigma = 2.65$, and COV = 52.92%).

The minimum uncorrected blowcount of 3 occurs at a depth of 2.5m in SPT-PS3.

Seymen Tea Garden

The 1999 Kocaeli earthquake also triggered liquefaction failure around the city of Seymen. The extensive failures occurred at Seymen Tea Garden site. The failures were causing the movement of soil mass toward the Bay of Izmit.

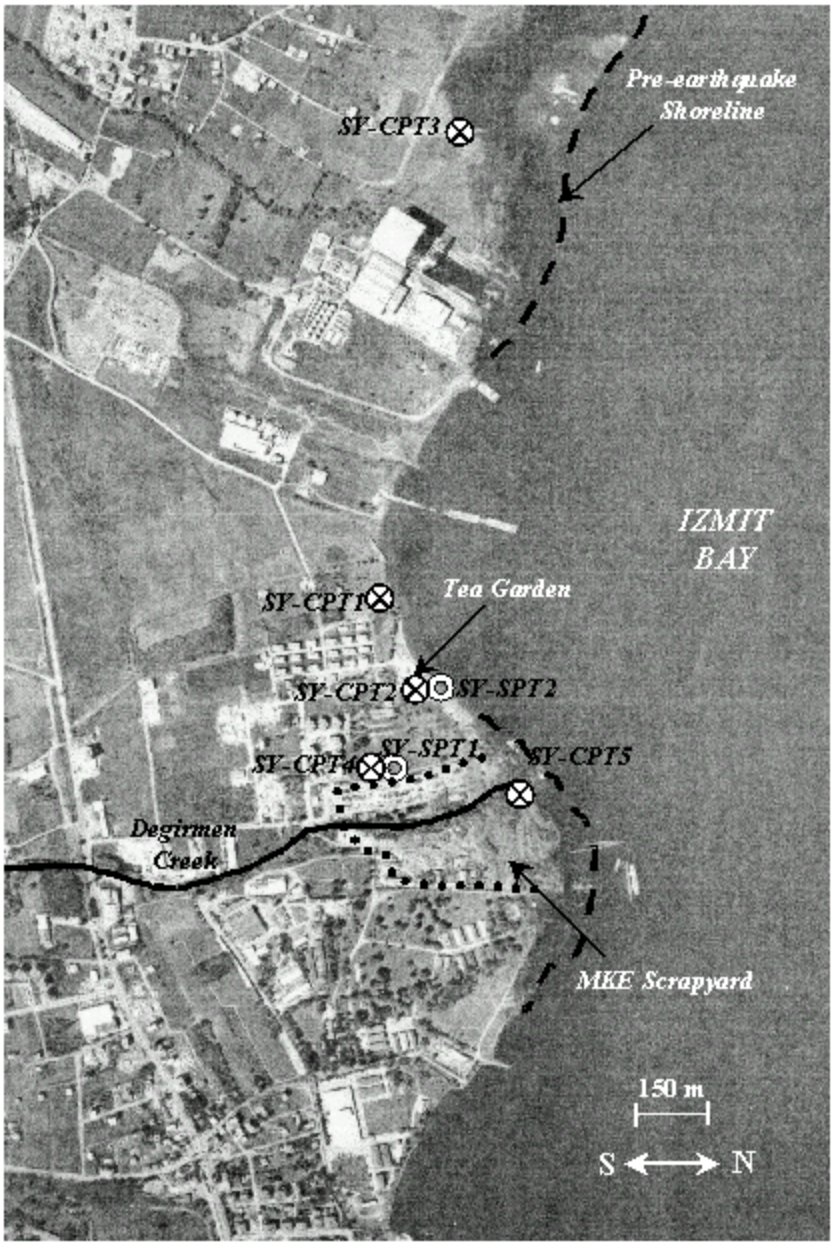

Figure A.19 - Aerial photograph taken after the 1999 Kocaeli earthquake (http://www.ce.utexas.edu/prof/rathje/research/turkey.html)

Figure A.20 - Liquefaction location at Seymen Tea Garden site
(http://www.ce.utexas.edu/prof/rathje/research/turkey.html)

Source of data:

Rathje, E. M., Karatas, I., Wright, S. G., and Bachhuber, J. (2004). "Coastal failures during the 1999 Kocaeli earthquake in Turkey." *Soil Dynamics and Earthquake Engineering*, Vol. 24, pp.699-712.

Soil Type/Description:

The upper 5m of the site consists of silty clay (CL/CH). From 5m to 21m the site consists of silty sand with clay. Below 21m the soils return to a silty clay (CH) layer.

Failure modes:

Failure occurs as a result of liquefaction within the 16m thick silty sand layer.

Failure surface/ground surface slope angle, α:

Rathje et al. (2004) report that the slope angle is approximately 1^{O} to 3^{O}, therefore the mean is assumed to be 2^{O}, with a standard deviation of 0.2^{O}.

Depth to water table, H_d:

The depth to the water table is between 0 and 2m (μ = 1m, σ = 0.1m).

Height of water above the failure surface, H_w:

The depth to the middle of the silty sand layer is 13m. The mean height of water above the failure surface is assumed to be the depth to the middle of the layer minus the mean depth to the water table equal to 12m, with an assumed coefficient of variation of 30%.

Saturated unit weight of soil above failure surface, γ_{sat}:

The saturated unit weight of soil above the failure surface is estimated to be 21.5kN/m^3 based on typical unit weights of soils (Coduto, 1999). Assuming a COV of 5%, the standard deviation is equal to 1.075kN/m^3.

Dry unit weight of soil above water table, γ_d:

The dry unit weight of soil above the water table is estimated to be 20.0kN/m^3 based on typical unit weights of soils (Coduto, 1999). Assuming a COV of 5%, the standard deviation is equal to 1.0 kN/m^3.

Fines content, FC:

The fines content of the silty sand layer ranges from 20% to 40%, this results in a mean of 30% and a standard deviation of 3.0%.

SPT data:

The uncorrected blowcounts (energy corrected) within the silty sand layer from 5m to 21m range from 6 to 16 blows/30cm. The energy corrected blowcounts have a mean of 10.73 and a standard deviation of 3.31.

The minimum energy corrected blowcount of 7 at a depth of 15m.

Soccer Field

Soccer Field site was the other area along the south shore of the Bay of Izmit where the liquefaction failures also occurred. This site was located to the east from the Police Station site. The failures were causing extensive ground cracking in the area.

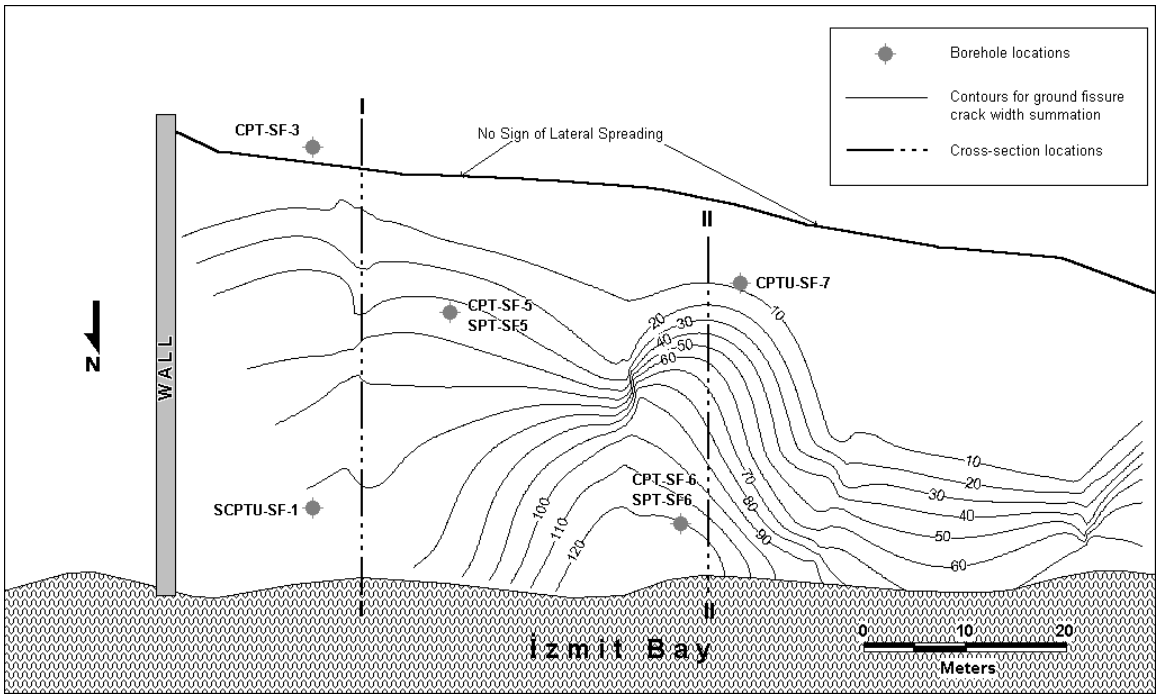

Figure A.21 - Soccer Field site map (PEER, 2000)

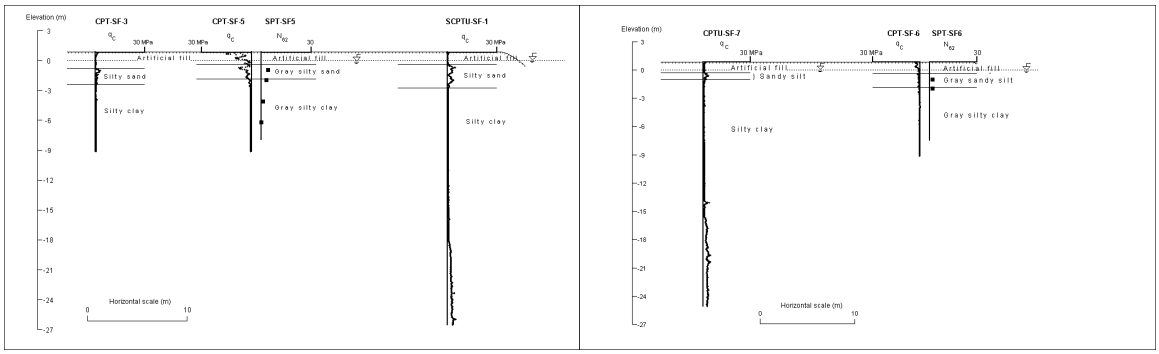

Figure A.22a-b - Cross sections of Soccer Field site (PEER, 2000)

Source of data:

PEER (2000). Documenting Incidents of Ground Failure Resulting from the August 17, 1999 Kocaeli, Turkey Earthquake. Berkeley, CA. (http://peer.berkeley.edu/turkey/adapazari/).

Soil Type/Description:

The site is stratified with alternating strata of loose silts, clays, and sands. The liquefiable layer consists of silty sand and sandy silt from a depth of 1.2m to 3.5m. The borings indicate that depths below 3.5m contain silty clay. The top 1.2m at the site contain man-made fill.

Failure modes:

Failure mode of the site is because of the liquefaction of liquefiable layer.

Failure surface/ground surface slope angle, α:

The slope angle is estimated from the above cross section. The surface angle is approximately 0.1^{O}, with an assumed coefficient of variation of 10%.

Depth to water table, H_d:

The depth to the water table at the site is estimated to have a mean of 0.8m, with a standard deviation of 0.08m.

Height of water above the failure surface, H_w:

The failure surface is assumed to go through the middle of the liquefiable layer (which occurs at a depth of 2.4m). The height of water above the failure surface is therefore 1.6m on average, with an assumed coefficient of variation of 30%.

Saturated unit weight of soil above failure surface, γ_{sat}:

The saturated unit weight of soil above the failure surface is estimated to be $21.5 kN/m^3$ based on typical unit weights of soils (Coduto, 1999). Assuming a COV of 5%, the standard deviation is equal to $1.075 kN/m^3$.

Dry unit weight of soil above water table, γ_d:

The dry unit weight of soil above the water table is estimated to be 20.0kN/m^3 based on typical unit weights of soils (Coduto, 1999). Assuming a COV of 5%, the standard deviation is equal to 1.0 kN/m^3.

Fines content, FC:

The fines content in the liquefiable layer range from 16% to 66%. Fines contents were estimated from three samples within the liquefiable layer; 16%, 52%, and 66% (μ = 44.7%, σ = 25.8%, and COV = 57.7%).

SPT data:

The uncorrected blowcounts, N_M, in the liquefiable layer range from 2 to 4 blows per 30cm. Uncorrected blowcounts were obtained from 3 samples within the liquefiable layer; 2, 3, and 4 (μ = 3, σ = 1, and COV = 33.3%).

The minimum uncorrected blowcount of 2 occurred at a depth of 3m.

Yakin Street

Soccer Field site was the other area along the south shore of the Bay of Izmit where the liquefaction failures also occurred. This site was located to the east from the Police Station site. The failures were causing extensive ground cracking in the area.

Yakin Street site also was located in the downtown area of city of Adapazari. Extensive failures occurred in this area. The failures were causing massive damage to buildings and infrastructures in this area.

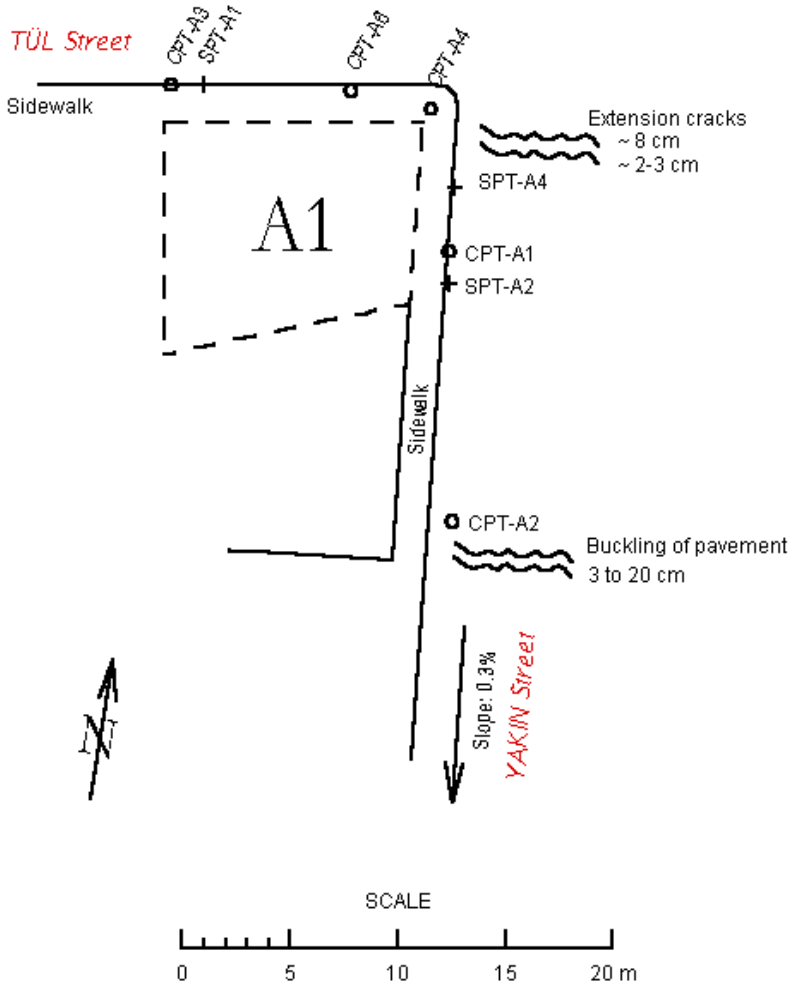

Figure A.23 - Yakin Street site map (PEER, 2000)

Source of data:

PEER (2000). Documenting Incidents of Ground Failure Resulting from the August 17, 1999 Kocaeli, Turkey Earthquake. Berkeley, CA. (http://peer.berkeley.edu/turkey/adapazari/).

Soil Type/Description:

The upper one meter of the site contains asphalt and subgrade material. From 1m to 8.5m the site consists of a stratum containing interbedded layers of loose, high plasticity clays (CH) and low plasticity silts (ML). Below 8.5m, the soils transition to a medium dense sandy stratum.

Failure modes:

Liquefaction of loose low-plasticity silt (ML) within a stratum containing predominately loose CL and CH materials; the deformations likely occurred near the end or shortly after the earthquake shaking because of the low hydraulic conductivities involved.

Failure surface/ground surface slope angle, α:

As indicated on the above figure, Yakin Street slopes to the south at a 0.3% grade. Assuming a coefficient of variation equal to 10%, the slope has a mean of 0.17^{O} and a standard deviation of 0.017^{O}.

Depth to water table, H_d:

Ten measurements were taken to investigate the depth to the water table; 0.9m, 0.77m, 0.77m, 0.7m, 0.79m, 0.85m, 0.87m, 0.7m, 0.72m, and 0.82m. The average depth to the water table is 0.8m, with a standard deviation equal to 0.08m.

Height of water above the failure surface, H_w:

The failure surface is assumed to go through the middle of the liquefiable layer (which occurs at a depth of 4.5m). The height of water above the failure surface is therefore 3.7m on average, with an assumed coefficient of variation of 30%.

Saturated unit weight of soil above failure surface, γ_{sat}:

The saturated unit weight of soil above the failure surface is estimated to be 16.0kN/m^3 based on typical unit weights of ML and CH soils (Coduto, 1999). Assuming a COV of 5%, the standard deviation is equal to 0.8kN/m^3.

Dry unit weight of soil above water table, γ_d:

The dry unit weight of soil above the water table is estimated to be 15.0kN/m^3 based on typical unit weights of soils (Coduto, 1999). Assuming a COV of 5%, the standard deviation is equal to 0.75kN/m^3.

Fines content, FC:

The fines content in the liquefiable layer range from 58% to 100%. Fines contents were estimated from 23 samples within the liquefiable layer; 90, 94, 100, 87, 74, 92, 97, 70, 58, 74, 86, 100, 85, 93, 95, 99, 85, 99, 99, 79, 91, 96, 88, 80, 94, 99, 97, 98, 92, and 66 (μ = 89.65%, σ = 8.65%, and COV = 9.65%).

SPT data:

The uncorrected blowcounts, N_M, in the liquefiable layer range from 2 to 14 blows per 30cm. Uncorrected blowcounts were obtained from 20 samples within the liquefiable layer; 6, 7, 7, 4, 4, 3, 3, 3, 4, 2, 7, 3, 10, 3, 5, 4, 5, 4, 14, 6, and 3 (μ = 6.30, σ = 4.23, and COV = 67.17%).

The minimum uncorrected blowcount of 2 occurs at a depth of 3.5m within a classification of CL/CH (the lowest blowcount in a ML material is 4 at a depth of 5.8m).

Yalova Harbor

The 1999 Kocaeli earthquake also triggered liquefaction failure in the city of Yalova. The liquefaction failures were observed across portions of the harbor in Yalova. Failure toward the water was observed in the marina at the west end of the harbor.

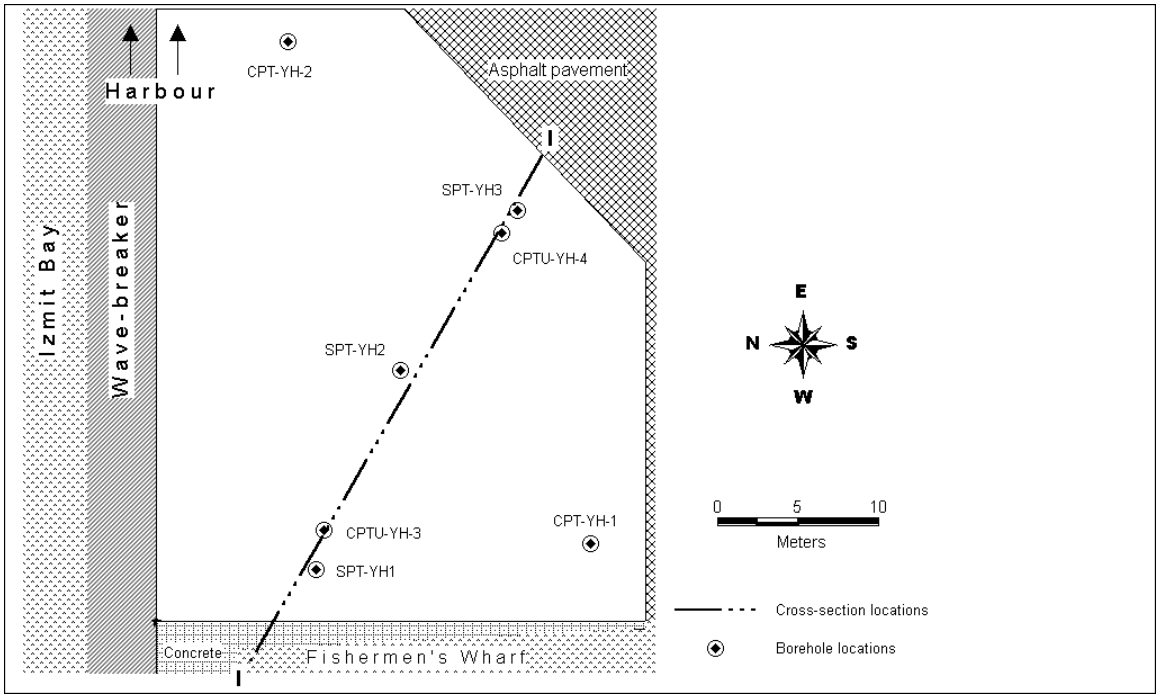

Figure A.24 - Yalova Harbor site map (PEER, 2000)

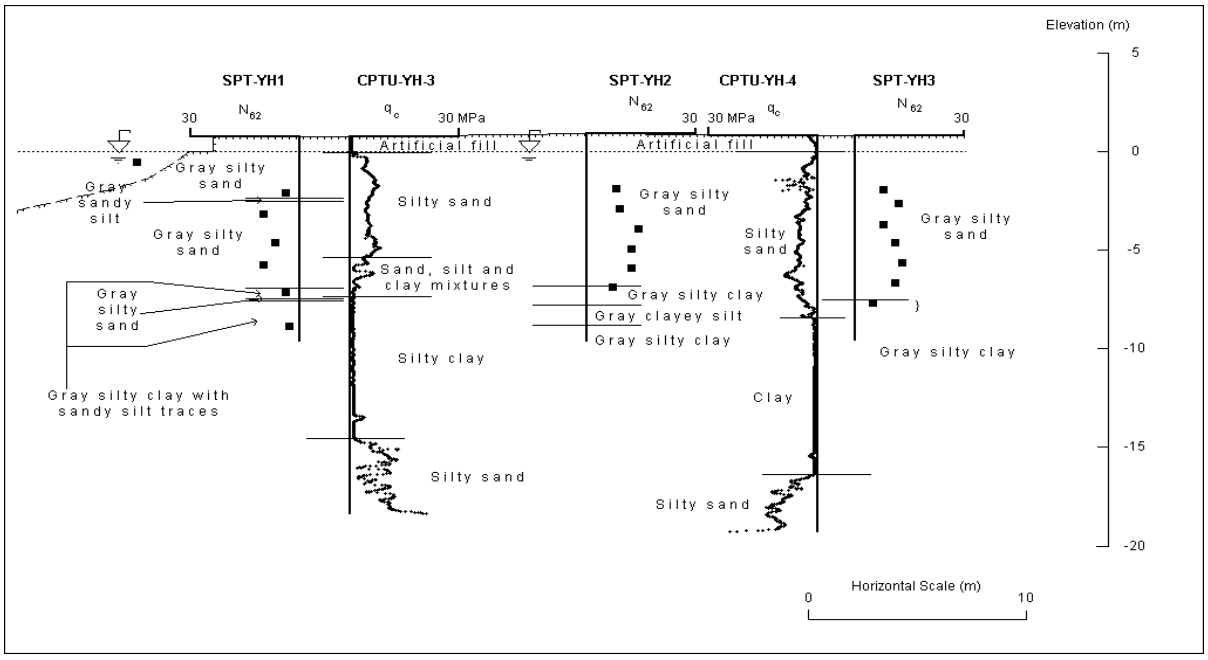

Figure A.25 - Cross Section of Yalova Harbor site (PEER, 2000)

Figure A.26 - Ground Cracking at Yalova Harbor site (PEER, 2000)

Source of data:

PEER (2000). Documenting Incidents of Ground Failure Resulting from the August 17, 1999 Kocaeli, Turkey Earthquake. Berkeley, CA. (http://peer.berkeley.edu/turkey/adapazari/).

Soil Type/Description:

The site consists predominately of silty sand (SM) to poorly-graded sand (SP) in the top 8m (this layer as small seams of sandy silt material, ML). The sands are underlain by low plasticity clays.

Failure modes:

The likely failure mode is liquefaction of the SM and SP material.

Failure surface/ground surface slope angle, α:

Based on the cross-section above, the average slope of the ground surface is 0.5% (equal to 0.286^{O}). Assuming a COV equal to 10%, the standard deviation is 0.0286^{O}.

Depth to water table, H_d:

Three water table measurements were recorded at the site; 0.7m, 0.9m, and 0.8m. The average depth to the water table is 0.8m, with a standard deviation equal to 0.08m.

Height of water above the failure surface, H_w:

The failure surface is assumed to go through the middle of the liquefiable layer (which occurs at a depth of 4.4m). The height of water above the failure surface is therefore 3.6m on average, with an assumed coefficient of variation of 30%.

Saturated unit weight of soil above failure surface, γ_{sat}:

The saturated unit weight of soil above the failure surface is estimated to be $22.0kN/m^3$ based on typical unit weights of silty sand (Coduto, 1999). Assuming a COV of 5%, the standard deviation is equal to $1.1kN/m^3$.

Dry unit weight of soil above water table, γ_d:

The dry unit weight of soil above the water table is estimated to be $21.0kN/m^3$ based on typical unit weights of silty sand (Coduto, 1999). Assuming a COV of 5%, the standard deviation is equal to $1.05kN/m^3$.

Fines content, FC:

The fines content in the liquefiable layer range from 5% to 45%. Fines contents were estimated from 14 samples within the liquefiable layer; 7, 9, 10, 23, 29, 7, 12, 26, 16, 13, 10, 11, 17, and 33 (μ = 15.93%, σ = 8.51%, and COV = 53.41%).

SPT data:

The uncorrected blowcounts, N_M, in the liquefiable layer range from 4 to 14 blows per 30cm. Uncorrected blowcounts were obtained from 16 samples within the liquefiable layer; 4, 10, 7, 10, 4, 8, 9, 14, 12, 12, 8, 12, 8, 11, 13, and 11 (μ = 9.56, σ = 2.94, and COV = 30.78%).

The minimum uncorrected blowcount of 4 occurs at a depth of 3m.

APPENDIX B

APPENDIX B

Appendix B contains reliability index analyses for all of the case histories. All of the case histories are analyzed using the same procedure described in Hotel Sapanca failure case. The equations are implemented in Microsoft Excel to calculate the reliability index, β. Figure B.1 to Figure B.9 showed spreadsheet implementation for all of the case histories.

	DistName	Para1	Para2	Para3	Para4	$x_{initial}$	x^*	m^N	s^N	nx
γ_d	Normal	17.50	0.88			17.50	17.55	17.50	0.88	0.06
γ_{sat}	Normal	20.50	1.03			20.50	20.56	20.50	1.03	0.06
H_d	Normal	2.60	0.26			2.60	2.61	2.60	0.26	0.03
H_w	Normal	1.80	0.54			1.80	1.83	1.80	0.54	0.05
α	Normal	1.00	0.10			1.00	1.01	1.00	0.10	0.10
$(N_1)_{60cs}$	Normal	10.02	1.92			10.02	9.37	10.02	1.92	-0.34
C_1	Normal	1.00	0.30			1.00	0.10	1.00	0.30	-3.00

	γ_d	γ_{sat}	H_d	H_w	α	$(N_1)_{60cs}$	C_1
γ_d	**1.00**	0.90	0.00	0.00	0.00	0.00	0.00
γ_{sat}	0.90	**1.00**	0.00	0.00	0.00	0.00	0.00
H_d	0.00	0.00	**1.00**	-0.50	0.00	0.00	0.00
H_w	0.00	0.00	-0.50	**1.00**	0.00	0.00	0.00
α	0.00	0.00	0.00	0.00	**1.00**	0.00	0.00
$(N_1)_{60cs}$	0.00	0.00	0.00	0.00	0.00	**1.00**	0.00
C_1	0.00	0.00	0.00	0.00	0.00	0.00	**1.00**

reset design points, x*

Options	Para1	Para2	Para3	Para4
None	value			
Normal	mean	StDev		
Lognorm	mean	StDev		
ExtValue1	mean	StDev		
Uniform	Use BetaDist (1,1,min,max)			
Expo	mean			
Gamma	α	λ		
Weibull	α	λ		
Triang	min	mode	max	
BetaDist	α	λ	min	max
PERTdist	min	mode	max	

	Min.	Max.
γ_d	12.50	22.50
γ_{sat}	15.50	25.50
H_d	0.00	10.00
H_w	0.00	25.00
α	0.00	2.00
$(N_1)_{60cs}$	0.00	20.00
C_1	0.00	2.00

FS
1.00
β
3.021
Pf
0.0013

UNITS ARE IN KILOPASCALS & METERS

Stability computations are based on Ishihara et al (1990).

Reliability computations are based on Low and Tang (2004).

A best-fit line through the Seed and Harder (1990) data is used to estimate the liquefied shear strength based on the input $(N_1)_{60}$

Figure B.1 Reliability computations of Cark Canal case using mean value of $(N_1)_{60\text{-}cs}$

	DistName	Para1	Para2	Para3	Para4	$x_{initial}$	x^*	m^N	s^N	Nx
γ_d	Normal	15.00	0.75			15.00	15.01	15.00	0.75	0.01
γ_{sat}	Normal	16.00	0.80			16.00	16.01	16.00	0.80	0.01
H_d	Normal	1.10	0.11			1.10	1.10	1.10	0.11	0.00
H_w	Normal	3.60	1.08			3.60	3.62	3.60	1.08	0.02
α	Normal	0.17	0.02			0.17	0.17	0.17	0.02	0.01
$(N_1)_{60cs}$	Normal	10.12	2.69			10.12	9.99	10.12	2.69	-0.05
C_1	Normal	1.00	0.30			1.00	0.01	1.00	0.30	-3.30

	γ_d	γ_{sat}	H_d	H_w	α	$(N_1)_{60cs}$	C_1
γ_d	**1.00**	0.90	0.00	0.00	0.00	0.00	0.00
γ_{sat}	0.90	**1.00**	0.00	0.00	0.00	0.00	0.00
H_d	0.00	0.00	**1.00**	-0.50	0.00	0.00	0.00
H_w	0.00	0.00	-0.50	**1.00**	0.00	0.00	0.00
α	0.00	0.00	0.00	0.00	**1.00**	0.00	0.00
$(N_1)_{60cs}$	0.00	0.00	0.00	0.00	0.00	**1.00**	0.00
C_1	0.00	0.00	0.00	0.00	0.00	0.00	**1.00**

reset design points, x*

Options	Para1	Para2	Para3	Para4
None	value			
Normal	mean	StDev		
Lognorm	mean	StDev		
ExtValue1	mean	StDev		
Uniform	Use BetaDist (1,1,min,max)			
Expo	mean			
Gamma	α	λ		
Weibull	α	λ		
Triang	min	mode	max	
BetaDist	α	λ	min	max
PERTdist	min	mode	max	

	Min.	Max.
γ_d	10.00	20.00
γ_{sat}	11.00	21.00
H_d	0.00	10.00
H_w	0.00	25.00
α	0.00	0.34
$(N_1)_{60cs}$	0.00	20.00
C_1	0.00	2.00

FS
1.00
β
3.303
Pf
0.0005

UNITS ARE IN KILOPASCALS & METERS

Stability computations are based on Ishihara et al (1990).

Reliability computations are based on Low and Tang (2004).

A best-fit line through the Seed and Harder (1990) data is used to estimate the liquefied shear strength based on the input $(N_1)_{60}$

Figure B.2 Reliability computations of Cumruhiyet Avenue case using mean value of $(N_1)_{60\text{-}cs}$

	DistName	Para1	Para2	Para3	Para4	$x_{initial}$	x^*	m^N	s^N	nx
γ_d	Normal	21.00	1.05			21.00	21.18	21.00	1.05	0.17
γ_{sat}	Normal	22.00	1.10			22.00	22.19	22.00	1.10	0.17
H_d	Normal	1.70	0.17			1.70	1.70	1.70	0.17	0.02
H_w	Normal	1.70	0.51			1.70	1.81	1.70	0.51	0.22
α	Normal	8.90	0.89			8.90	9.13	8.90	0.89	0.26
$(N_1)_{60cs}$	Normal	16.69	3.28			16.69	11.70	16.69	3.28	-1.52
C_1	Normal	1.00	0.30			1.00	0.54	1.00	0.30	-1.54

	γ_d	γ_{sat}	H_d	H_w	α	$(N_1)_{60cs}$	C_1
γ_d	**1.00**	0.90	0.00	0.00	0.00	0.00	0.00
γ_{sat}	0.90	**1.00**	0.00	0.00	0.00	0.00	0.00
H_d	0.00	0.00	**1.00**	-0.50	0.00	0.00	0.00
H_w	0.00	0.00	-0.50	**1.00**	0.00	0.00	0.00
α	0.00	0.00	0.00	0.00	**1.00**	0.00	0.00
$(N_1)_{60cs}$	0.00	0.00	0.00	0.00	0.00	**1.00**	0.00
C_1	0.00	0.00	0.00	0.00	0.00	0.00	**1.00**

reset design points, x*

Options	Para1	Para2	Para3	Para4
None	value			
Normal	mean	StDev		
Lognorm	mean	StDev		
ExtValue1	mean	StDev		
Uniform	Use BetaDist (1,1,min,max)			
Expo	mean			
Gamma	α	λ		
Weibull	α	λ		
Triang	min	mode	max	
BetaDist	α	λ	min	max
PERTdist	min	mode	max	

	Min.	Max.
γ_d	16.00	26.00
γ_{sat}	17.00	27.00
H_d	0.00	10.00
H_w	0.00	25.00
α	0.00	17.80
$(N_1)_{60cs}$	0.00	33.00
C_1	0.00	2.00

FS
1.00
β
2.200
Pf
0.0139

UNITS ARE IN KILOPASCALS & METERS

Stability computations are based on Ishihara et al (1990).

Reliability computations are based on Low and Tang (2004).

A best-fit line through the Seed and Harder (1990) data is used to estimate the liquefied shear strength based on the input $(N_1)_{60}$

Figure B.3 Reliability computations of Degirmendere Nose case using mean value of $(N_1)_{60\text{-}cs}$

	DistName	Para1	Para2	Para3	Para4	$x_{initial}$	x^*	m^N	s^N	nx
γ_d	Normal	21.00	1.05			21.00	21.21	21.00	1.05	0.20
γ_{sat}	Normal	22.00	1.10			22.00	22.23	22.00	1.10	0.21
H_d	Normal	1.00	0.10			1.00	0.98	1.00	0.10	-0.24
H_w	Normal	7.00	2.10			7.00	8.14	7.00	2.10	0.54
α	Normal	3.00	0.30			3.00	3.08	3.00	0.30	0.26
$(N_1)_{60cs}$	Normal	14.82	3.55			14.82	8.98	14.82	3.55	-1.64
C_1	Normal	1.00	0.30			1.00	0.61	1.00	0.30	-1.30

	γ_d	γ_{sat}	H_d	H_w	α	$(N_1)_{60cs}$	C_1
γ_d	**1.00**	0.90	0.00	0.00	0.00	0.00	0.00
γ_{sat}	0.90	**1.00**	0.00	0.00	0.00	0.00	0.00
H_d	0.00	0.00	**1.00**	-0.50	0.00	0.00	0.00
H_w	0.00	0.00	-0.50	**1.00**	0.00	0.00	0.00
α	0.00	0.00	0.00	0.00	**1.00**	0.00	0.00
$(N_1)_{60cs}$	0.00	0.00	0.00	0.00	0.00	**1.00**	0.00
C_1	0.00	0.00	0.00	0.00	0.00	0.00	**1.00**

reset design points, x*

Options	Para1	Para2	Para3	Para4
None	value			
Normal	mean	StDev		
Lognorm	mean	StDev		
ExtValue1	mean	StDev		
Uniform	Use BetaDist (1,1,min,max)			
Expo	mean			
Gamma	α	λ		
Weibull	α	λ		
Triang	min	mode	max	
BetaDist	α	λ	min	max
PERTdist	min	mode	max	

	Min.	Max.
γ_d	16.00	26.00
γ_{sat}	17.00	27.00
H_d	0.00	10.00
H_w	0.00	25.00
α	0.00	6.00
$(N_1)_{60cs}$	0.00	30.00
C_1	0.00	2.00

FS
1.00
β
2.190
Pf
0.0143

UNITS ARE IN KILOPASCALS & METERS

Stability computations are based on Ishihara et al (1990).

Reliability computations are based on Low and Tang (2004).

A best-fit line through the Seed and Harder (1990) data is used to estimate the liquefied shear strength based on the input $(N_1)_{60}$

Figure B.4 Reliability computations of Esme Nose case using mean value of $(N_1)_{60\text{-}cs}$

	DistName	Para1	Para2	Para3	Para4	$x_{initial}$	x^*	m^N	s^N	nx
γ_d	Normal	20.00	1.00			20.00	20.03	20.00	1.00	0.03
γ_{sat}	Normal	21.50	1.08			21.50	21.53	21.50	1.08	0.03
H_d	Normal	1.10	0.11			1.10	1.10	1.10	0.11	0.00
H_w	Normal	1.40	0.42			1.40	1.42	1.40	0.42	0.04
α	Normal	0.70	0.07			0.70	0.70	0.70	0.07	0.04
$(N_1)_{60cs}$	Normal	10.25	3.13			10.25	9.51	10.25	3.13	-0.24
C_1	Normal	1.00	0.30			1.00	0.04	1.00	0.30	-3.20

	γ_d	γ_{sat}	H_d	H_w	α	$(N_1)_{60cs}$	C_1
γ_d	**1.00**	0.90	0.00	0.00	0.00	0.00	0.00
γ_{sat}	0.90	**1.00**	0.00	0.00	0.00	0.00	0.00
H_d	0.00	0.00	**1.00**	-0.50	0.00	0.00	0.00
H_w	0.00	0.00	-0.50	**1.00**	0.00	0.00	0.00
α	0.00	0.00	0.00	0.00	**1.00**	0.00	0.00
$(N_1)_{60cs}$	0.00	0.00	0.00	0.00	0.00	**1.00**	0.00
C_1	0.00	0.00	0.00	0.00	0.00	0.00	**1.00**

reset design points, x*

Options	Para1	Para2	Para3	Para4
None	value			
Normal	mean	StDev		
Lognorm	mean	StDev		
ExtValue1	mean	StDev		
Uniform	Use BetaDist (1,1,min,max)			
Expo	mean			
Gamma	α	λ		
Weibull	α	λ		
Triang	min	mode	max	
BetaDist	α	λ	min	max
PERTdist	min	mode	max	

	Min.	Max.
γ_d	15.00	25.00
γ_{sat}	16.50	26.50
H_d	0.00	10.00
H_w	0.00	25.00
α	0.00	1.40
$(N_1)_{60cs}$	0.00	21.00
C_1	0.00	2.00

FS
1.00
β
3.208
Pf
0.0007

UNITS ARE IN KILOPASCALS & METERS

Stability computations are based on Ishihara et al (1990).

Reliability computations are based on Low and Tang (2004).

A best-fit line through the Seed and Harder (1990) data is used to estimate the liquefied shear strength based on the input $(N_1)_{60}$

Figure B.5 Reliability computations of Police Station case using mean value of $(N_1)_{60\text{-}cs}$

	DistName	Para1	Para2	Para3	Para4	$x_{initial}$	x^*	m^N	s^N	nx
γ_d	Normal	20.00	1.00			20.00	20.21	20.00	1.00	0.21
γ_{sat}	Normal	21.50	1.08			21.50	21.75	21.50	1.08	0.23
H_d	Normal	1.00	0.10			1.00	0.97	1.00	0.10	-0.28
H_w	Normal	12.00	3.60			12.00	14.17	12.00	3.60	0.60
α	Normal	2.00	0.20			2.00	2.05	2.00	0.20	0.26
$(N_1)_{60cs}$	Normal	13.63	2.94			13.63	9.52	13.63	2.94	-1.40
C_1	Normal	1.00	0.30			1.00	0.57	1.00	0.30	-1.42

	γ_d	γ_{sat}	H_d	H_w	α	$(N_1)_{60cs}$	C_1
γ_d	**1.00**	0.90	0.00	0.00	0.00	0.00	0.00
γ_{sat}	0.90	**1.00**	0.00	0.00	0.00	0.00	0.00
H_d	0.00	0.00	**1.00**	-0.50	0.00	0.00	0.00
H_w	0.00	0.00	-0.50	**1.00**	0.00	0.00	0.00
α	0.00	0.00	0.00	0.00	**1.00**	0.00	0.00
$(N_1)_{60cs}$	0.00	0.00	0.00	0.00	0.00	**1.00**	0.00
C_1	0.00	0.00	0.00	0.00	0.00	0.00	**1.00**

reset design points, x*

Options	Para1	Para2	Para3	Para4
None	value			
Normal	mean	StDev		
Lognorm	mean	StDev		
ExtValue1	mean	StDev		
Uniform	Use BetaDist (1,1,min,max)			
Expo	mean			
Gamma	α	λ		
Weibull	α	λ		
Triang	min	mode	max	
BetaDist	α	λ	min	max
PERTdist	min	mode	max	

	Min.	Max.
γ_d	15.00	25.00
γ_{sat}	16.50	26.50
H_d	0.00	10.00
H_w	0.00	25.00
α	0.00	4.00
$(N_1)_{60cs}$	0.00	27.00
C_1	0.00	2.00

FS
1.00
β
2.110
Pf
0.0174

UNITS ARE IN KILOPASCALS & METERS

Stability computations are based on Ishihara et al (1990).

Reliability computations are based on Low and Tang (2004).

A best-fit line through the Seed and Harder (1990) data is used to estimate the liquefied shear strength based on the input $(N_1)_{60}$

Figure B.6 Reliability computations of Seymen Tea Garden case using mean value of $(N_1)_{60\text{-}cs}$

	DistName	Para1	Para2	Para3	Para4	$x_{initial}$	x^*	m^N	s^N	nx
γ_d	Normal	20.00	1.00			20.00	20.00	20.00	1.00	0.00
γ_{sat}	Normal	21.50	1.08			21.50	21.51	21.50	1.08	0.01
H_d	Normal	0.80	0.08			0.80	0.80	0.80	0.08	0.00
H_w	Normal	1.60	0.48			1.60	1.61	1.60	0.48	0.01
α	Normal	0.10	0.01			0.10	0.10	0.10	0.01	0.01
$(N_1)_{60cs}$	Normal	7.64	1.85			7.64	7.46	7.64	1.85	-0.09
C_1	Normal	1.00	0.30			1.00	0.01	1.00	0.30	-3.31

	γ_d	γ_{sat}	H_d	H_w	α	$(N_1)_{60cs}$	C_1
γ_d	**1.00**	0.90	0.00	0.00	0.00	0.00	0.00
γ_{sat}	0.90	**1.00**	0.00	0.00	0.00	0.00	0.00
H_d	0.00	0.00	**1.00**	-0.50	0.00	0.00	0.00
H_w	0.00	0.00	-0.50	**1.00**	0.00	0.00	0.00
α	0.00	0.00	0.00	0.00	**1.00**	0.00	0.00
$(N_1)_{60cs}$	0.00	0.00	0.00	0.00	0.00	**1.00**	0.00
C_1	0.00	0.00	0.00	0.00	0.00	0.00	**1.00**

reset design points, x*

Options	Para1	Para2	Para3	Para4
None	value			
Normal	mean	StDev		
Lognorm	mean	StDev		
ExtValue1	mean	StDev		
Uniform	Use BetaDist (1,1,min,max)			
Expo	mean			
Gamma	α	λ		
Weibull	α	λ		
Triang	min	mode	max	
BetaDist	α	λ	min	max
PERTdist	min	mode	max	

	Min.	Max.
γ_d	15.00	25.00
γ_{sat}	16.50	26.50
H_d	0.00	10.00
H_w	0.00	25.00
α	0.00	0.20
$(N_1)_{60cs}$	0.00	15.00
C_1	0.00	2.00

FS
1.00
β
3.310
Pf
0.0005

UNITS ARE IN KILOPASCALS & METERS

Stability computations are based on Ishihara et al (1990).

Reliability computations are based on Low and Tang (2004).

A best-fit line through the Seed and Harder (1990) data is used to estimate the liquefied shear strength based on the input $(N_1)_{60}$

Figure B.7 Reliability computations of Soccer Field case using mean value of $(N_1)_{60\text{-}cs}$

	DistName	Para1	Para2	Para3	Para4	$x_{initial}$	x^*	m^N	s^N	nx
γ_d	Normal	15.00	0.75			15.00	15.00	15.00	0.75	0.01
γ_{sat}	Normal	16.00	0.80			16.00	16.01	16.00	0.80	0.01
H_d	Normal	0.80	0.08			0.80	0.80	0.80	0.08	0.00
H_w	Normal	3.70	1.11			3.70	3.71	3.70	1.11	0.01
α	Normal	0.17	0.02			0.17	0.17	0.17	0.02	0.01
$(N_1)_{60cs}$	Normal	12.06	3.46			12.06	11.87	12.06	3.46	-0.05
C_1	Normal	1.00	0.30			1.00	0.01	1.00	0.30	-3.31

	γ_d	γ_{sat}	H_d	H_w	α	$(N_1)_{60cs}$	C_1
γ_d	**1.00**	0.90	0.00	0.00	0.00	0.00	0.00
γ_{sat}	0.90	**1.00**	0.00	0.00	0.00	0.00	0.00
H_d	0.00	0.00	**1.00**	-0.50	0.00	0.00	0.00
H_w	0.00	0.00	-0.50	**1.00**	0.00	0.00	0.00
α	0.00	0.00	0.00	0.00	**1.00**	0.00	0.00
$(N_1)_{60cs}$	0.00	0.00	0.00	0.00	0.00	**1.00**	0.00
C_1	0.00	0.00	0.00	0.00	0.00	0.00	**1.00**

reset design points, x*

Options	Para1	Para2	Para3	Para4
None	value			
Normal	mean	StDev		
Lognorm	mean	StDev		
ExtValue1	mean	StDev		
Uniform	Use BetaDist (1,1,min,max)			
Expo	mean			
Gamma	α	λ		
Weibull	α	λ		
Triang	min	mode	max	
BetaDist	α	λ	min	max
PERTdist	min	mode	max	

	Min.	Max.
γ_d	10.00	20.00
γ_{sat}	11.00	21.00
H_d	0.00	10.00
H_w	0.00	25.00
α	0.00	0.34
$(N_1)_{60cs}$	0.00	24.00
C_1	0.00	2.00

FS
1.00
β
3.314
Pf
0.0005

UNITS ARE IN KILOPASCALS & METERS

Stability computations are based on Ishihara et al (1990).

Reliability computations are based on Low and Tang (2004).

A best-fit line through the Seed and Harder (1990) data is used to estimate the liquefied shear strength based on the input $(N_1)_{60}$

Figure B.8 Reliability computations of Yakin Street case using mean value of $(N_1)_{60\text{-}cs}$

	DistName	Para1	Para2	Para3	Para4	$x_{initial}$	x^*	m^N	s^N	nx
γ_d	Normal	21.00	1.05			21.00	21.02	21.00	1.05	0.02
γ_{sat}	Normal	22.00	1.10			22.00	22.02	22.00	1.10	0.02
H_d	Normal	0.80	0.08			0.80	0.80	0.80	0.08	-0.01
H_w	Normal	3.60	1.08			3.60	3.64	3.60	1.08	0.03
α	Normal	0.29	0.03			0.29	0.29	0.29	0.03	0.02
$(N_1)_{60cs}$	Normal	12.81	3.32			12.81	12.48	12.81	3.32	-0.10
C_1	Normal	1.00	0.30			1.00	0.02	1.00	0.30	-3.28

	γ_d	γ_{sat}	H_d	H_w	α	$(N_1)_{60cs}$	C_1
γ_d	**1.00**	0.90	0.00	0.00	0.00	0.00	0.00
γ_{sat}	0.90	**1.00**	0.00	0.00	0.00	0.00	0.00
H_d	0.00	0.00	**1.00**	-0.50	0.00	0.00	0.00
H_w	0.00	0.00	-0.50	**1.00**	0.00	0.00	0.00
α	0.00	0.00	0.00	0.00	**1.00**	0.00	0.00
$(N_1)_{60cs}$	0.00	0.00	0.00	0.00	0.00	**1.00**	0.00
C_1	0.00	0.00	0.00	0.00	0.00	0.00	**1.00**

reset design points, x*

Options	Para1	Para2	Para3	Para4
None	value			
Normal	mean	StDev		
Lognorm	mean	StDev		
ExtValue1	mean	StDev		
Uniform	Use BetaDist (1,1,min,max)			
Expo	mean			
Gamma	α	λ		
Weibull	α	λ		
Triang	min	mode	max	
BetaDist	α	λ	min	max
PERTdist	min	mode	max	

	Min.	Max.
γ_d	16.00	26.00
γ_{sat}	17.00	27.00
H_d	0.00	10.00
H_w	0.00	25.00
α	0.00	0.58
$(N_1)_{60cs}$	0.00	26.00
C_1	0.00	2.00

FS
1.00
β
3.283
Pf
0.0005

UNITS ARE IN KILOPASCALS & METERS

Stability computations are based on Ishihara et al (1990).

Reliability computations are based on Low and Tang (2004).

A best-fit line through the Seed and Harder (1990) data is used to estimate the liquefied shear strength based on the input $(N_1)_{60}$

Figure B.9 Reliability computations of Yalova Harbor case using mean value of $(N_1)_{60\text{-}cs}$

	DistName	Para1	Para2	Para3	Para4	$x_{initial}$	x^*	m^N	s^N	nx
γ_d	Normal	17.50	0.88			17.50	17.61	17.50	0.88	0.13
γ_{sat}	Normal	20.50	1.03			20.50	20.63	20.50	1.03	0.13
H_d	Normal	2.60	0.26			2.60	2.61	2.60	0.26	0.05
H_w	Normal	1.80	0.54			1.80	1.86	1.80	0.54	0.11
α	Normal	1.00	0.10			1.00	1.02	1.00	0.10	0.20
$(N_1)_{60cs}$	Normal	4.00	0.77			4.00	3.84	4.00	0.77	-0.21
C_1	Normal	1.00	0.30			1.00	0.25	1.00	0.30	-2.49

	γ_d	γ_{sat}	H_d	H_w	α	$(N_1)_{60cs}$	C_1
γ_d	**1.00**	0.90	0.00	0.00	0.00	0.00	0.00
γ_{sat}	0.90	**1.00**	0.00	0.00	0.00	0.00	0.00
H_d	0.00	0.00	**1.00**	-0.50	0.00	0.00	0.00
H_w	0.00	0.00	-0.50	**1.00**	0.00	0.00	0.00
α	0.00	0.00	0.00	0.00	**1.00**	0.00	0.00
$(N_1)_{60cs}$	0.00	0.00	0.00	0.00	0.00	**1.00**	0.00
C_1	0.00	0.00	0.00	0.00	0.00	0.00	**1.00**

reset design points, x*

Options	Para1	Para2	Para3	Para4
None	value			
Normal	mean	StDev		
Lognorm	mean	StDev		
ExtValue1	mean	StDev		
Uniform	Use BetaDist (1,1,min,max)			
Expo	mean			
Gamma	α	λ		
Weibull	α	λ		
Triang	min	mode	max	
BetaDist	α	λ	min	max
PERTdist	min	mode	max	

	Min.	Max.
γ_d	12.50	22.50
γ_{sat}	15.50	25.50
H_d	0.00	10.00
H_w	0.00	25.00
α	0.00	2.00
$(N_1)_{60cs}$	0.00	20.00
C_1	0.00	2.00

FS
1.00
β
2.520
Pf
0.006

UNITS ARE IN KILOPASCALS & METERS

Stability computations are based on Ishihara et al (1990).

Reliability computations are based on Low and Tang (2004).

A best-fit line through the Seed and Harder (1990) data is used to estimate the liquefied shear strength based on the input $(N_1)_{60}$

Figure B.10 Reliability computations of Cark Canal case using minimum value of $(N_1)_{60\text{-}cs}$

	DistName	Para1	Para2	Para3	Para4	$x_{initial}$	x^*	m^N	s^N	nx
γ_d	Normal	15.00	0.75			15.00	15.02	15.00	0.75	0.03
γ_{sat}	Normal	16.00	0.80			16.00	16.02	16.00	0.80	0.03
H_d	Normal	1.10	0.11			1.10	1.10	1.10	0.11	-0.01
H_w	Normal	3.60	1.08			3.60	3.65	3.60	1.08	0.05
α	Normal	0.17	0.02			0.17	0.17	0.17	0.02	0.03
$(N_1)_{60cs}$	Normal	3.00	0.80			3.00	2.98	3.00	0.80	-0.03
C_1	Normal	1.00	0.30			1.00	0.03	1.00	0.30	-3.24

	γ_d	γ_{sat}	H_d	H_w	α	$(N_1)_{60cs}$	C_1
γ_d	**1.00**	0.90	0.00	0.00	0.00	0.00	0.00
γ_{sat}	0.90	**1.00**	0.00	0.00	0.00	0.00	0.00
H_d	0.00	0.00	**1.00**	-0.50	0.00	0.00	0.00
H_w	0.00	0.00	-0.50	**1.00**	0.00	0.00	0.00
α	0.00	0.00	0.00	0.00	**1.00**	0.00	0.00
$(N_1)_{60cs}$	0.00	0.00	0.00	0.00	0.00	**1.00**	0.00
C_1	0.00	0.00	0.00	0.00	0.00	0.00	**1.00**

reset design points, x*

Options	Para1	Para2	Para3	Para4
None	value			
Normal	mean	StDev		
Lognorm	mean	StDev		
ExtValue1	mean	StDev		
Uniform	Use BetaDist (1,1,min,max)			
Expo	mean			
Gamma	α	λ		
Weibull	α	λ		
Triang	min	mode	max	
BetaDist	α	λ	min	max
PERTdist	min	mode	max	

	Min.	Max.
γ_d	10.00	20.00
γ_{sat}	11.00	21.00
H_d	0.00	10.00
H_w	0.00	25.00
α	0.00	0.34
$(N_1)_{60cs}$	0.00	20.00
C_1	0.00	2.00

FS
1.00
β
3.241
Pf
0.001

UNITS ARE IN KILOPASCALS & METERS

Stability computations are based on Ishihara et al (1990).

Reliability computations are based on Low and Tang (2004).

A best-fit line through the Seed and Harder (1990) data is used to estimate the liquefied shear strength based on the input $(N_1)_{60}$

Figure B.11 Reliability computations of Cumruhiyet Avenue case using minimum value of $(N_1)_{60\text{-}cs}$

	DistName	Para1	Para2	Para3	Para4	$x_{initial}$	x^*	m^N	s^N	nx
γ_d	Normal	21.00	1.05			21.00	21.01	21.00	1.05	0.01
γ_{sat}	Normal	22.00	1.10			22.00	22.01	22.00	1.10	0.01
H_d	Normal	1.70	0.17			1.70	1.70	1.70	0.17	0.00
H_w	Normal	1.70	0.51			1.70	1.71	1.70	0.51	0.02
α	Normal	8.90	0.89			8.90	8.92	8.90	0.89	0.02
$(N_1)_{60cs}$	Normal	8.00	1.57			8.00	7.91	8.00	1.57	-0.06
C_1	Normal	1.00	0.30			1.00	0.98	1.00	0.30	-0.06

	γ_d	γ_{sat}	H_d	H_w	α	$(N_1)_{60cs}$	C_1
γ_d	**1.00**	0.90	0.00	0.00	0.00	0.00	0.00
γ_{sat}	0.90	**1.00**	0.00	0.00	0.00	0.00	0.00
H_d	0.00	0.00	**1.00**	-0.50	0.00	0.00	0.00
H_w	0.00	0.00	-0.50	**1.00**	0.00	0.00	0.00
α	0.00	0.00	0.00	0.00	**1.00**	0.00	0.00
$(N_1)_{60cs}$	0.00	0.00	0.00	0.00	0.00	**1.00**	0.00
C_1	0.00	0.00	0.00	0.00	0.00	0.00	**1.00**

reset design points, x*

Options	Para1	Para2	Para3	Para4
None	value			
Normal	mean	StDev		
Lognorm	mean	StDev		
ExtValue1	mean	StDev		
Uniform	Use BetaDist (1,1,min,max)			
Expo	mean			
Gamma	α	λ		
Weibull	α	λ		
Triang	min	mode	max	
BetaDist	α	λ	min	max
PERTdist	min	mode	max	

	Min.	Max.
γ_d	16.00	26.00
γ_{sat}	17.00	27.00
H_d	0.00	10.00
H_w	0.00	25.00
α	0.00	17.80
$(N_1)_{60cs}$	0.00	33.00
C_1	0.00	2.00

FS
1.00
β
0.089
Pf
0.465

UNITS ARE IN KILOPASCALS & METERS

Stability computations are based on Ishihara et al (1990).

Reliability computations are based on Low and Tang (2004).

A best-fit line through the Seed and Harder (1990) data is used to estimate the liquefied shear strength based on the input $(N_1)_{60}$

Figure B.12 Reliability computations of Degirmendere Nose case using minimum value of $(N_1)_{60\text{-}cs}$

	DistName	Para1	Para2	Para3	Para4	$x_{initial}$	x^*	m^N	s^N	nx
γ_d	Normal	21.00	1.05			21.00	21.05	21.00	1.05	0.05
γ_{sat}	Normal	22.00	1.10			22.00	22.06	22.00	1.10	0.05
H_d	Normal	1.00	0.10			1.00	0.99	1.00	0.10	-0.06
H_w	Normal	7.00	2.10			7.00	7.31	7.00	2.10	0.15
α	Normal	3.00	0.30			3.00	3.02	3.00	0.30	0.07
$(N_1)_{60cs}$	Normal	6.00	1.44			6.00	5.78	6.00	1.44	-0.15
C_1	Normal	1.00	0.30			1.00	0.94	1.00	0.30	-0.21

	γ_d	γ_{sat}	H_d	H_w	α	$(N_1)_{60cs}$	C_1
γ_d	**1.00**	0.90	0.00	0.00	0.00	0.00	0.00
γ_{sat}	0.90	**1.00**	0.00	0.00	0.00	0.00	0.00
H_d	0.00	0.00	**1.00**	-0.50	0.00	0.00	0.00
H_w	0.00	0.00	-0.50	**1.00**	0.00	0.00	0.00
α	0.00	0.00	0.00	0.00	**1.00**	0.00	0.00
$(N_1)_{60cs}$	0.00	0.00	0.00	0.00	0.00	**1.00**	0.00
C_1	0.00	0.00	0.00	0.00	0.00	0.00	**1.00**

reset design points, x*

Options	Para1	Para2	Para3	Para4
None	value			
Normal	mean	StDev		
Lognorm	mean	StDev		
ExtValue1	mean	StDev		
Uniform	Use BetaDist (1,1,min,max)			
Expo	mean			
Gamma	α	λ		
Weibull	α	λ		
Triang	min	mode	max	
BetaDist	α	λ	min	max
PERTdist	min	mode	max	

	Min.	Max.
γ_d	16.00	26.00
γ_{sat}	17.00	27.00
H_d	0.00	10.00
H_w	0.00	25.00
α	0.00	6.00
$(N_1)_{60cs}$	0.00	30.00
C_1	0.00	2.00

FS
1.00
β
0.310
Pf
0.378

UNITS ARE IN KILOPASCALS & METERS

Stability computations are based on Ishihara et al (1990).

Reliability computations are based on Low and Tang (2004).

A best-fit line through the Seed and Harder (1990) data is used to estimate the liquefied shear strength based on the input $(N_1)_{60}$

Figure B.13 Reliability computations of Esme Nose case using minimum value of $(N_1)_{60\text{-}cs}$

	DistName	Para1	Para2	Para3	Para4	$x_{initial}$	x^*	m^N	s^N	nx
γ_d	Normal	20.00	1.00			20.00	20.07	20.00	1.00	0.07
γ_{sat}	Normal	21.50	1.08			21.50	21.58	21.50	1.08	0.07
H_d	Normal	1.10	0.11			1.10	1.10	1.10	0.11	-0.01
H_w	Normal	1.40	0.42			1.40	1.45	1.40	0.42	0.11
α	Normal	0.70	0.07			0.70	0.71	0.70	0.07	0.11
$(N_1)_{60cs}$	Normal	3.00	0.92			3.00	2.90	3.00	0.92	-0.11
C_1	Normal	1.00	0.30			1.00	0.12	1.00	0.30	-2.95

	γ_d	γ_{sat}	H_d	H_w	α	$(N_1)_{60cs}$	C_1
γ_d	**1.00**	0.90	0.00	0.00	0.00	0.00	0.00
γ_{sat}	0.90	**1.00**	0.00	0.00	0.00	0.00	0.00
H_d	0.00	0.00	**1.00**	-0.50	0.00	0.00	0.00
H_w	0.00	0.00	-0.50	**1.00**	0.00	0.00	0.00
α	0.00	0.00	0.00	0.00	**1.00**	0.00	0.00
$(N_1)_{60cs}$	0.00	0.00	0.00	0.00	0.00	**1.00**	0.00
C_1	0.00	0.00	0.00	0.00	0.00	0.00	**1.00**

reset design points, x*

Options	Para1	Para2	Para3	Para4
None	value			
Normal	mean	StDev		
Lognorm	mean	StDev		
ExtValue1	mean	StDev		
Uniform	Use BetaDist (1,1,min,max)			
Expo	mean			
Gamma	α	λ		
Weibull	α	λ		
Triang	min	mode	max	
BetaDist	α	λ	min	max
PERTdist	min	mode	max	

	Min.	Max.
γ_d	15.00	25.00
γ_{sat}	16.50	26.50
H_d	0.00	10.00
H_w	0.00	25.00
α	0.00	1.40
$(N_1)_{60cs}$	0.00	21.00
C_1	0.00	2.00

FS
1.00
β
2.956
Pf
0.002

UNITS ARE IN KILOPASCALS & METERS

Stability computations are based on Ishihara et al (1990).

Reliability computations are based on Low and Tang (2004).

A best-fit line through the Seed and Harder (1990) data is used to estimate the liquefied shear strength based on the input $(N_1)_{60}$

Figure B.14 Reliability computations of Police Station case using minimum value of $(N_1)_{60\text{-}cs}$

	DistName	Para1	Para2	Para3	Para4	$x_{initial}$	x^*	m^N	s^N	nx
γ_d	Normal	20.00	1.00			20.00	20.10	20.00	1.00	0.10
γ_{sat}	Normal	21.50	1.08			21.50	21.61	21.50	1.08	0.10
H_d	Normal	1.00	0.10			1.00	0.99	1.00	0.10	-0.14
H_w	Normal	12.00	3.60			12.00	13.05	12.00	3.60	0.29
α	Normal	2.00	0.20			2.00	2.02	2.00	0.20	0.12
$(N_1)_{60cs}$	Normal	7.00	1.51			7.00	6.54	7.00	1.51	-0.31
C_1	Normal	1.00	0.30			1.00	0.87	1.00	0.30	-0.42

	γ_d	γ_{sat}	H_d	H_w	α	$(N_1)_{60cs}$	C_1
γ_d	**1.00**	0.90	0.00	0.00	0.00	0.00	0.00
γ_{sat}	0.90	**1.00**	0.00	0.00	0.00	0.00	0.00
H_d	0.00	0.00	**1.00**	-0.50	0.00	0.00	0.00
H_w	0.00	0.00	-0.50	**1.00**	0.00	0.00	0.00
α	0.00	0.00	0.00	0.00	**1.00**	0.00	0.00
$(N_1)_{60cs}$	0.00	0.00	0.00	0.00	0.00	**1.00**	0.00
C_1	0.00	0.00	0.00	0.00	0.00	0.00	**1.00**

reset design points, x*

Options	Para1	Para2	Para3	Para4
None	value			
Normal	mean	StDev		
Lognorm	mean	StDev		
ExtValue1	mean	StDev		
Uniform	Use BetaDist (1,1,min,max)			
Expo	mean			
Gamma	α	λ		
Weibull	α	λ		
Triang	min	mode	max	
BetaDist	α	λ	min	max
PERTdist	min	mode	max	

	Min.	Max.
γ_d	15.00	25.00
γ_{sat}	16.50	26.50
H_d	0.00	10.00
H_w	0.00	25.00
α	0.00	4.00
$(N_1)_{60cs}$	0.00	27.00
C_1	0.00	2.00

FS
1.00
β
0.617
Pf
0.269

UNITS ARE IN KILOPASCALS & METERS

Stability computations are based on Ishihara et al (1990).

Reliability computations are based on Low and Tang (2004).

A best-fit line through the Seed and Harder (1990) data is used to estimate the liquefied shear strength based on the input $(N_1)_{60}$

Figure B.15 Reliability computations of Seymen Tea Garden case using minimum value of $(N_1)_{60\text{-}cs}$

	DistName	Para1	Para2	Para3	Para4	$x_{initial}$	x^*	m^N	s^N	nx
γ_d	Normal	20.00	1.00			20.00	20.01	20.00	1.00	0.01
γ_{sat}	Normal	21.50	1.08			21.50	21.51	21.50	1.08	0.01
H_d	Normal	0.80	0.08			0.80	0.80	0.80	0.08	-0.01
H_w	Normal	1.60	0.48			1.60	1.61	1.60	0.48	0.02
α	Normal	0.10	0.01			0.10	0.10	0.10	0.01	0.02
$(N_1)_{60cs}$	Normal	2.00	0.49			2.00	2.00	2.00	0.49	-0.01
C_1	Normal	1.00	0.30			1.00	0.02	1.00	0.30	-3.28

	γ_d	γ_{sat}	H_d	H_w	α	$(N_1)_{60cs}$	C_1
γ_d	**1.00**	0.90	0.00	0.00	0.00	0.00	0.00
γ_{sat}	0.90	**1.00**	0.00	0.00	0.00	0.00	0.00
H_d	0.00	0.00	**1.00**	-0.50	0.00	0.00	0.00
H_w	0.00	0.00	-0.50	**1.00**	0.00	0.00	0.00
α	0.00	0.00	0.00	0.00	**1.00**	0.00	0.00
$(N_1)_{60cs}$	0.00	0.00	0.00	0.00	0.00	**1.00**	0.00
C_1	0.00	0.00	0.00	0.00	0.00	0.00	**1.00**

reset design points, x*

Options	Para1	Para2	Para3	Para4
None	value			
Normal	mean	StDev		
Lognorm	mean	StDev		
ExtValue1	mean	StDev		
Uniform	Use BetaDist (1,1,min,max)			
Expo	mean			
Gamma	α	λ		
Weibull	α	λ		
Triang	min	mode	max	
BetaDist	α	λ	min	max
PERTdist	min	mode	max	

	Min.	Max.
γ_d	15.00	25.00
γ_{sat}	16.50	26.50
H_d	0.00	10.00
H_w	0.00	25.00
α	0.00	0.20
$(N_1)_{60cs}$	0.00	15.00
C_1	0.00	2.00

FS
1.00
β
3.280
Pf
0.001

UNITS ARE IN KILOPASCALS & METERS

Stability computations are based on Ishihara et al (1990).

Reliability computations are based on Low and Tang (2004).

A best-fit line through the Seed and Harder (1990) data is used to estimate the liquefied shear strength based on the input $(N_1)_{60}$

Figure B.16 Reliability computations of Soccer Field case using minimum value of $(N_1)_{60\text{-}cs}$

	DistName	Para1	Para2	Para3	Para4	$x_{initial}$	x^*	m^N	s^N	nx
γ_d	Normal	15.00	0.75			15.00	15.02	15.00	0.75	0.03
γ_{sat}	Normal	16.00	0.80			16.00	16.02	16.00	0.80	0.03
H_d	Normal	0.80	0.08			0.80	0.80	0.80	0.08	-0.02
H_w	Normal	3.70	1.11			3.70	3.76	3.70	1.11	0.05
α	Normal	0.17	0.02			0.17	0.17	0.17	0.02	0.03
$(N_1)_{60cs}$	Normal	2.00	0.57			2.00	1.99	2.00	0.57	-0.02
C_1	Normal	1.00	0.30			1.00	0.03	1.00	0.30	-3.24

	γ_d	γ_{sat}	H_d	H_w	α	$(N_1)_{60cs}$	C_1
γ_d	**1.00**	0.90	0.00	0.00	0.00	0.00	0.00
γ_{sat}	0.90	**1.00**	0.00	0.00	0.00	0.00	0.00
H_d	0.00	0.00	**1.00**	-0.50	0.00	0.00	0.00
H_w	0.00	0.00	-0.50	**1.00**	0.00	0.00	0.00
α	0.00	0.00	0.00	0.00	**1.00**	0.00	0.00
$(N_1)_{60cs}$	0.00	0.00	0.00	0.00	0.00	**1.00**	0.00
C_1	0.00	0.00	0.00	0.00	0.00	0.00	**1.00**

reset design points, x*

Options	Para1	Para2	Para3	Para4
None	value			
Normal	mean	StDev		
Lognorm	mean	StDev		
ExtValue1	mean	StDev		
Uniform	Use BetaDist (1,1,min,max)			
Expo	mean			
Gamma	α	λ		
Weibull	α	λ		
Triang	min	mode	max	
BetaDist	α	λ	min	max
PERTdist	min	mode	max	

	Min.	Max.
γ_d	10.00	20.00
γ_{sat}	11.00	21.00
H_d	0.00	10.00
H_w	0.00	25.00
α	0.00	0.34
$(N_1)_{60cs}$	0.00	24.00
C_1	0.00	2.00

FS
1.00
β
3.242
Pf
0.001

UNITS ARE IN KILOPASCALS & METERS

Stability computations are based on Ishihara et al (1990).

Reliability computations are based on Low and Tang (2004).

A best-fit line through the Seed and Harder (1990) data is used to estimate the liquefied shear strength based on the input $(N_1)_{60}$

Figure B.17 Reliability computations of Yakin Street case using minimum value of $(N_1)_{60\text{-}cs}$

	DistName	Para1	Para2	Para3	Para4	$x_{initial}$	x^*	m^N	s^N	nx
γ_d	Normal	21.00	1.05			21.00	21.05	21.00	1.05	0.05
γ_{sat}	Normal	22.00	1.10			22.00	22.06	22.00	1.10	0.05
H_d	Normal	0.80	0.08			0.80	0.80	0.80	0.08	-0.05
H_w	Normal	3.60	1.08			3.60	3.75	3.60	1.08	0.14
α	Normal	0.29	0.03			0.29	0.29	0.29	0.03	0.07
$(N_1)_{60cs}$	Normal	4.00	1.04			4.00	3.90	4.00	1.04	-0.09
C_1	Normal	1.00	0.30			1.00	0.07	1.00	0.30	-3.11

	γ_d	γ_{sat}	H_d	H_w	α	$(N_1)_{60cs}$	C_1
γ_d	**1.00**	0.90	0.00	0.00	0.00	0.00	0.00
γ_{sat}	0.90	**1.00**	0.00	0.00	0.00	0.00	0.00
H_d	0.00	0.00	**1.00**	-0.50	0.00	0.00	0.00
H_w	0.00	0.00	-0.50	**1.00**	0.00	0.00	0.00
α	0.00	0.00	0.00	0.00	**1.00**	0.00	0.00
$(N_1)_{60cs}$	0.00	0.00	0.00	0.00	0.00	**1.00**	0.00
C_1	0.00	0.00	0.00	0.00	0.00	0.00	**1.00**

reset design points, x*

Options	Para1	Para2	Para3	Para4
None	value			
Normal	mean	StDev		
Lognorm	mean	StDev		
ExtValue1	mean	StDev		
Uniform	Use BetaDist (1,1,min,max)			
Expo	mean			
Gamma	α	λ		
Weibull	α	λ		
Triang	min	mode	max	
BetaDist	α	λ	min	max
PERTdist	min	mode	max	

	Min.	Max.
γ_d	16.00	26.00
γ_{sat}	17.00	27.00
H_d	0.00	10.00
H_w	0.00	25.00
α	0.00	0.58
$(N_1)_{60cs}$	0.00	26.00
C_1	0.00	2.00

FS
1.00
β
3.117
Pf
0.001

UNITS ARE IN KILOPASCALS & METERS

Stability computations are based on Ishihara et al (1990).

Reliability computations are based on Low and Tang (2004).

A best-fit line through the Seed and Harder (1990) data is used to estimate the liquefied shear strength based on the input $(N_1)_{60}$

Figure B.18 Reliability computations of Yalova Harbor case using minimum value of $(N_1)_{60\text{-}cs}$

VITA

P. Mamora H. Lumbantoruan received a B.S. in Civil Engineering from Parahyangan Catholic University, Bandung, Indonesia in 1997. He worked for Totalindo Eka Persada Company, Jakarta from 1997 to 1998. He received his M.S. in Civil Engineering in 2000 from Parahyangan Catholic University. He was an instructor at Mercu Buana University, Jakarta, before he began his study at Virginia Polytechnic Institute and State University in 2004.